JAERI-M
93-139

ASSESSMENT OF TRAC-PF1/MOD1 CODE FOR THERMAL-HYDRAULIC BEHAVIOR IN PRESSURE VESSEL DURING REFLOOD IN SCTF TEST WITH A RADIAL POWER DISTRIBUTION

July 1993

Akira OHNUKI, Hajime AKIMOTO and Yoshio MURAO

日本原子力研究所
Japan Atomic Energy Research Institute

JAERI-Mレポートは，日本原子力研究所が不定期に公刊している研究報告書です。
入手の問合わせは，日本原子力研究所技術情報部情報資料課（〒319-11茨城県那珂郡東海村）あて，お申しこしください。なお，このほかに財団法人原子力弘済会資料センター（〒319-11 茨城県那珂郡東海村日本原子力研究所内）で複写による実費頒布をおこなっております。

JAERI-M reports are issued irregularly.
Inquiries about availability of the reports should be addressed to Information Division Department of Technical Information, Japan Atomic Energy Research Institute, Tokai-mura, Naka-gun, Ibaraki-ken 319-11, Japan.

編集兼発行　日本原子力研究所
印　　刷　いばらき印刷㈱

JAERI-M 93-139

Assessment of TRAC-PF1/MOD1 Code for Thermal-hydraulic Behavior in Pressure Vessel during Reflood in SCTF Test with a Radial Power Distribution

Akira OHNUKI, Hajime AKIMOTO and Yoshio MURAO

Department of Reactor Engineering
Tokai Research Establishment
Japan Atomic Energy Research Institute
Tokai-mura, Naka-gun, Ibaraki-ken

(Received June 8, 1993)

Post test calculations for two tests with steep or flat radial core power distribution using the Slab Core Test Facility (SCTF) were performed to assess the TRAC-PF1/MOD1 code for the thermal-hydraulic behaviors in pressure vessel during reflood phase of a PWR-LOCA. The predictive capability for the two-dimensional thermal-hydraulic behavior in pressure vessel was also assessed in this report. The TRAC code predicted transients of clad surface temperature well including radial distribution of clad surface temperature caused by different bundle power. However, the TRAC predictions showed poor agreement on void fractions in the core and in the upper plenum. For the radial distribution of void fraction, the TRAC code predicted a peculiar distribution in the core which was not observed in the SCTF tests, and predicted a flatter distribution in the upper plenum compared to measured results. Recommendation was made for the future improvement on hydraulic and heat transfer models based on this assessment study.

Keywords: Reactor Safety, Heat Transfer, Void Fraction, Two-phase Flow, Reflood, Film Boiling, Numerical Simulation, TRAC Code

半径方向出力分布を有するＳＣＴＦ試験の圧力容器内における再冠水時熱水力学的挙動に対するＴＲＡＣ－ＰＦ１／ＭＯＤ１コードの予測性能評価

日本原子力研究所東海研究所原子炉工学部
大貫　晃・秋本　肇・村尾　良夫

（1993年６月８日受理）

ＰＷＲ－ＬＯＣＡ時再冠水過程での圧力容器内熱水力挙動に対するＴＲＡＣ－ＰＦ１／ＭＯＤ１コードの予測性能を評価するために，平板炉心試験装置（ＳＣＴＦ）を使い急峻，あるいは平坦の各炉心半径方向出力分布により行った二つの試験に対する試験後解析を行った。本報告では，圧力容器内の２次元的な熱水力挙動に対する予測性能についても併せて評価した。ＴＲＡＣコードは被覆管温度の遷移に対し，出力の違いにより生ずる半径方向の分布を含め良く予測した。しかしながら，炉心内及び上部プレナム内でのボイド率の予測に対しては良くなかった。ＴＲＡＣコードはボイド率の半径方向の分布に対し，炉心内ではＳＣＴＦ試験ではみられなかった特殊な分布を予測し，上部プレナム内では測定結果に対しより平坦な分布を予測した。本予測性能評価に基づき，水力及び熱伝達モデルに対し改良すべき点を示した。

東海研究所：〒319-11　茨城県那珂郡東海村白方字白根2-4

Contents

1. Introduction 1
2. Facility and Test Description 2
2.1 Test Facility 2
2.2 Test Conditions and Procedure 2
3. Code and Model Description 3
3.1 Input Schematics 3
3.2 Initial and Boundary Conditions 4
4. Results and Discussion 5
4.1 Hydraulic Behavior in Pressure Vessel except Core 5
4.2 Hydraulic Behavior in Core 7
4.3 Thermal Behavior in Core 9
4.4 Run Statistics 11
5. Conclusions 12
Acknowledgments 13
References 13

目　　次

1. 序　論 …… 1
2. 試験装置及び試験条件 …… 2
2.1 試験装置 …… 2
2.2 試験条件及び試験手順 …… 2
3. 計算コード及び入力モデル …… 3
3.1 入力モデル …… 3
3.2 初期条件及び境界条件 …… 4
4. 結果及び考察 …… 5
4.1 炉心部を除く圧力容器内の水力挙動 …… 5
4.2 炉心内の水力挙動 …… 7
4.3 炉心内の熱伝達挙動 …… 9
4.4 計算時間 …… 11
5. 結　論 …… 12
謝　辞 …… 13
参考文献 …… 13

List of Tables

Table 1 ICAP assessment matrix − Japan
Table 2.1.1 Principal dimensions of SCTF core−II
Table 2.1.2 Comparison of dimensions between SCTF and the reference PWR
Table 2.2.1 Test conditions for flat power test S2−14
Table 2.2.2 Test conditions for steep power test S2−16
Table 2.2.3 Chronology of major events for flat power test S2−14
Table 2.2.4 Chronology of major events for steep power test S2−16

List of Figures

Fig.2.1.1 Vertical cross sections of pressure vessel
Fig.2.1.2 Bird's−eye view of SCTF
Fig.2.1.3 Comparison of dimensions between SCTF and the reference PWR
Fig.2.1.4 Arrangement of rod bundles
Fig.2.1.5 Dimension, Configuration and axial power distribution of heater rods
Fig.2.1.6 Horizontal cross sections in upper head and in upper plenum

Fig.3.1.1 Input model for SCTF pressure vessel
Fig.3.1.2 Input model for hot leg and for ECC injection line
Fig.3.2.1 Comparison of ECC mass flow rate and ECC water temperature for flat power test S2−14
Fig.3.2.2 Comparison of ECC mass flow rate and ECC water temperature for steep power test S2−16
Fig.3.2.3 Comparison of core power for flat power test S2−14
Fig.3.2.4 Comparison of core power for steep power test S2−16
Fig.3.2.5 Comparison of relative axial power ratio for both tests
Fig.3.2.6 Comparison of pressure at exit of hot leg

Fig.4.1.1 Comparison of pressure in pressure vessel for flat power test
Fig.4.1.2 Comparison of pressure in pressure vessel for steep power test
Fig.4.1.3 Comparison of core inlet mass flow rate

Fig.4.1.4 Comparison of fluid temperature at inlet of core
Fig.4.1.5 Comparison of core exit liquid mass flow rate
Fig.4.1.6 Comparison of steam and water mass flow rates at exit of hot leg for flat power test
Fig.4.1.7 Comparison of steam and water mass flow rates at exit of hot leg for steep power test
Fig.4.1.8(1) Comparison of differential pressure in upper plenum for flat power test
Fig.4.1.8(2) Comparison of differential pressure in upper plenum for flat power test
Fig.4.1.9(1) Comparison of differential pressure in upper plenum for steep power test
Fig.4.1.9(2) Comparison of differential pressure in upper plenum for steep power test
Fig.4.1.10 Comparison of difference of differential pressure in upper plenum between above bundle 8 and above bundle 1
Fig.4.1.11 Comparison of void fraction in upper plenum for steep power test

Fig.4.2.1 Comparison of sectional differential pressure in bundle 4 for flat power test
Fig.4.2.2(1) Comparison of sectional differential pressure in bundle 2 for steep power test
Fig.4.2.2(2) Comparison of sectional differential pressure in bundle 4 for steep power test
Fig.4.2.2(3) Comparison of sectional differential pressure in bundle 8 for steep power test
Fig.4.2.3 Comparison of upper and lower half differential pressures in bundle 4 for flat power test
Fig.4.2.4(1) Comparison of upper and lower half differential pressures in bundle 2 for steep power test
Fig.4.2.4(2) Comparison of upper and lower half differential pressures in bundle 4 for steep power test
Fig.4.2.4(3) Comparison of upper and lower half differential pressures in bundle 8 for steep power test
Fig.4.2.5 Comparison of total core differential pressure for flat power test
Fig.4.2.6 Comparison of total core differential pressure for steep power test
Fig.4.2.7 Comparison of differential pressure in core baffle region
Fig.4.2.8 Comparison of sectional void fraction in bundle 4 for flat power test
Fig.4.2.9 Comparison of radial distribution of sectional void fraction for flat power test

Fig.4.2.10(1) Comparison of sectional void fraction in bundle 2 for steep power test
Fig.4.2.10(2) Comparison of sectional void fraction in bundle 4 for steep power test
Fig.4.2.10(3) Comparison of sectional void fraction in bundle 8 for steep power test
Fig.4.2.11 Comparison of void fraction in each computational cell in bundle 4 for steep power test
Fig.4.2.12(1) Comparison of radial distribution of sectional void fraction for steep power test
Fig.4.2.12(2) Comparison of radial distribution of sectional void fraction for steep power test
Fig.4.2.13(1) Two-dimensional mass flow rate distribution in core at 150 sec for flat power test
Fig.4.2.13(2) Two-dimensional mass flow rate distribution in core at 200 sec for flat power test
Fig.4.2.13(3) Two-dimensional mass flow rate distribution in core at 300 sec for flat power test
Fig.4.2.13(4) Two-dimensional mass flow rate distribution in core at 400 sec for flat power test
Fig.4.2.14(1) Two-dimensional mass flow rate distribution in core at 200 sec for steep power test
Fig.4.2.14(2) Two-dimensional mass flow rate distribution in core at 250 sec for steep power test
Fig.4.2.14(3) Two-dimensional mass flow rate distribution in core at 300 sec for steep power test
Fig.4.2.14(4) Two-dimensional mass flow rate distribution in core at 400 sec for steep power test
Fig.4.2.14(5) Two-dimensional mass flow rate distribution in core at 500 sec for steep power test

Fig.4.3.1 Comparison of clad surface temperature in bundle 4 for flat power test
Fig.4.3.2 Comparison of turnaround time after flood for flat power test
Fig.4.3.3 Comparison of turnaround temperature for flat power test
Fig.4.3.4 Comparison of quench time after flood for flat power test
Fig.4.3.5 Comparison of quench temperature for flat power test
Fig.4.3.6(1) Comparison of clad surface temperature in bundle 2 for steep power test

Fig.4.3.6(2) Comparison of clad surface temperature in bundle 4 for steep power test
Fig.4.3.6(3) Comparison of clad surface temperature in bundle 8 for steep power test
Fig.4.3.7 Comparison of turnaround time after flood for steep power test
Fig.4.3.8 Comparison of turnaround temperature for steep power test
Fig.4.3.9 Comparison of quench time after flood for steep power test
Fig.4.3.10 Comparison of quench temperature for steep power test

Fig.4.4.1 Total CPU time and time step size for flat power test
Fig.4.4.2 Total CPU time and time step size for steep power test

1. Introduction

The International Thermal-Hydraulic Code Assessment and Application Program (ICAP) was conducted by several countries and coordinated by the United States Nuclear Regulatory Commission (USNRC).[1] The purpose of ICAP is to make qualitative and quantitative statement regarding the accuracy of the current thermal-hydraulic computer programs developed under the auspices of the USNRC.

Japan's contributions to ICAP include the assessment of TRAC-PWR[2], TRAC-BWR[3] and RELAP5[4] codes. The assessment matrix is shown in Table 1. The assessment calculations were conducted by Japan Atomic Energy Research Institute (JAERI) and Japanese industrial groups.

In this report, the predictive capability of TRAC-PF1/MOD1 code[2] is presented for the thermal-hydraulic behaviors including two-dimensional behaviors in pressure vessel during reflood phase of a postulated Large Break Loss-of-Coolant Accident (LBLOCA) in a PWR. In the previous studies at JAERI[5][6], the integral predictive capability of the TRAC-PF1/MOD1 code was assessed in the calculation of the Cylindrical Core Test Facility (CCTF)[7] test with the model including the primary loops, and then the separate assessments with one-dimensional core model were conduced with the CCTF and the Slab Core Test Facility (SCTF)[8] data. In the present study, a multidimensional predictive capability is assessed with two-dimensional VESSEL model by comparisons with data from the SCTF. The predictive capability for the multidimensional behaviors has not been analyzed in detail yet as far as the authors understand.

The SCTF has a full-height core with full radial size and one bundle depth to a reference actual PWR. Experimental results from SCTF indicate that radial power distribution affects the two-dimensional thermal-hydraulic behaviors in the pressure vessel[9]. So two SCTF tests with different radial power distribution were selected for the assessment in this report. One is Test S2-14, that is flat radial power distribution test, and the other is Test S2-16[10], that is steep radial power distribution test.

This report is organized as follows: Chapter 2 describes the test facility and test conditions and chapter 3 describes the TRAC-PF1/MOD1 model used to simulate the tests. In chapter 4, results from the simulations are presented and discussed. Conclusions and recommendation are presented in chapter 5.

2. Facility and Test Description

2.1 Test Facility

The SCTF was designed to properly simulate the two-dimensional core heat transfer and hydraulic behaviors during refill-reflood phase. The pressure vessel is of slab geometry as shown in Fig. 2.1.1. Full scale radial and axial section of a reference PWR is provided as a simulated core with single bundle depth. The reference reactor is the Trojan reactor in the United States which is a four loop 3300 MWt PWR. The simulated core consists of 8 bundles arranged in a row. On the other hand, simplified primary coolant loops are provided. Bird's-eye view of pressure vessel and the coolant loop is shown in Fig. 2.1.2. The scaling of flow area and fluid volume of each component is in accordance with the core flow area scaling. The principal dimensions of the facility is shown in Table 2.1.1, and the comparison of dimensions between the SCTF and the referred PWR is shown in Table 2.1.2 and in Fig. 2.1.3.

Each bundle has 234 electrically heated rods and 22 non-heated rods. The arrangement of rod bundles is shown in Fig. 2.1.4. The dimensions of the heater rods are based on a 15x15 type fuel assembly and the heated length and the outer diameter of each heater rod are 3.66 m and 10.7 mm, respectively. The dimension, configuration and axial power distribution of each heater rod are shown in Fig. 2.1.5. The axial peaking factor is 1.4.

The design of upper plenum internals is based on that of the new Westinghouse 17x17 array fuel assemblies. The internals consist of control rod guide tubes, support columns, orifice plate and open holes and the arrangement is shown in Fig. 2.1.6. The radius of each component is scaled down by factor 8/15 from that of an actual reactor.

Mode detailed information on the SCTF is available in reference (8).

2.2 Test Conditions and Procedure

Emergency core cooling (ECC) water was injected directly into the lower plenum in the tests examined in this report. The downcomer had been isolated from the lower plenum by inserting a blocking plate. This method is called the forced-feed reflooding.

Two forced feed tests were selected in this report to meet objectives in Introduction, those are Tests S2-14 and S2-16. These two tests were performed under the different radial power distribution. In Test S2-14, the distribution was flat. On the other hand, the normalized radial power factors in Bundles 1 and 2, 3 and 4, 5 and 6 and 7 and 8

were 1.0, 1.2, 1.0 and 0.8 in Test S2-16. Additionally, water extraction from the upper plenum was performed in Test S2-14 to maintain the flat distribution of collapsed liquid level because non-uniform distribution of liquid level in upper plenum was found to affect the two-dimensional core thermal-hydraulic behaviors as described in reference (9). Therefore, data from Test S2-14 are considered to give information under the condition without inducing two-dimensional thermal-hydraulic behaviors due to test conditions. Major specified and measured test conditions are listed in Tables 2.2.1 and 2.2.2.

The test procedure for these two tests is as follows. After setting the initial conditions (pressure and saturation condition etc.), core heating was initiated. When four cladding temperatures exceeded 910 K and 1137 K for Tests S2-14 and S2-16, respectively, the accumulator (Acc) injection into the lower plenum was initiated. The initial saturation water level in the lower plenum was about 0.15 m below the bottom of heated part. The maximum cladding temperature at the reflood initiation was intended to be 922 K and 1160 K for Tests S2-14 and S2-16, respectively. After keeping the core power constant for 0 second in Test S2-14 and for 40 sec in Test S2-16 from the Acc injection start, the core power decay simulation started from the value at 40 sec after shutdown of an actual reactor. The decay curve was based on the "1.02 x (ANS standard + actinides)". Chronologies of major events for both tests are shown in Tables 2.2.3 and 2.2.4.

3. Code and Model Description

The two-dimensional reflood simulations for SCTF Tests S2-14 and S2-16 were performed with TRAC-PF1/MOD1 code Version 12.5.

3.1 Input Schematics

The TRAC input in this report modeled the pressure vessel, ECC injection piping and a hot leg in SCTF. Intact and broken cold legs and steam/water separator were not modeled because of the following reasons:

(1) Main assessment subject is the two-dimensional thermal-hydraulic behaviors in the pressure vessel in this report.

(2) Since the bottom of the downcomer is blocked in the tests, two-phase flow through the cold legs to the downcomer does not affect the core thermal-hydraulics.

were 1.0, 1.2, 1.0 and 0.8 in Test S2-16. Additionally, water extraction from the upper plenum was performed in Test S2-14 to maintain the flat distribution of collapsed liquid level because non-uniform distribution of liquid level in upper plenum was found to affect the two-dimensional core thermal-hydraulic behaviors as described in reference (9). Therefore, data from Test S2-14 are considered to give information under the condition without inducing two-dimensional thermal-hydraulic behaviors due to test conditions. Major specified and measured test conditions are listed in Tables 2.2.1 and 2.2.2.

The test procedure for these two tests is as follows. After setting the initial conditions (pressure and saturation condition etc.), core heating was initiated. When four cladding temperatures exceeded 910 K and 1137 K for Tests S2-14 and S2-16, respectively, the accumulator (Acc) injection into the lower plenum was initiated. The initial saturation water level in the lower plenum was about 0.15 m below the bottom of heated part. The maximum cladding temperature at the reflood initiation was intended to be 922 K and 1160 K for Tests S2-14 and S2-16, respectively. After keeping the core power constant for 0 second in Test S2-14 and for 40 sec in Test S2-16 from the Acc injection start, the core power decay simulation started from the value at 40 sec after shutdown of an actual reactor. The decay curve was based on the "1.02 x (ANS standard + actinides)". Chronologies of major events for both tests are shown in Tables 2.2.3 and 2.2.4.

3. Code and Model Description

The two-dimensional reflood simulations for SCTF Tests S2-14 and S2-16 were performed with TRAC-PF1/MOD1 code Version 12.5.

3.1 Input Schematics

The TRAC input in this report modeled the pressure vessel, ECC injection piping and a hot leg in SCTF. Intact and broken cold legs and steam/water separator were not modeled because of the following reasons:

(1) Main assessment subject is the two-dimensional thermal-hydraulic behaviors in the pressure vessel in this report.

(2) Since the bottom of the downcomer is blocked in the tests, two-phase flow through the cold legs to the downcomer does not affect the core thermal-hydraulics.

(3) Since the SCTF has the steam/water separator instead of steam generators to measure carry-over flow rate accurately, the effect of the feed back from the exit of the hot leg is negligible small on the core behaviors in the SCTF.

The pressure vessel was represented by VESSEL component as shown in Fig. 3.1.1. The input consists of 15 axial levels, 11 radial sections and 1 azimuthal section. Levels 4 through 11 and radial sections 1 through 8 represent the heated core.

The ECC injection piping and the hot leg were modeled by PIPE components as shown in Fig. 3.1.2. Mass flow rate and fluid temperature of ECC water was supplied by FILL component. The boundary condition at the exit of the hot leg was supplied by BREAK component in terms of the pressure measured at the steam/water separator in the tests.

The ECC injection piping is connected to the cell of level 1 and radial section 9 of VESSEL component as shown in Fig. 3.1.1. And the hot leg is connected to the cell of level 14 and radial section 9 of VESSEL component as also shown in Fig. 3.1.1.

3.2 Initial and Boundary Conditions

The initial and time-dependent boundary conditions were determined based on the measured results. The conditions for FILL, supplied core power and BREAK are shown in Figs. 3.2.1 through 3.2.6. These values are plotted against the time after core power on.

The conditions for FILL are shown in Figs. 3.2.1 and 3.2.2 for flat power test S2-14 and steep power test S2-16, respectively. The input values for TRAC calculations are almost the same as the measured results.

The total supplied power for each bundle and relative axial power ratio are compared in Figs. 3.2.3 through 3.2.5. Radial distribution of supplied power and the shape of decay curve are agreed well with each other. Since the axial noding for the core is course against the axial power step in the tests as shown in Fig. 3.2.5, the axial peak power was supplied at 1.58 m elevation from the bottom of heated core for TRAC calculations. The integrated power density at top and bottom regions in the core was slightly higher than the measured results but the difference was negligible small as already shown in Figs. 3.2.3 and 3.2.4.

The conditions for BREAK are compared in Fig. 3.2.6. The initial and time-dependent values are agreed well with each other.

4. Results and Discussion

4.1 Hydraulic Behavior in Pressure Vessel except Core

In this section, the assessment results are discussed on the pressure, on the core inlet fluid conditions, on the mass flow rate at the core exit and at the hot leg exit and on the two-dimensional hydraulic behaviors in the upper plenum.

Figures 4.1.1 and 4.1.2 show the comparison of the pressure in the upper plenum, in the core and in the lower plenum for flat power test and for steep power test, respectively. The whole transients are predicted well qualitatively and quantitatively for both tests. However, the TRAC code slightly overestimates in the lower plenum after about 200 sec for flat power test and in the period between about 250 sec and about 450 sec for steep power test. These differences were caused by the overestimation for core differential pressures as will be presented in Figs. 4.2.5 and 4.2.6. And the pressure in the lower plenum after about 600 sec for steep power test is slightly underestimated as shown in Fig. 4.1.2. This was caused by the underestimation for liquid fraction in the upper plenum in that period as will be shown in Figs. 4.1.9(1) and 4.1.9(2) because the core differential pressure was almost the same between each other in that period as will be shown in Fig. 4.2.6.

Figure 4.1.3 shows the comparisons of the core inlet mass flow rates for both tests. The measured values were estimated by subtracting the accumulated rate in the lower plenum from the ECC injection rate because the bottom of downcomer was blocked. The measured results and the TRAC predictions are almost the same between each other for both tests.

Figure 4.1.4 shows the comparison of the fluid temperature just below bundles 1, 4 and 8 for both tests. For flat power test, the predicted results are slightly lower than the data during whole transients. Since the pressure in the lower plenum is slightly overestimated as shown in Fig. 4.1.1, the core inlet subcooling in the TRAC calculation is higher than data. For steep power test, the predicted results are almost the same as the data until about 400 sec, and however the degree of measured radial distribution after about 500 sec is underestimated. The radial distribution is also recognized in the flat power test in the period between about 160 sec and about 450 sec. The TRAC code underestimates the degree of that distribution. The underestimation for the distribution indicates that the degree of fluid mixing in the lower plenum is higher in the TRAC calculations.

Figure 4.1.5 shows the comparison of the liquid mass flow rate at the exit of core for both tests. The TRAC predictions almost agree with the measured results except in the following two periods,

(1) Early period in the transients −− Underestimate,

(2) Around 550 sec for flat power test and around 600 sec for steep power test
−− The TRAC code predicts the down−flow from the upper plenum into the core.

Figures 4.1.6 and 4.1.7 show the comparisons of steam and water mass flow rate at the exit of hot leg for flat and steep power tests, respectively. For the steam mass flow rate, the TRAC predictions almost agree with the measured results qualitatively and quantitatively although relatively long period oscillations are recognized. On the other hand, the water mass flow rate is not predicted qualitatively and quantitatively. For both tests, the TRAC predictions give almost zero value until about 400 sec. After that, the TRAC code tends to overestimate the mass flow rates although the predicted value falls to zero in the periods when the mass flow rate at the exit of core is negative as shown in Fig. 4.1.5. Since the water mass flow rate at the exit of hot leg affects the core inlet coolant velocity due to the steam binding in an actual reactor, the improvement for the carry−over characteristics is recommended.

Figures 4.1.8 and 4.1.9 show the comparison of differential pressure in the upper plenum above bundles 1, 3, 6 and 8 for flat and steep power tests, respectively. For flat power test, the assessment of the TRAC code for the hydraulic behaviors is difficult until about 500 sec because the water in the upper plenum was extracted until that time in the test as mentioned in Chapter 2. After that time, the TRAC code underestimates the differential pressure. For steep power test, the TRAC code overestimates the differential pressure until about 550 sec, and, after that, tends to underestimate the value.

Figure 4.1.10 shows the comparison of the degree of radial distribution of differential pressure in the upper plenum, that is (differential pressure above bundle 8 − differential pressure above bundle 1). Even though the radial distribution was tried to be flat in the flat power test by extracting the water, the TRAC prediction indicates flatter distribution than the measured results. For steep power test, the TRAC prediction also gives flatter distribution, and the difference is getting large after about 400 sec.

Figure 4.1.11 shows the comparisons of void fraction in the upper plenum above bundles 1, 3, 6 and 8 for steep power test. The measured results were estimated from the differential pressure shown in Fig. 4.1.9 under the assumption that the frictional and acceleratory pressure drops are negligible small. Until about 350 sec above bundles 1, 3

and 6 and about 250 sec above bundle 8, the TRAC prediction shows almost zero liquid fraction (1−void fraction). This indicates that the higher differential pressure of TRAC in this period shown in Fig. 4.1.9 is caused by the frictional and acceleratory pressure drops mainly due to the steam flow because the water up−flow rate from the core is small as shown in Fig. 4.1.5. In the period between after those times mentioned above and about 500 sec, the TRAC code slightly overestimates the liquid fraction. After about 500 sec, the TRAC code underestimates the liquid fraction. These characteristics for the liquid fraction are correspond to those for the differential pressures shown in Fig. 4.1.9. The assessment results for the hydraulic behaviors in the upper plenum and for the carry−over flow rate described above indicate the necessity of the hydraulic model improvements in the upper plenum.

4.2 Hydraulic Behavior in Core

Figure 4.2.1 and Figs. 4.2.2(1) through 4.2.2(3) show the comparison of sectional differential pressure in core for flat and steep power tests, respectively. The TRAC code has a tendency to overestimate the differential pressure below the middle elevation of the core. On the other hand, the TRAC predictions almost agree with the measured results at the upper region of the core until about 300 sec for flat power test and until about 400 sec for steep power test. After those times, the TRAC code overestimates the differential pressure.

The comparison of the differential pressure at the lower half and at the upper half of core is shown in Figs. 4.2.3 and 4.2.4(1) through 4.2.4(3). The tendency of TRAC predictions mentioned above is also observed in these figures although the periods of underestimation at the upper half are different. The predicted values at the upper half show relatively good agreement with the measured results against the lower half. And for the steep power test, the TRAC predictions almost agree with the measured results after about 600 sec in both regions.

The comparison of total core differential pressure is shown in Figs. 4.2.5 and 4.2.6. The TRAC predictions for both tests overestimate the differential pressure except for the initial rapid increasing period and for the period after about 600 sec in steep power test. The tendency of the overestimation is due to the overestimation at the lower half of the core as shown in Figs. 4.2.3 and 4.2.4. In the initial period, the increasing rate of predicted results is slightly lower, and after about 600 sec in steep power test the differential pressure is almost agreed with each other. These characteristics are also

recognized in the sectional differential pressure shown in Figs. 4.2.1 through 4.2.4.

Figure 4.2.7 shows the comparison of differential pressure in core baffle region for both tests. The TRAC code overestimates the differential pressure except for the initial rapid increasing period. The tendency of the overestimation is correspond to that for the total core differential pressure discussed above. In the initial period, the increasing rate of TRAC is almost the same with the measured results and however the time of initial increase is later than the measured result.

Figure 4.2.8 shows the comparison of sectional void fraction at three axial sections in bundle 4 in flat power test. The locations of these axial sections are the same as those for the sectional differential pressure shown in Fig. 4.2.1. The method for estimating the void fraction was the same as that in Fig. 4.1.11. The TRAC code tends to underestimate the void fraction below the middle elevation of core. The tendency of underestimation is also recognized in the upper part of core after about 350 sec. In the upper part of core, no water accumulation is calculated until about 300 sec. Even in the region below the middle elevation, no water accumulation is calculated early in the transients. After those periods, the TRAC code predicts a faster decrease of void fraction than the measured results.

Figures 4.2.9 shows the comparison of radial difference of void fraction at almost middle section of core in flat power test. TRAC predictions show the almost flat distribution as in the data.

Figure 4.2.10 (1) through 4.2.10(3) show the comparison of sectional void fraction in bundles 2 4 and 8 in steep power test. The tendency of the difference between predicted and measured results in these different power bundles is the same as that observed in flat power test mentioned above. In order to make clear the characteristics of predicted water accumulation, the void fraction in each computational cell in bundle 4 in steep power test is compared in Fig. 4.2.11. This comparison indicates that the water accumulation in one cell starts after that the void fraction of the adjacent lower cell is almost saturated except for the cell just above the core. On the other hand, the void fraction in some cells suddenly increases from a saturated value after a time period. This peculiar nature of transients is considered to relate to the interface sharpener model in the TRAC code[2]. For example, the void fraction in fifth level of core is reduced at about 300 sec because the model was on (the model is on under the condition that the void fraction in the upper and the lower cells are greater than 0.7 and less than 0.3, respectively). However, the void fraction is suddenly increased at about 550 sec. Since

the void fraction condition in the adjacent cells is not satisfied to the condition of application of the model at that time, the behavior is considered to be caused by the model termination. In the upper figure of Fig. 4.2.11, the void fraction in the level just above the core is also shown. The beginning of decrease of void fraction in this cell is faster than that of the adjacent lower cell in the core because the interface sharpener model is only applied to the cells of core.

Figures 4.2.12(1) and 4.2.12(2) show radial difference of void fraction in bundles 2, 4 and 8 in steep power test at almost middle regions of core. The TRAC predictions indicate almost flat radial distribution during the decreasing period of void fraction in which the interface sharpener model described above was on and, after that, the sharpener model produces a peculiar distribution. On the other hand, a radial distribution is slightly observed in the measured results. The void fraction in low power bundle (bundle 8) is lower in the region between 1.365 m and 1.905 m elevations, and is higher at around 350 sec in the region between 2.03 m and 2.57 m elevations.

Figures 4.2.13(1) through 4.2.13(4) and 4.2.14(1) through 4.2.14(5) show the predicted two-dimensional steam and liquid mass flow rate distribution in the core at a specified time for flat and steep power tests, respectively. These figures also includes the location of quench front calculated by the code at each time. The following remarks are recognized from these figures,

(1) Steam mass flow rate is gradually increased from around the quench front to the top of core, and the radial distribution of steam mass flow rate becomes almost flat even for the steep power test due to a cross flow in the core,

(2) Negligible small liquid mass flow rate is calculated in the upper part of core for both tests,

(3) For flat power test, the radial distribution of liquid mass flow rate is almost flat above the quench front and however a systematic distribution is not recognized below around the quench front and

(4) For steep power test, the liquid mass flow rate in higher power bundles tends to be higher than that in lower power bundles for both regions below and above the quench front except at 500 sec. This tendency is realized by the flow circulation around the quench front.

4.3 Thermal Behavior in Core

Figure 4.3.1 shows the comparison of clad surface temperature in bundle 4 in flat

power test. Although the TRAC code gives a higher turnaround temperature, the shape of transient curve and the time of quench are almost predicted. Since the heat transfer at the clad surface is dependent on the local void fraction in the TRAC models[2], the agreement for the clad surface temperature means the necessity of improvement of heat transfer model because the void fraction was not predicted well as discussed in section 4.2.

Figures 4.3.2 through 4.3.5 show the comparison of important parameters on the clad surface temperature along the axial direction, those are the turnaround time ,the turnaround temperature, the quench time and the quench temperature in bundles 2, 4 and 8 for flat power test. For the turnaround items, the TRAC code overestimates the turnaround time and the turnaround temperature at almost all elevations and bundles. For the quench items, the TRAC predictions almost agree with the measured results. No significant differences among bundles are recognized in the measured results for both items in this test and the TRAC code predicts the tendency.

Figures 4.3.6(1) through 4.3.6(3) show the comparison of clad surface temperature in bundles 2, 4 and 8, respectively, for steep power test. The characteristics of the qualitative and quantitative agreement are almost the same as those for flat power test shown in Fig. 4.3.1. Figures 4.3.7 through 4.3.10 show the comparison of the important parameters mentioned above in bundles 2, 4 and 7 for steep power test. For the turnaround items, the TRAC code qualitatively predicts the difference among bundles, the difference which is the shorter turnaround time and the higher turnaround temperature in higher power bundle, although the overestimation for the turnaround items are also recognized for all bundles as those in the flat power test. For the quench items, the TRAC predictions almost agree with the measured results qualitatively and quantitatively. The TRAC code predicts qualitatively the variation along axial direction for the difference of quench time among different power bundles, the variation which is that the difference of quench time becomes smaller with propagating the quench front to the upper elevation. This result might support the remark that the TRAC code has a capability to predict the heat transfer enhancement in higher power bundles[9], and the enhancement is supposed to be caused by the higher liquid up-flow rate in higher power bundles as shown in Figs. 4.2.14(1) through 4.2.14(5). However since the void fraction was not predicted as discussed in section 4.2, the investigation of the mechanism of heat transfer enhancement would be the future subject after improving the one-dimensional thermal-hydraulic model in core.

4.4 Run Statistics

Total CPU time and time step size are plotted in Figs. 4.4.1 and 4.4.2 for flat and steep power tests, respectively. Time step size for both tests is reduced after the reflood initiation for each test. Time step size is not significantly affected by the difference of the radial power profile in core and however total CPU time divided by total transient time or by total time step number are higher in steep power test as shown in the following table. These two calculations were conducted on a FACOM M−780 computer.

Summary table for run statistics as follows:

Test name	Transi. time (s) RT	Total CPU time (s) CPU	Total time step num. ST	CPU/RT	CPU/ST (s)	RT/ST (s)
Flat power test	599.5	10630	31546	17.731	0.337	0.019
Steep power test	969.0	19280	52536	19.897	0.367	0.018

5. Conclusions

The predictive capability of TRAC-PF1/MOD1 code version 12.5 was assessed for the thermal-hydraulic behaviors including two-dimensional behaviors in the pressure vessel during reflood phase of a LBLOCA in a PWR. The assessments were performed by the measured results using SCTF at JAERI, the results which were obtained under the flat or the steep radial power distribution.

Main conclusions derived from this study are as follows:

(1) The TRAC code slightly overestimated the turnaround time and the turnaround temperature but the transients of the clad surface temperature were almost predicted especially for the quench front propagation. Radial distribution of the clad surface temperature caused by the different bundle power were also predicted well. Heat transfer in higher power bundles was predicted to be enhanced.

(2) The TRAC code predicted well the pressure transients in the pressure vessel and the steam mass flow rate generated in the core. However, the following defects were observed for the hydraulic behaviors in the pressure vessel:

   1) The axial and the radial distribution of void fraction in the core were not predicted qualitatively and quantitatively. The mechanism for the water accumulation was different between the prediction and the test. The prediction showed a peculiar axial and radial distributions of void fraction. The peculiar void distribution was caused by the interface sharpener model in the code.

   2) The TRAC code underestimated the liquid carry-over flow rate from the core to the upper plenum and from the upper plenum to the exit of the hot leg in the early period. On the other hand, the flow rate from the upper plenum to the exit of the hot leg was overestimated in the later period.

   3) The TRAC code predicted a flatter radial distribution of the liquid fraction in the upper plenum compared to the measured results.

The results related to the hydraulic behaviors suggest the necessity of the hydraulic model improvement especially for the void fraction in the core and in the upper plenum such as the interface sharpener model and the interface friction model. Since the heat transfer model is closely related to the local void fraction in the code, the core heat transfer model should be improved.

Since the predicted void fraction distribution is different from the measured results qualitatively, the predicted two-dimensional behavior may be strongly distorted by the

error in the evaluation of the void fraction. As the first approach, it is recommended to improve the hydraulic models related to the qualitative difference of the void fraction between the prediction and the data. After the elimination of the difference, another assessment of two-dimensional flow behavior should be performed including the cross flow model in the radial direction.

Acknowledgments

The authors wish to express their thanks to the members of the SCTF analysis group, Drs. H. Adachi, T. Iwamura and Y. Abe for valuable discussions.

References

(1) USNRC: Guidelines and Procedures for the International Code Assessment and Applications Program, NUREG-1271 (1987).

(2) Liles, D.R., et al.: TRAC-PF1/MOD1 ; An Advanced Best-Estimate Computer Program for Pressurized Water Reactor Thermal-Hydraulic Analysis, NUREG/CR-3858 (1986).

(3) Taylor, D.D., et al.: TRAC-BD1/MOD1 ; An Advanced Best-Estimate Computer Program for Boiling Water Reactor Transient Analysis, NUREG/CR-3633 (1984).

(4) Ransom, V., et al.: RELAP5/MOD2 Code Manual, NUREG/CR-4312 (1985).

(5) Kikuta, M., et al.: Assessment of TRAC-PF1/MOD1 Code for Cylindrical Core Test Facility Base Case Test C2-4, To be published as JAERI-M report.

(6) Akimoto, H., et al.: Assessment of TRAC-PF1/MOD1 Code for Core Thermal Hydraulic Behavior during Reflood with CCTF and SCTF Data, JAERI-M 93-032 (1993).

(7) Murao, Y., et al.: Experimental Study of System Behavior during Reflood Phase of PWR-LOCA using CCTF, J. Nucl. Sci. Technol., 19(9) 705-719 (1982).

(8) Adachi, H., et al.: Design of Slab Core Test Facility (SCTF) in Large Scale Reflood Test Program, Part 1 : Core-1, JAERI-M 83-080 (1983).

(9) Iwamura, T., et al.: Two-Dimensional Thermal-Hydraulic Behavior in core in SCTF Core-II Cold Leg Injection Tests (Radial Power Profile Test Results), JAERI-M 85-106 (1985).

(10) Ohnuki, A., et al.: Study on ECC Injection Modes in Reflood Tests with SCTF Core II − Comparison between Gravity and Forced Feeds −, JAERI-M 91-001 (1991).

error in the evaluation of the void fraction. As the first approach, it is recommended to improve the hydraulic models related to the qualitative difference of the void fraction between the prediction and the data. After the elimination of the difference, another assessment of two-dimensional flow behavior should be performed including the cross flow model in the radial direction.

Acknowledgments

The authors wish to express their thanks to the members of the SCTF analysis group, Drs. H. Adachi, T. Iwamura and Y. Abe for valuable discussions.

References

(1) USNRC: Guidelines and Procedures for the International Code Assessment and Applications Program, NUREG-1271 (1987).

(2) Liles, D.R., et al.: TRAC-PF1/MOD1 ; An Advanced Best-Estimate Computer Program for Pressurized Water Reactor Thermal-Hydraulic Analysis, NUREG/CR-3858 (1986).

(3) Taylor, D.D., et al.: TRAC-BD1/MOD1 ; An Advanced Best-Estimate Computer Program for Boiling Water Reactor Transient Analysis, NUREG/CR-3633 (1984).

(4) Ransom, V., et al.: RELAP5/MOD2 Code Manual, NUREG/CR-4312 (1985).

(5) Kikuta, M., et al.: Assessment of TRAC-PF1/MOD1 Code for Cylindrical Core Test Facility Base Case Test C2-4, To be published as JAERI-M report.

(6) Akimoto, H., et al.: Assessment of TRAC-PF1/MOD1 Code for Core Thermal Hydraulic Behavior during Reflood with CCTF and SCTF Data, JAERI-M 93-032 (1993).

(7) Murao, Y., et al.: Experimental Study of System Behavior during Reflood Phase of PWR-LOCA using CCTF, J. Nucl. Sci. Technol., 19(9) 705-719 (1982).

(8) Adachi, H., et al.: Design of Slab Core Test Facility (SCTF) in Large Scale Reflood Test Program, Part 1 : Core-1, JAERI-M 83-080 (1983).

(9) Iwamura, T., et al.: Two-Dimensional Thermal-Hydraulic Behavior in core in SCTF Core-II Cold Leg Injection Tests (Radial Power Profile Test Results), JAERI-M 85-106 (1985).

(10) Ohnuki, A., et al.: Study on ECC Injection Modes in Reflood Tests with SCTF Core II - Comparison between Gravity and Forced Feeds -, JAERI-M 91-001 (1991).

error in the evaluation of the void fraction. As the first approach, it is recommended to improve the hydraulic models related to the qualitative difference of the void fraction between the prediction and the data. After the elimination of the difference, another assessment of two-dimensional flow behavior should be performed including the cross flow model in the radial direction.

Acknowledgments

The authors wish to express their thanks to the members of the SCTF analysis group, Drs. H. Adachi, T. Iwamura and Y. Abe for valuable discussions.

References

(1) USNRC: Guidelines and Procedures for the International Code Assessment and Applications Program, NUREG-1271 (1987).

(2) Liles, D.R., et al.: TRAC-PF1/MOD1 ; An Advanced Best-Estimate Computer Program for Pressurized Water Reactor Thermal-Hydraulic Analysis, NUREG/CR-3858 (1986).

(3) Taylor, D.D., et al.: TRAC-BD1/MOD1 ; An Advanced Best-Estimate Computer Program for Boiling Water Reactor Transient Analysis, NUREG/CR-3633 (1984).

(4) Ransom, V., et al.: RELAP5/MOD2 Code Manual, NUREG/CR-4312 (1985).

(5) Kikuta, M., et al.: Assessment of TRAC-PF1/MOD1 Code for Cylindrical Core Test Facility Base Case Test C2-4, To be published as JAERI-M report.

(6) Akimoto, H., et al.: Assessment of TRAC-PF1/MOD1 Code for Core Thermal Hydraulic Behavior during Reflood with CCTF and SCTF Data, JAERI-M 93-032 (1993).

(7) Murao, Y., et al.: Experimental Study of System Behavior during Reflood Phase of PWR-LOCA using CCTF, J. Nucl. Sci. Technol., 19(9) 705-719 (1982).

(8) Adachi, H., et al.: Design of Slab Core Test Facility (SCTF) in Large Scale Reflood Test Program, Part 1 : Core-1, JAERI-M 83-080 (1983).

(9) Iwamura, T., et al.: Two-Dimensional Thermal-Hydraulic Behavior in core in SCTF Core-II Cold Leg Injection Tests (Radial Power Profile Test Results), JAERI-M 85-106 (1985).

(10) Ohnuki, A., et al.: Study on ECC Injection Modes in Reflood Tests with SCTF Core II - Comparison between Gravity and Forced Feeds -, JAERI-M 91-001 (1991).

Table 1 ICAP assessment matrix - Japan

	LOCA type	TRAC-P				RELAP5				TRAC-B				
		88	89	90	91	88	89	90	91	88	89	90	91	
CCTF	PWR LB	9	1				5				5			Reflood
SCTF	PWR LB	3	5	3			1				1			Reflood
ROSA-Ⅱ	PWR LB								2					Blowdown
ROSA-Ⅲ	BWR LB/SB										1	1		Blowdown
ROSA-Ⅳ	PWR SB	1	1(0)			1	0(1)							
TBL	BWR LB/SB										1	1		Blowdown
Total		13	7(6)	3		1	6(7)		2		8	2		42

Table 2.1.1 Principal dimensions of SCTF core-II

1. Core Dimension			
(1)	Quantity of Bundle	8 Bundles	
(2)	Bundle Array	1 x 8	
(3)	Bundle Pitch	230 mm	
(4)	Rod Array in a Bundle	16x16	
(5)	Rod Pitch in a Bundle	14.3 mm	
(6)	Quantity of Heater Rod in a Bundle	234 rods	
(7)	Quantity of Non-Heated Rod in a Bundle	22 rods	
(8)	Total Quantity of Heater Rods	234x8=1872	rods
(9)	Total Quantity of Non-Heated Rods	22x8 =176	rods
(10)	Effective Heated Length of Heater Rod	3660 mm	
(11)	Diameter of Heater Rod	10.7 mm	
(12)	Diameter of Non-Heated Rod	13.8 mm	
2. Flow Area & Fluid Volume			
(1)	Core Flow Area	0.259 m^2	
(2)	Core Fluid Volume	0.92 m^3	
(3)	Baffle Region Flow Area	0.10 m^2	
(4)	Baffle Region Fluid Volume (nominal)	0.36 m^3	
(5)	Effective Core Area Based on the Measured Level-Volume Relationship Including Gap between Core Barrel and Pressure Vessel Wall and Various Penetration Holes	0.32 ~ 0.35 m^2	
(6)	Downcomer Flow Area	0.121 m^2	
(7)	Upper Annulus Flow Area	0.158 m^2	
(8)	Upper Plenum Horizontal Flow Area	0.525 m^2	
(9)	Upper Plenum Fluid Volume	1.16 m^3	
(10)	Upper Head Fluid Volume	0.86 m^3	
(11)	Lower Plenum Fluid Volume	1.305 m^3	
(12)	Steam Generator Inlet Plenum Simulator Flow Area	0.626 m^2	
(13)	Steam Generator Inlet Plenum Simulator Fluid Volume	0.931 m^3	
(14)	Steam Water Separator Fluid Volume	5.3 m^3	

Table 2.1.1 (Continued)

(15)	Flow Area at the Top Plate of Steam Generator Inlet Plenum Simulator	0.195	m^2
(16)	Hot Leg Flow Area	0.0826	m^2
(17)	Intact Cold Leg Flow Area (Diameter=297.9 mm)	0.0697	m^2
(18)	Broken Cold Leg Flow Area (Diameter=151.0 mm)	0.0179	m^2
(19)	Containment Tank−I Fluid Volume	30	m^3
(20)	Containment Tank−II Fluid Volume	50	m^3

3. Elevation & Height

(1)	Top Surface of Upper Core Support Plate (UCSP)	0	mm
(2)	Bottom Surface of UCSP	− 76	mm
(3)	Top of the Effective Heated Length of Heated Rod	− 393	mm
(4)	Bottom of the Skirt in the Lower Plenum	−5270	mm
(5)	Bottom of Intact Cold Leg	+ 724	mm
(6)	Bottom of Hot Leg	+1050	mm
(7)	Top of Upper Plenum	+2200	mm
(8)	Bottom of Steam Generator Inlet Plenum Simulator	+1933	mm
(9)	Centerline of Loop Seal Bottom	−2281	mm
(10)	Bottom Surface of End Box	−185.1	mm
(11)	Top of Upper Annulus of Downcomer	+2234	mm
(12)	Height of Steam Generator Inlet Plenum Simulator	1595	mm
(13)	Height of Loop Seal	3140	mm
(14)	Inner Height of Hot Leg Pipe	737	mm
(15)	Bottom of Lower Plenum	−5770	mm
(16)	Top of Upper Head	+2887	mm

Table 2.1.2 Comparison of dimensions between SCTF and the reference PWR

Item	SCTF	PWR	Ratio (SCTF/PWR)
Quantity of Bundle	8	193	1/24.1
Number of Heater Rod	1872	39372	1/21.0
Number of Rods	2048	43425	1/21.2
Effective Length of Heater Rod (mm)	3660	3660	1/1
Rod Pitch (mm)	14.30	14.30	1/1
Diameter of Heater Rod (mm)	10.70	10.72	1/1
Diameter of Unheated Rod (mm)	13.80	13.87	1/1
Flow Area between Core Walls (m^2)	0.259	4.76	1/17.7
Effective Core Area Based on the Measured Level-Volume Relationship (m^2)	0.32～0.35	4.76	1/13.6
Fluid Volume of Core Enveloped by Honeycomb Insulators*	0.92	17.95	1/19.5
Fluid Volume of Lower Plenum (m^3)	1.305	29.62	1/22.7
Fluid Volume of Upper Head (m^3)	0.86	19.8	1/23.0
Baffle Region Flow Area (m^2)	0.10	1.76	1/17.6
Upper Plenum Fluid Volume (m^3)	1.16	23.8	1/20.5
Downcomer Flow Area (m^2)	0.121	2.47	1/20.4
UCSP Thickness (m)	76	76	1/1
Steam Generator Inlet Plenum Simulator Volume (m^3)	0.931	4.25x4	1/18.3
Height of Steam Generator Inlet Plenum Simulator (m)	1.591	1.595	1/1
Flow Area at the Top Plate of Steam Generator Inlet Plenum Simulator (m^2)	0.19	4.0	1/21.2
Major Axis Length of Hot Leg Cross Section (mm)	737	736	1/1
Flow Area of hot Leg (m^2) (4 Loops)	0.0826	1.704	1/20.6
Flow Area of Intact Loop (m^2) (3 Loops)	0.0696	1.149	1/16.5

Table 2.1.2 (Continued)

Flow Area of Broken Cold Leg (m^2)	0.0179	0.383	1/21.4
* Fluid Volume of Core Including Gaps between Core Barrel and Pressure Vessel Wall (m^3)	1.74		

Table 2.2.1 Test conditions for flat power test S2-14

	Specified Conditions	Measured Conditions
Initial Pressure (Core Center)	0.20 MPa	0.20 MPa
Pressure (Containment-II)	0.20 MPa	0.22 MPa (Max.)
Max. Core Temp. (at reflood initiation)	922 K	940.7 K
Power Holding after Acc Initiation	0 s	0 s
Decay Curve	(ANS+Actinides)x1.02 from 40 sec (Reac. time)	see Fig. 3.2.3
Max. Ecc Injection Rate	26.1 kg/s	see Fig. 3.2.1
Injection rate in LPCI Period	4.8 kg/s	see Fig. 3.2.1
Max. Core Inlet Subcooling	not specified	16 K
Ecc Water Temperature in Acc Period	368 K	see Fig. 3.2.1
Ecc Water Temperature in LPCI Period	393 K	see Fig. 3.2.1
Set Value of Maximum Liquid Level above UCSP	0.13 m	see Fig. 4.1.8

Table 2.2.2 Test conditions for steep power test S2-16

	Specified Conditions	Measured Conditions
Initial Pressure (Core Center)	0.20 MPa	0.20 MPa
Pressure (Containment-II)	0.20 MPa	0.22 MPa (Max)
Max. Core Temp. (at reflood initiation)	1160 K	1158 K
Power Holding after ECC Initiation	40 sec (nominal)	40 s
Decay Curve	(ANS+Actinides)x1.02 from 40 sec (Reac. Time)	see Fig. 3.2.4
Max. Injection Rate	12.3 kg/s	see Fig. 3.2.2
Injection Rate in LPCI Period	5.06 kg/s	see Fig. 3.2.2
Max. Core Inlet Subcooling	not specified	19 K
ECC Water Temperature in Acc Period	363 K	see Fig. 3.2.2
ECC Water Temperature in LPCI Period	393 K	see Fig. 3.2.2

Table 2.2.3 Chronology of major events for flat power test S2-14

	TIME AFTER CORE POWER "ON"	TIME AFTER REFLOOD INITIATION
Core Power "ON"	0 sec	−114 sec
Ecc Injection Initiation	111	−3
Core Power Decay Initiation	111	−3
Reflood initiation	114	0
Maximum Core Temperature (965 K)	124	10
Maximum Containment−II Pressure (0.22 MPa)	137	23
Maximum Core Pressure (0.266 MPa)	142	28
Initiation Time for Controlling the Liquid Level above UCSP	191	77
Whole Core Quenched	482	368
Stop Time for Controlling the Liquid Level above UCSP	491	377

Table 2.2.4 Chronology of major events for steep power test S2-16

	TIME AFTER CORE POWER "ON"	TIME AFTER REFLOOD INITIATION
Core Power "ON"	0 sec	−149 sec
Ecc Injection Initiation	148	−1
Reflood Initiation	149	0
Maximum Containment−II Pressure (0.22 MPa)	175	26
Core Power Decay Initiation	188	39
Maximum Core Temperature (1224 K)	192	43
Maximum Core Pressure (0.273 MPa)	202	53
Whole Core Quenched	642	493

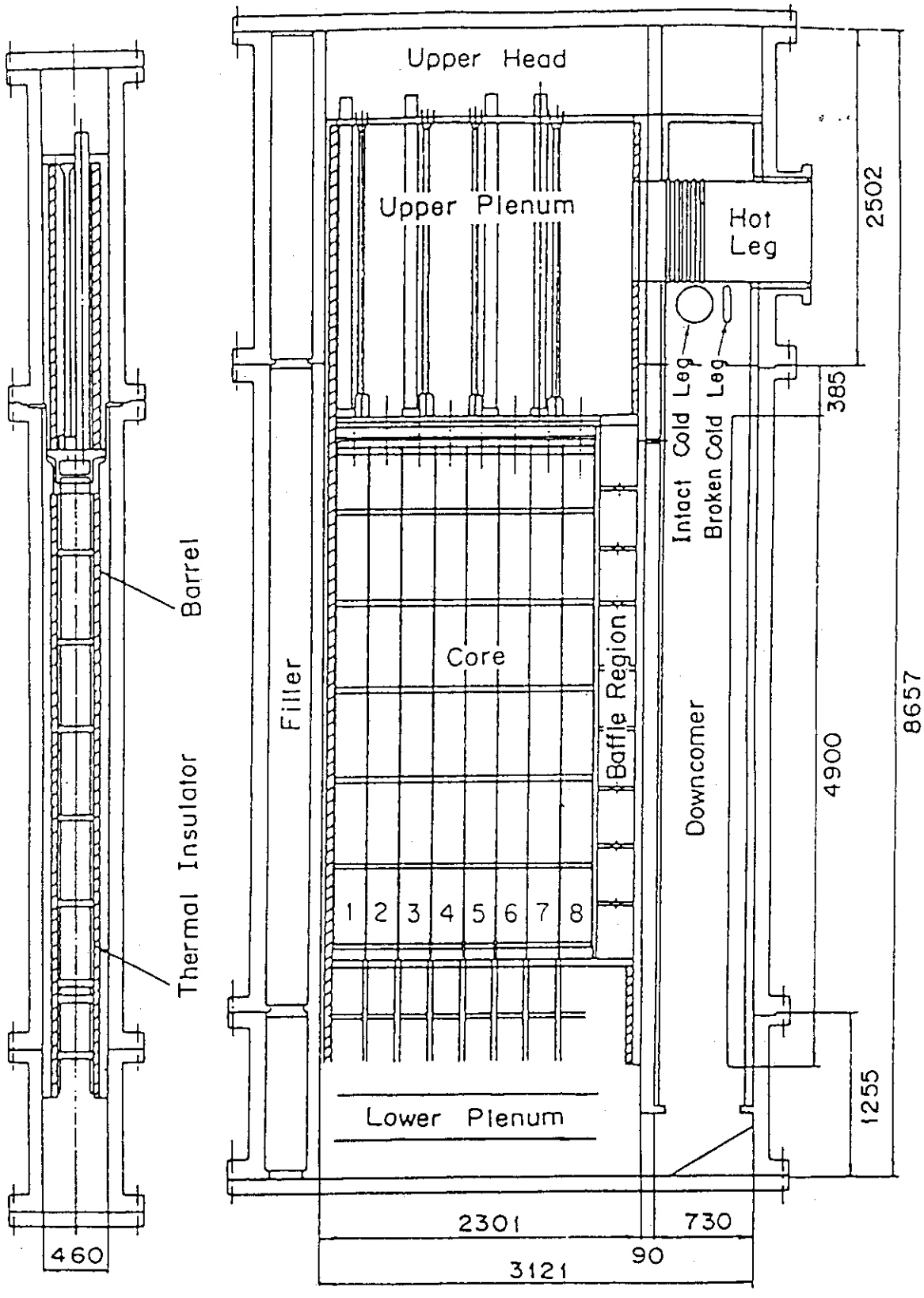

Fig. 2.1.1 Vertical cross sections of pressure vessel

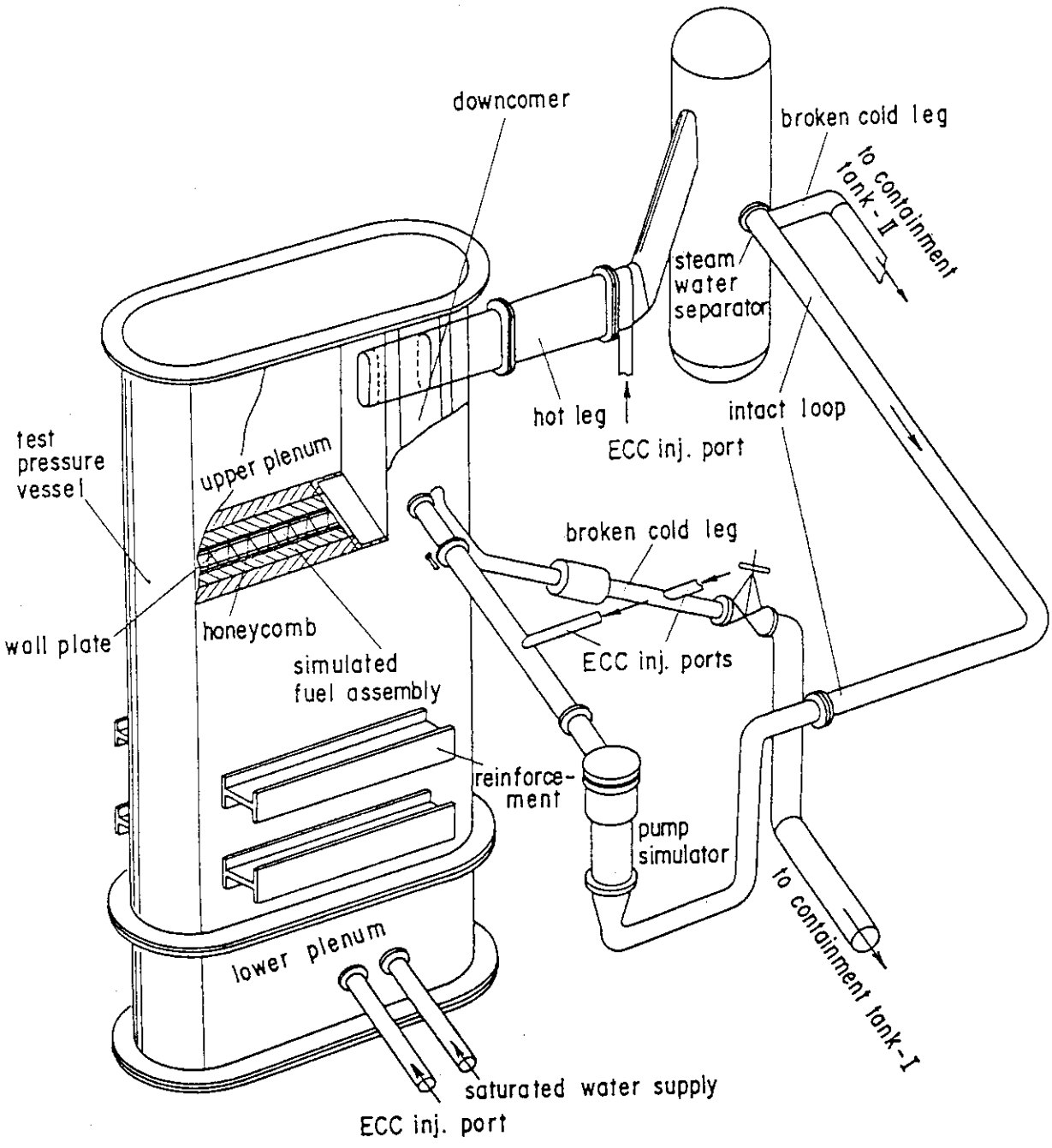

Fig.2.1.2 Bird's-eye view of SCTF

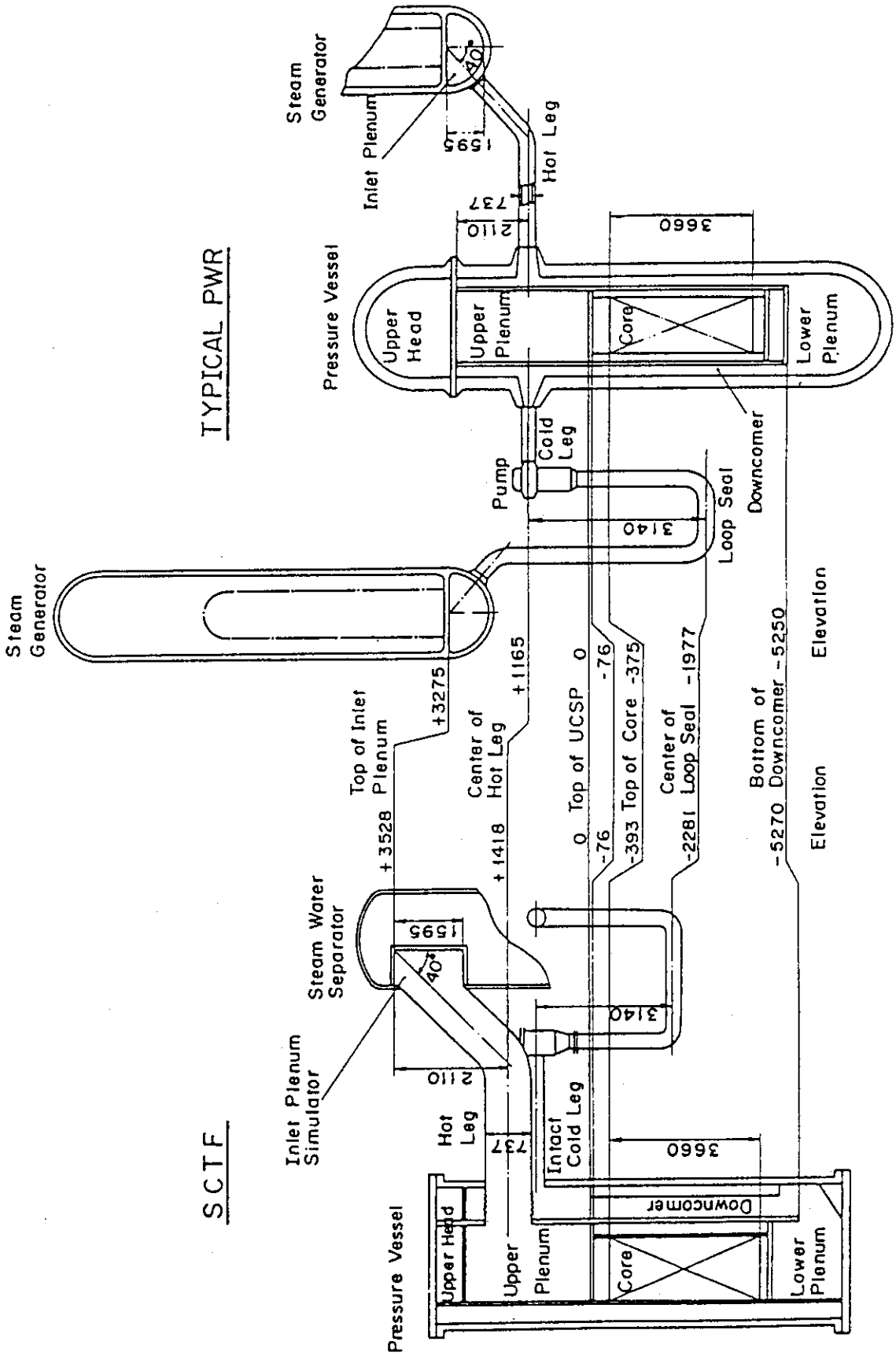

Fig.2.1.3 Comparison of dimensions between SCTF and the reference PWR

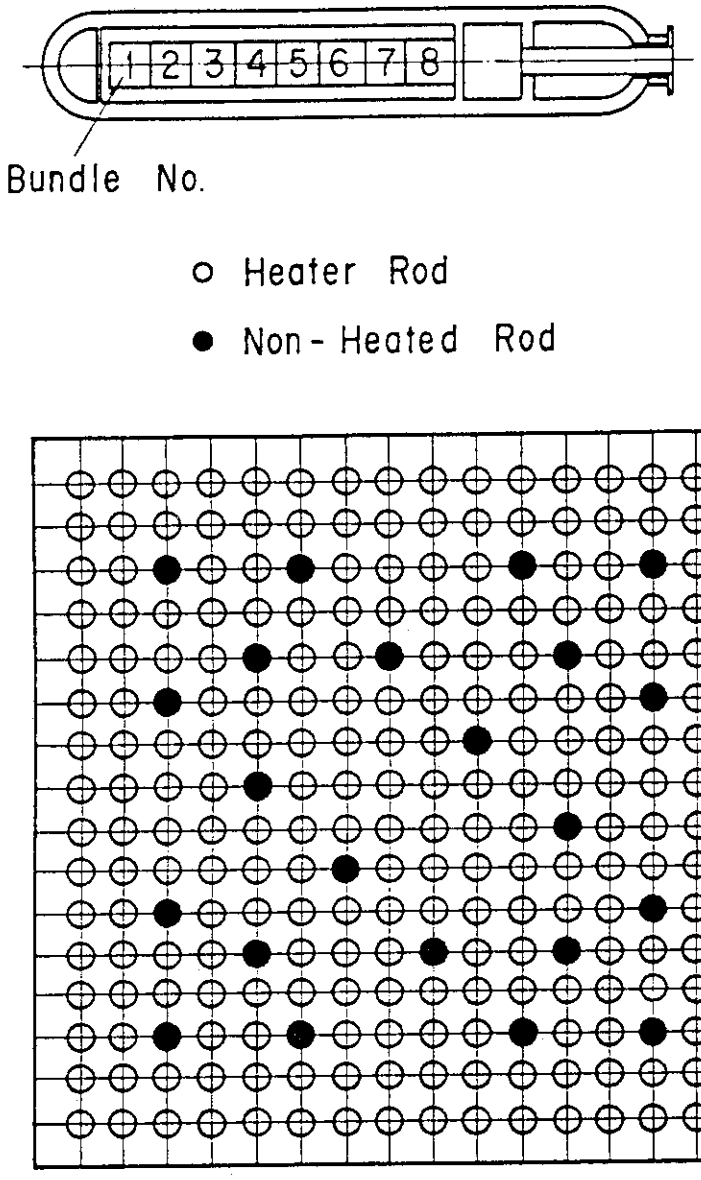

Fig.2.1.4 Arrangement of rod bundles

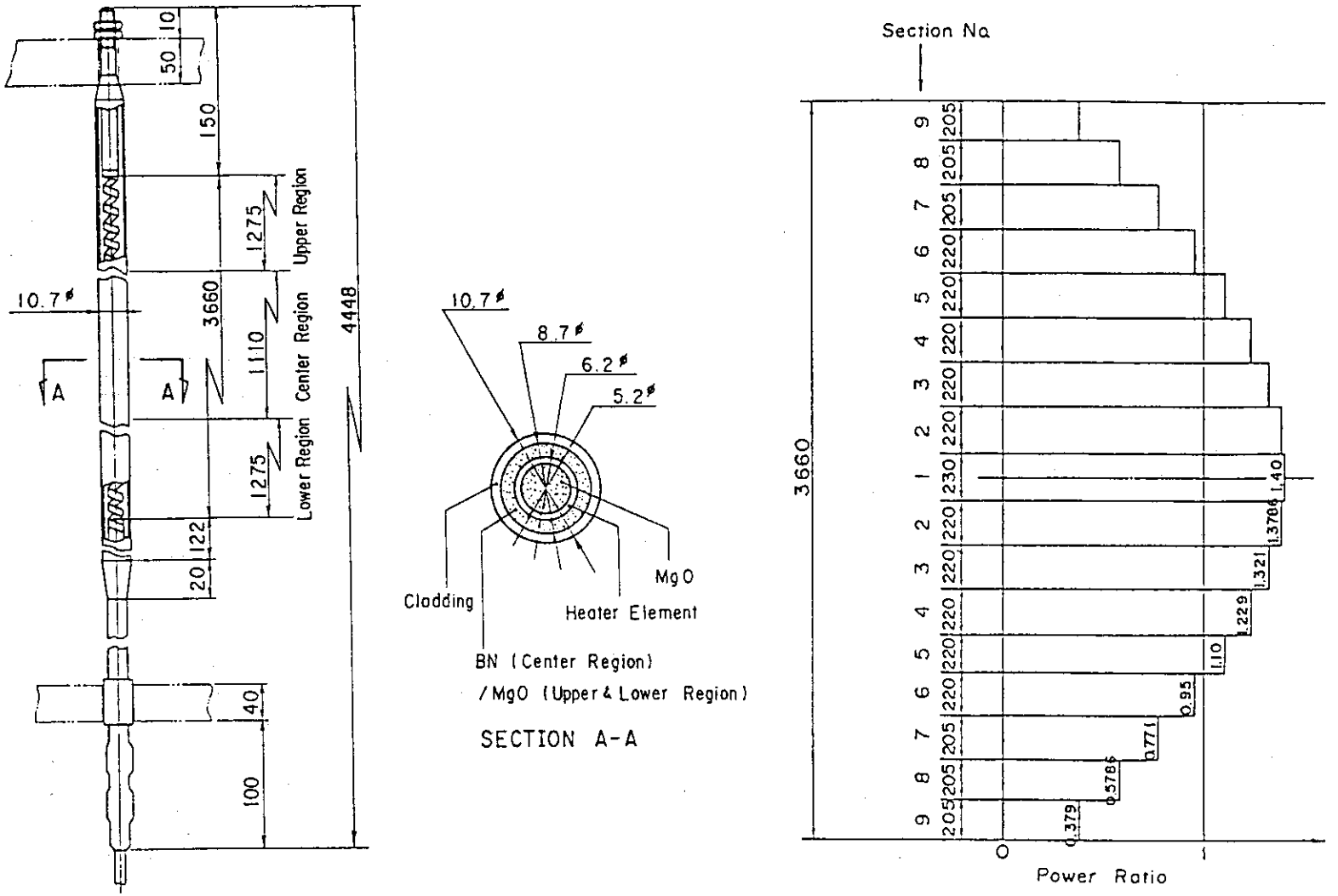

Fig. 2.1.5 Dimension, configuration and axial power distribution of heater rods

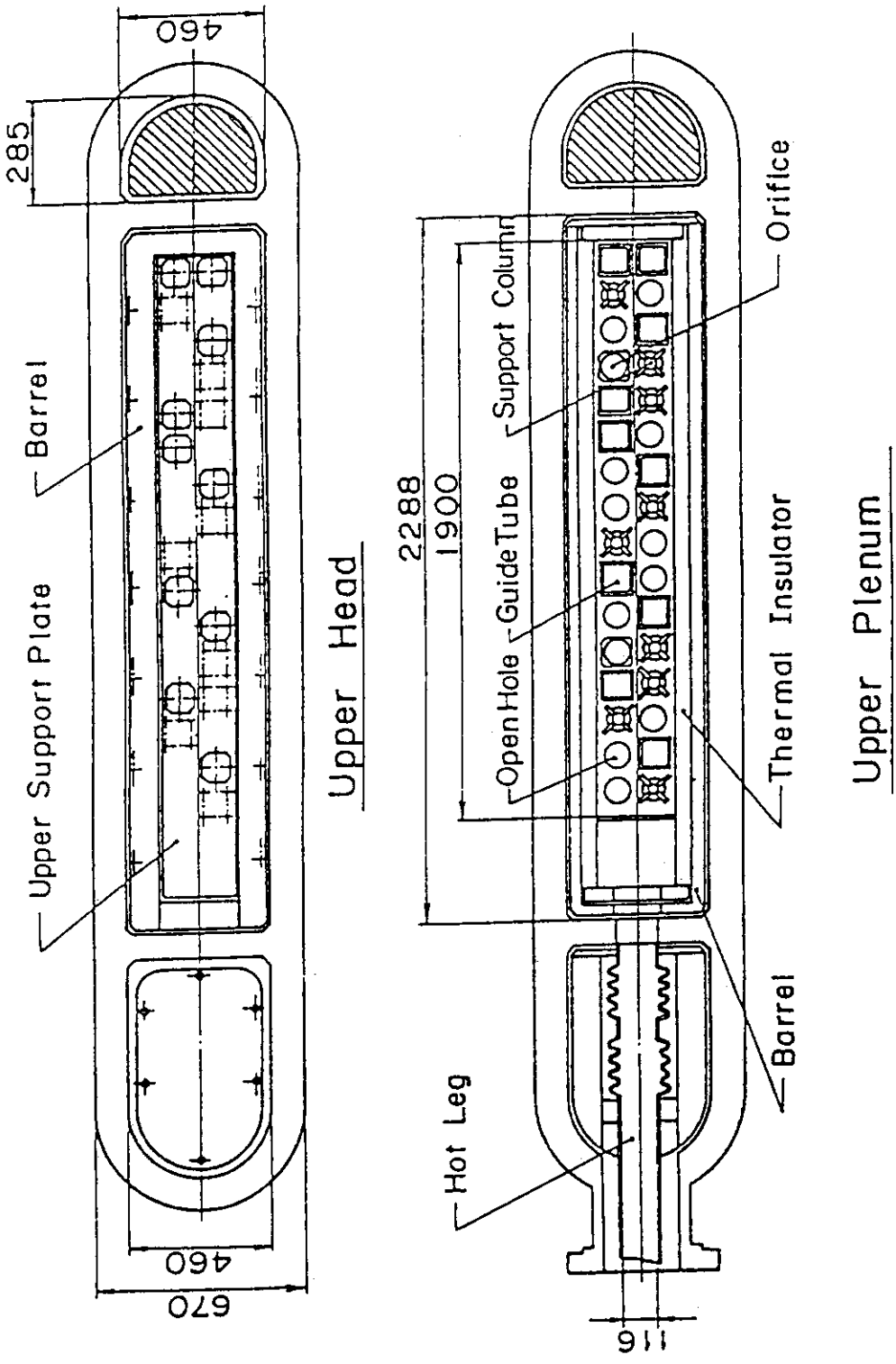

Fig.2.1.6 Horizontal cross sections in upper head and in upper plenum

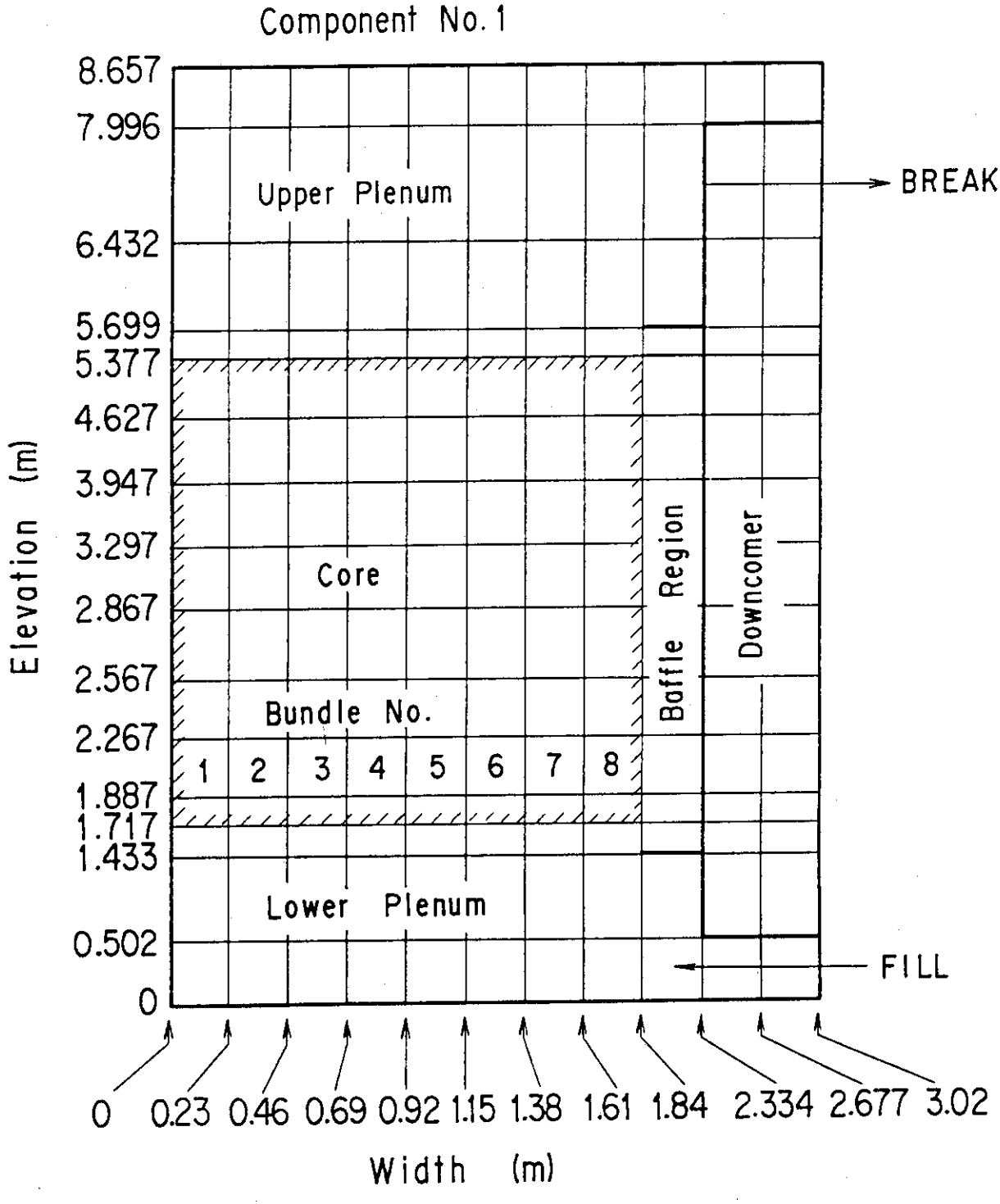

Fig.3.1.1 Noding model for SCTF pressure vessel

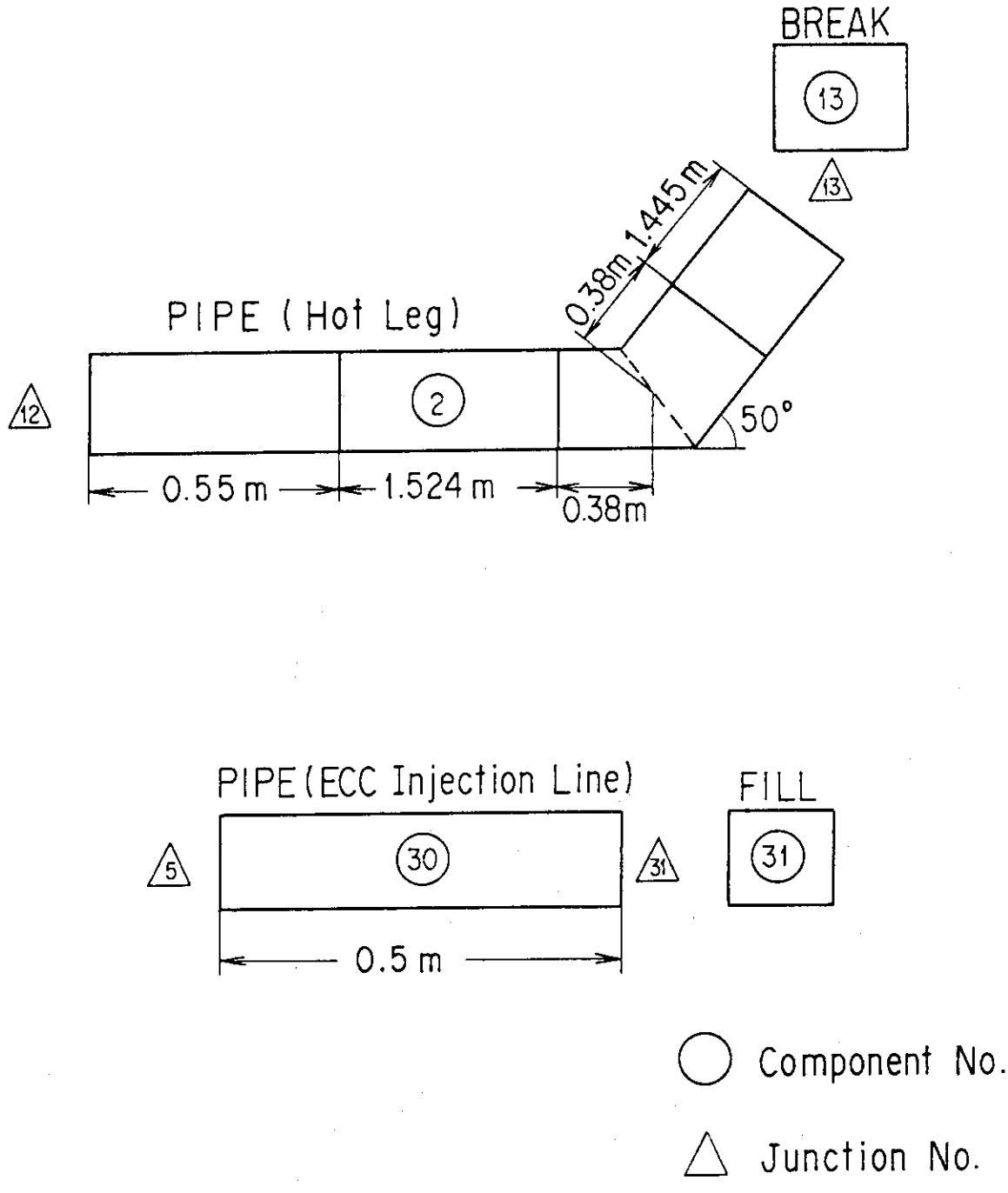

Fig.3.1.2 Noding model for hot leg and for ECC injection line

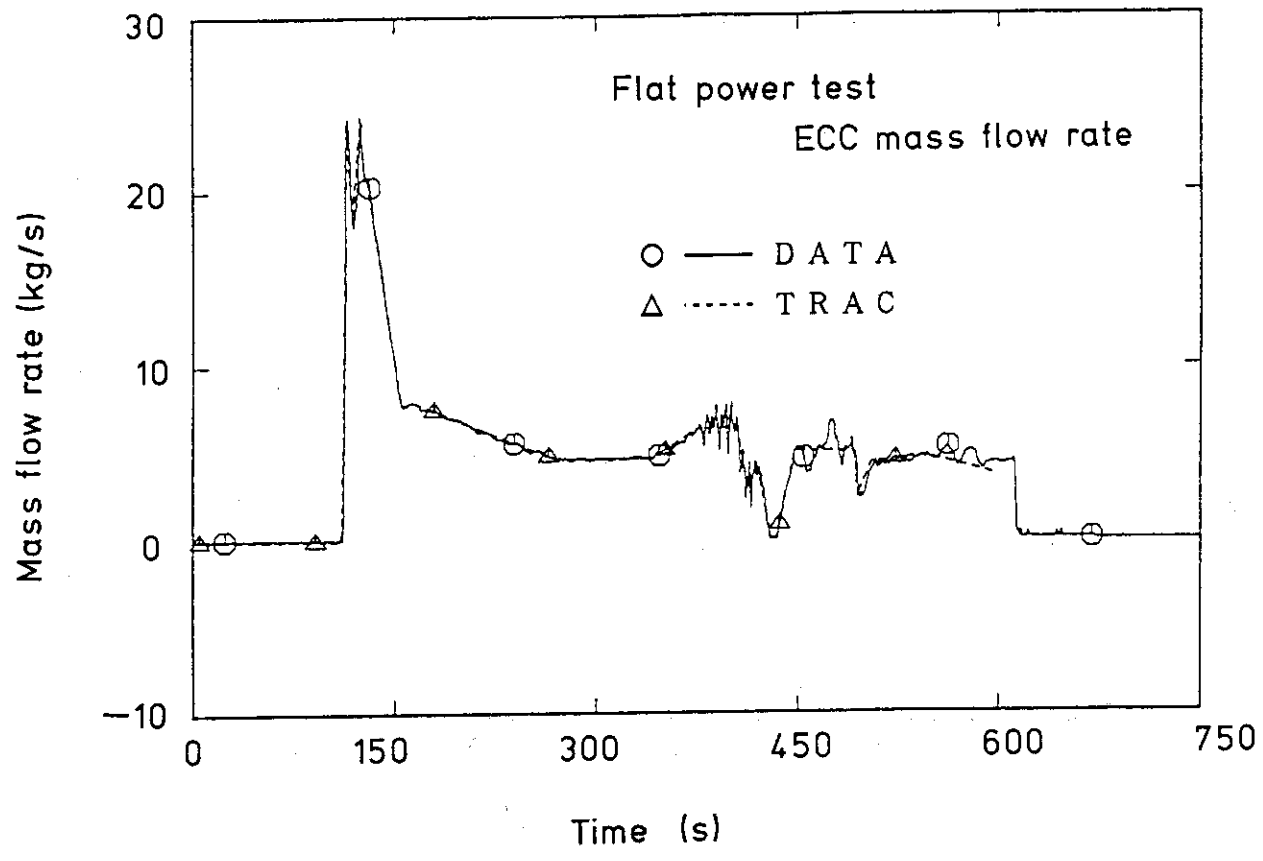

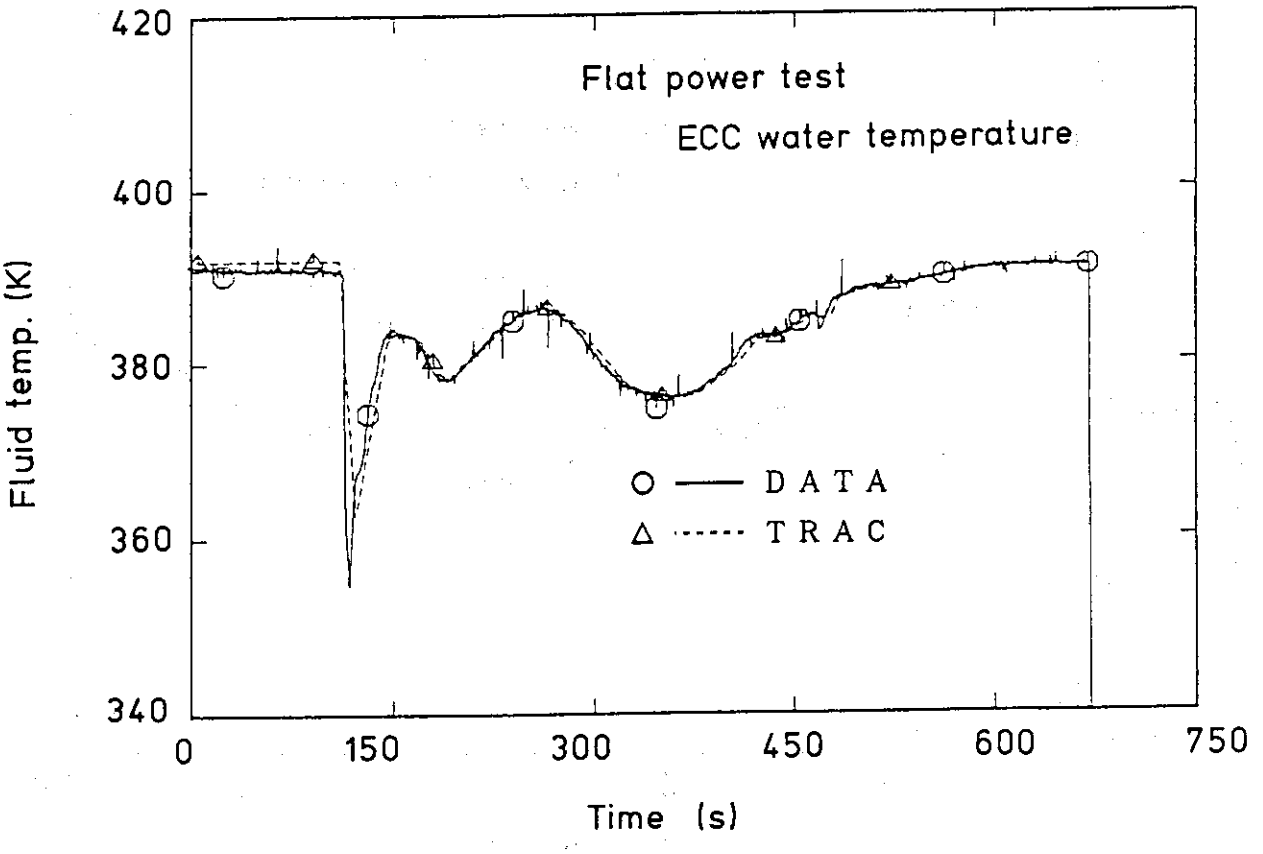

Fig.3.2.1 Comparison of ECC mass flow rate and ECC water temperature for flat power test S2-14

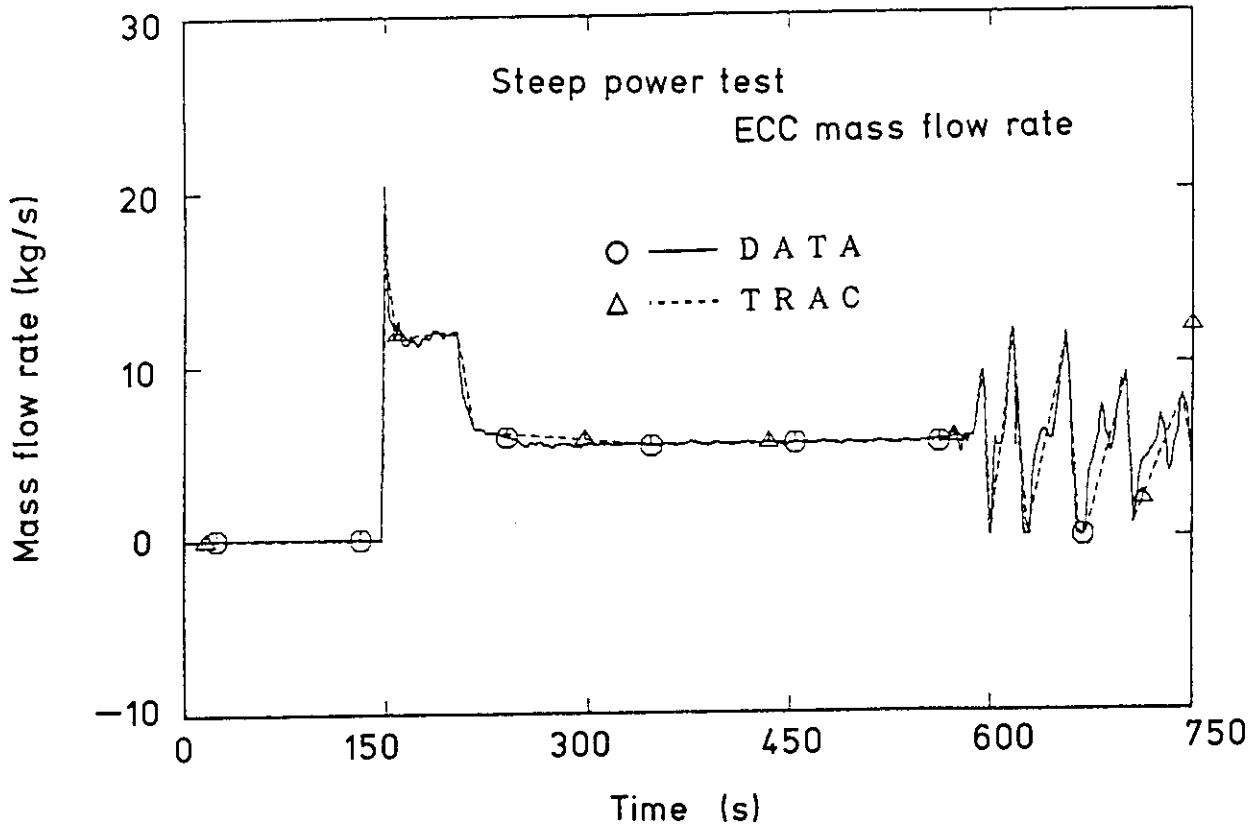

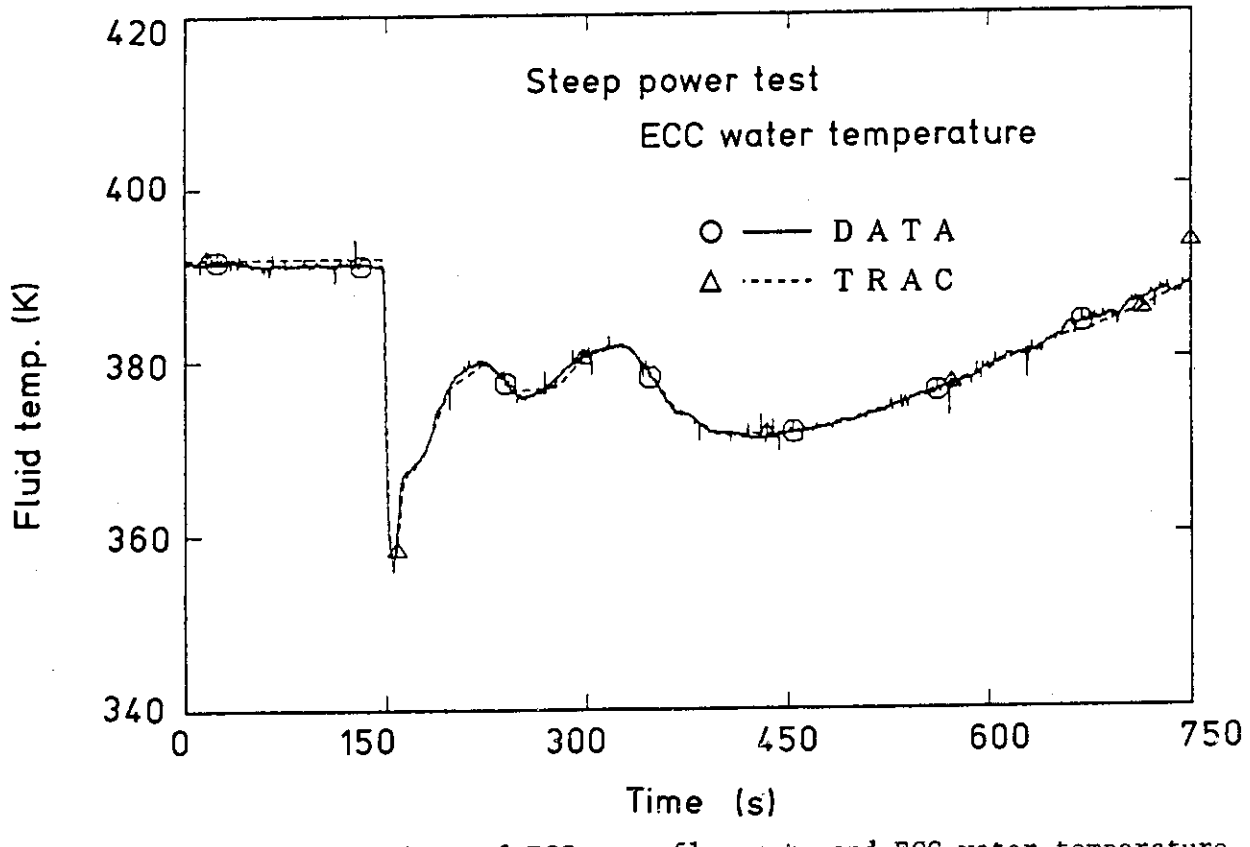

Fig.3.2.2 Comparison of ECC mass flow rate and ECC water temperature for steep power test S2-16

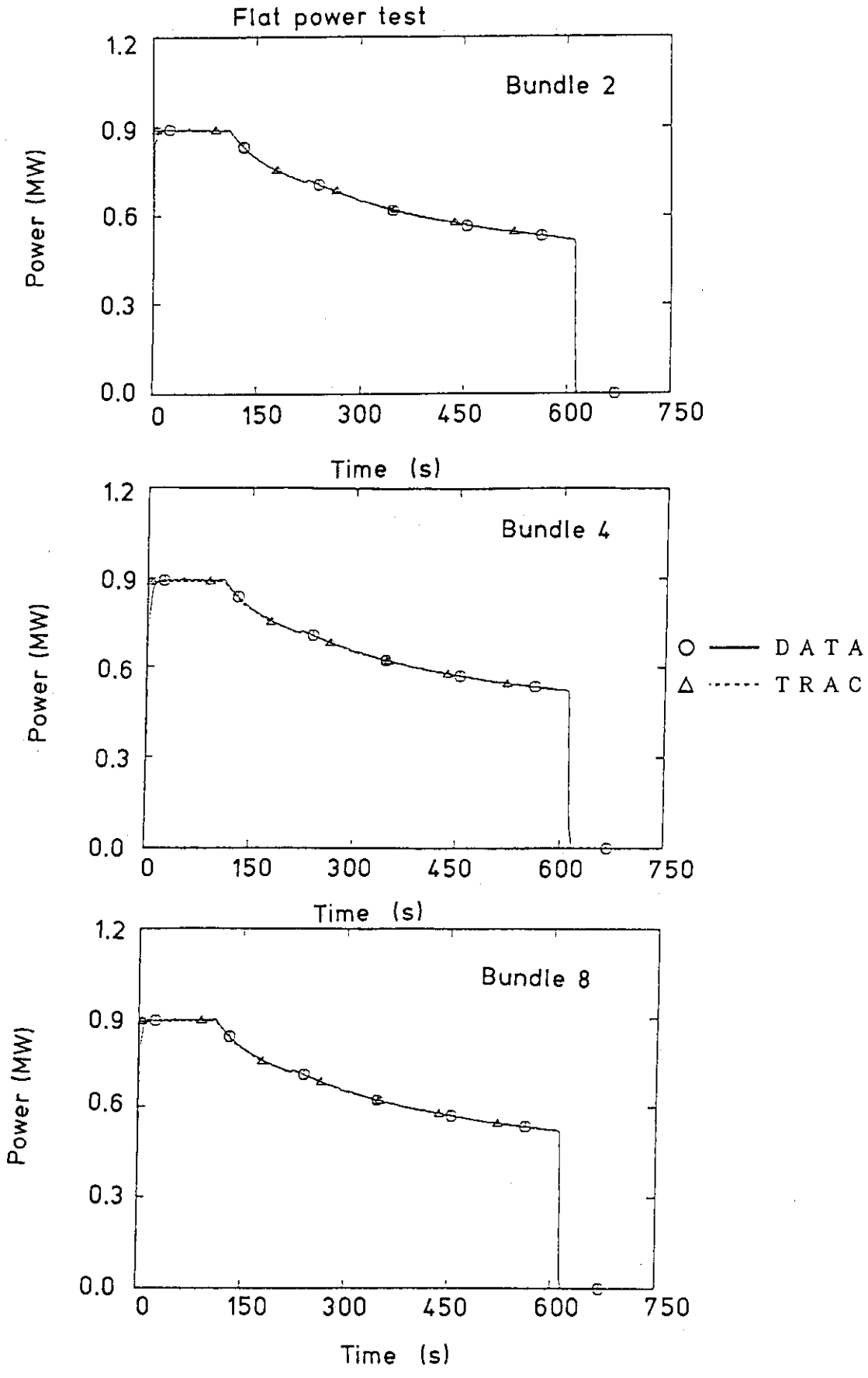

Fig.3.2.3 Comparison of core power for flat power test S2-14

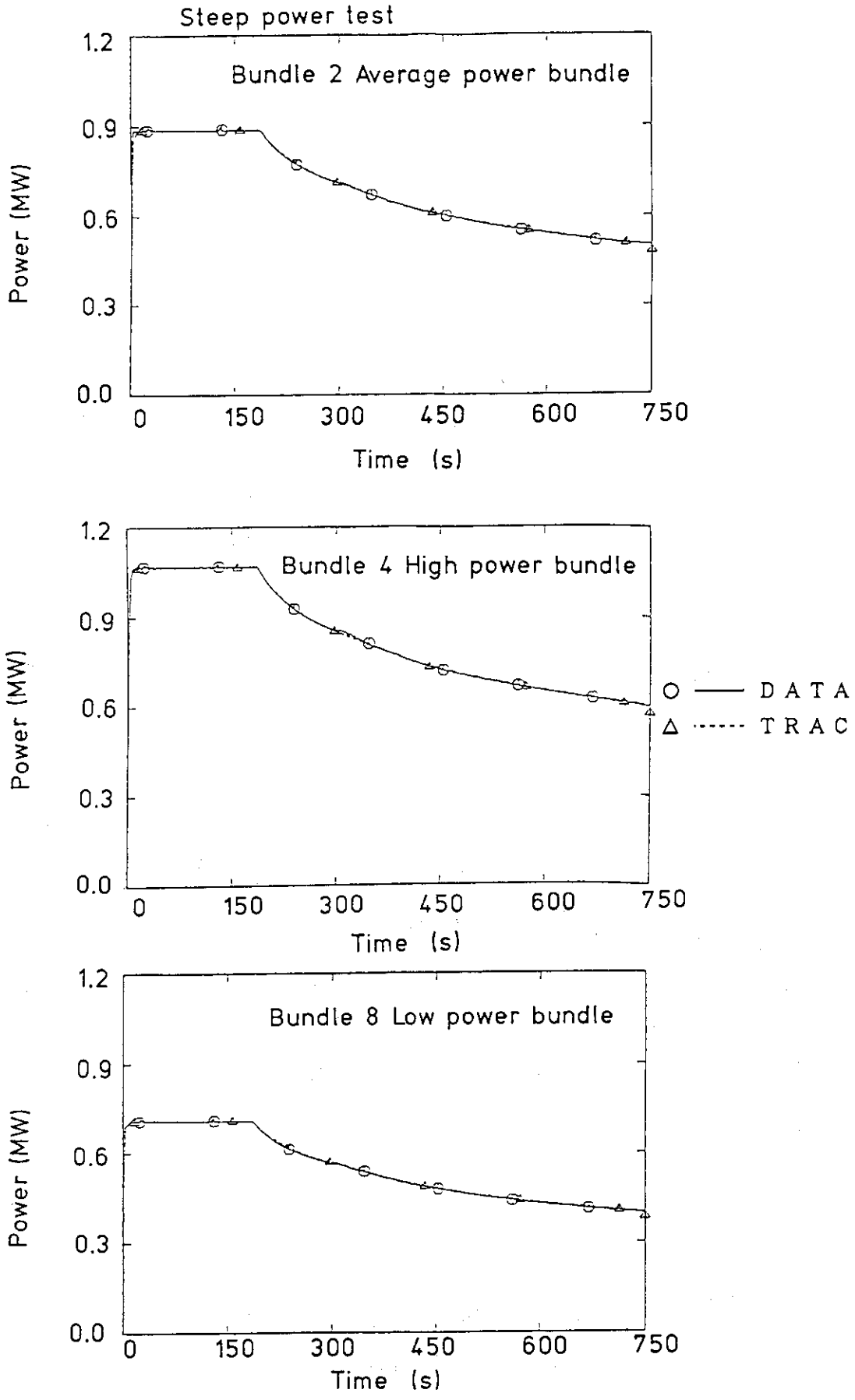

Fig.3.2.4 Comparison of core power for steep power test S2-16

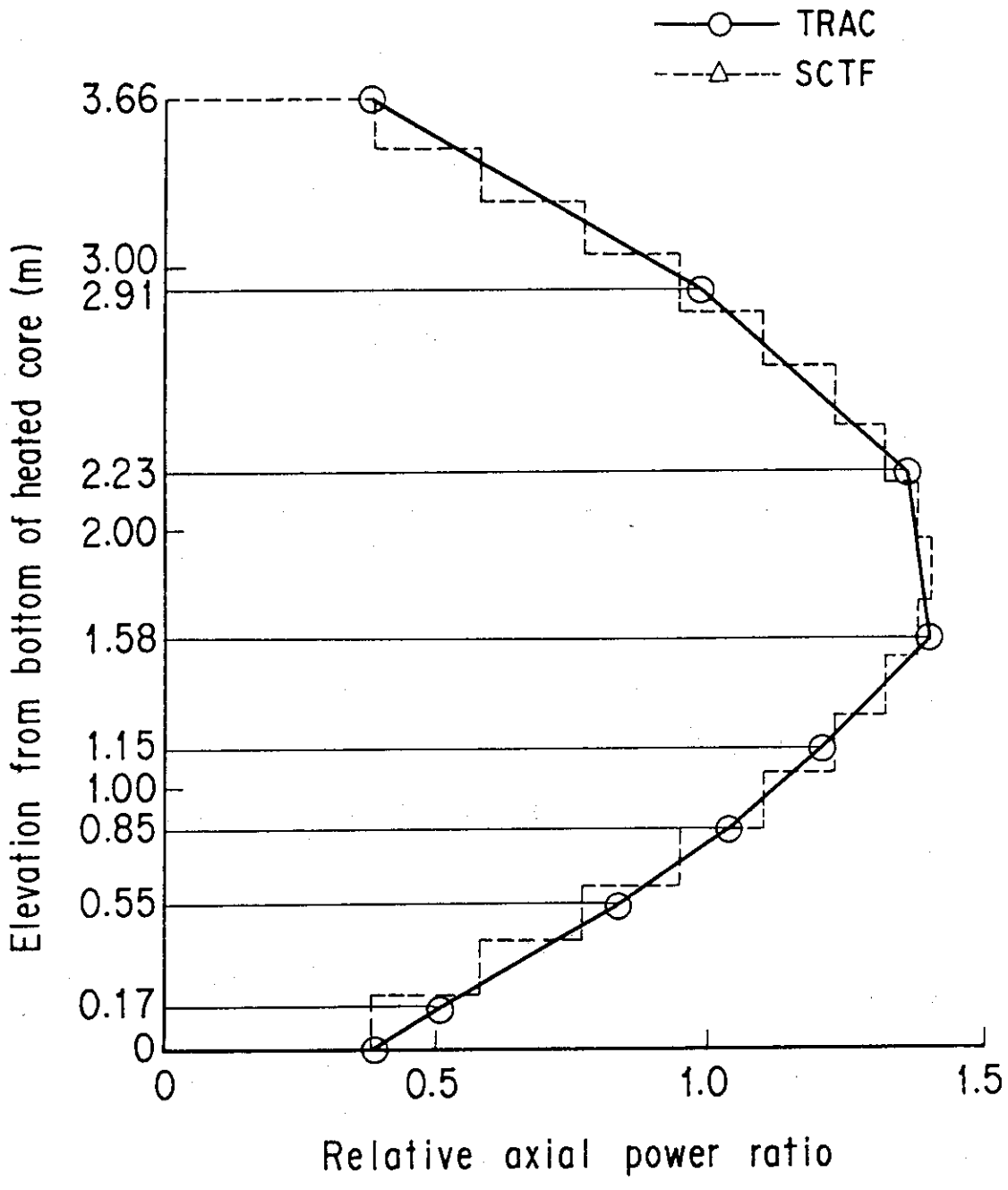

Fig.3.2.5 Comparison of relative axial power ratio for both tests

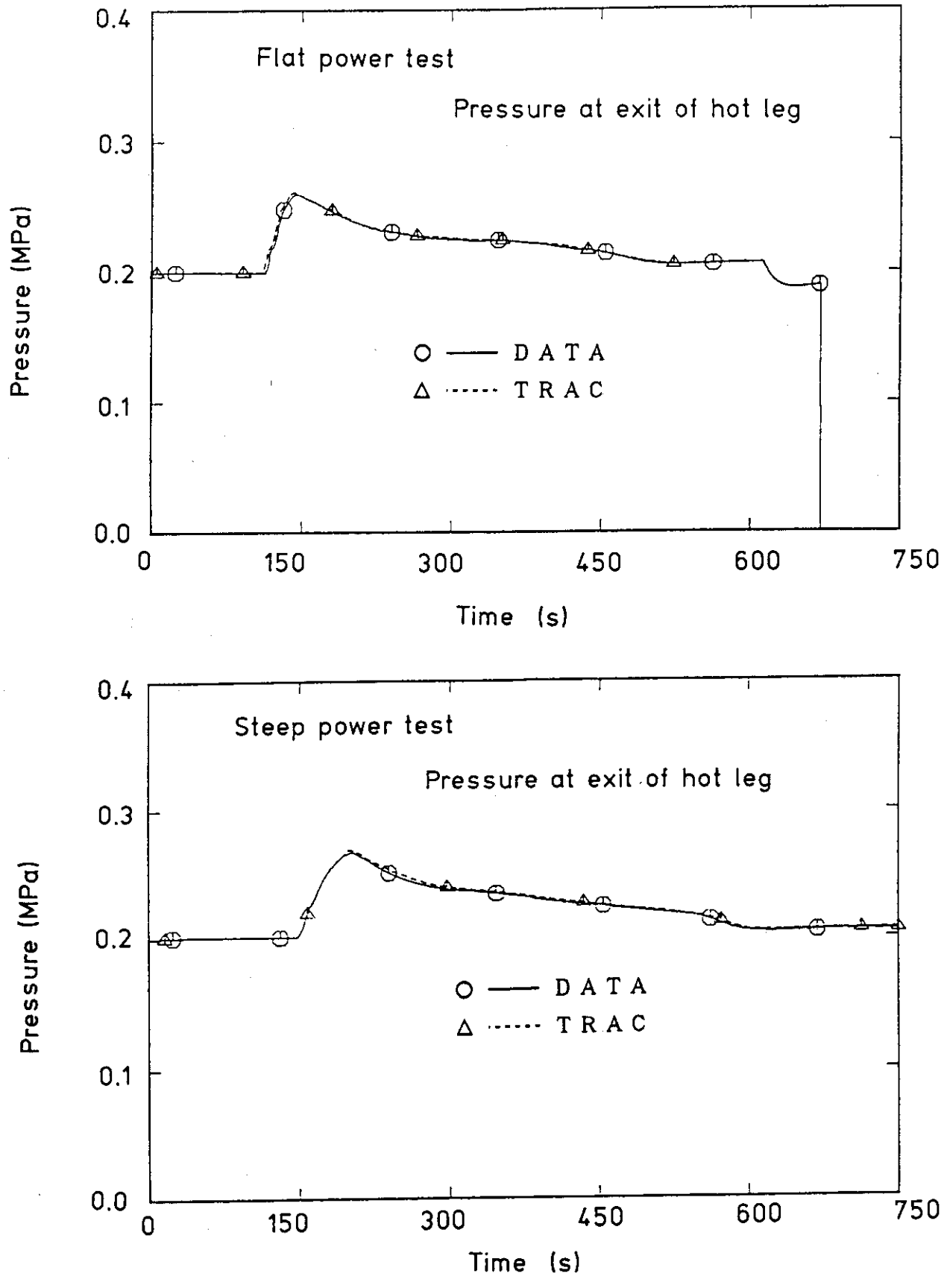

Fig.3.2.6 Comparison of pressure at exit of hot leg

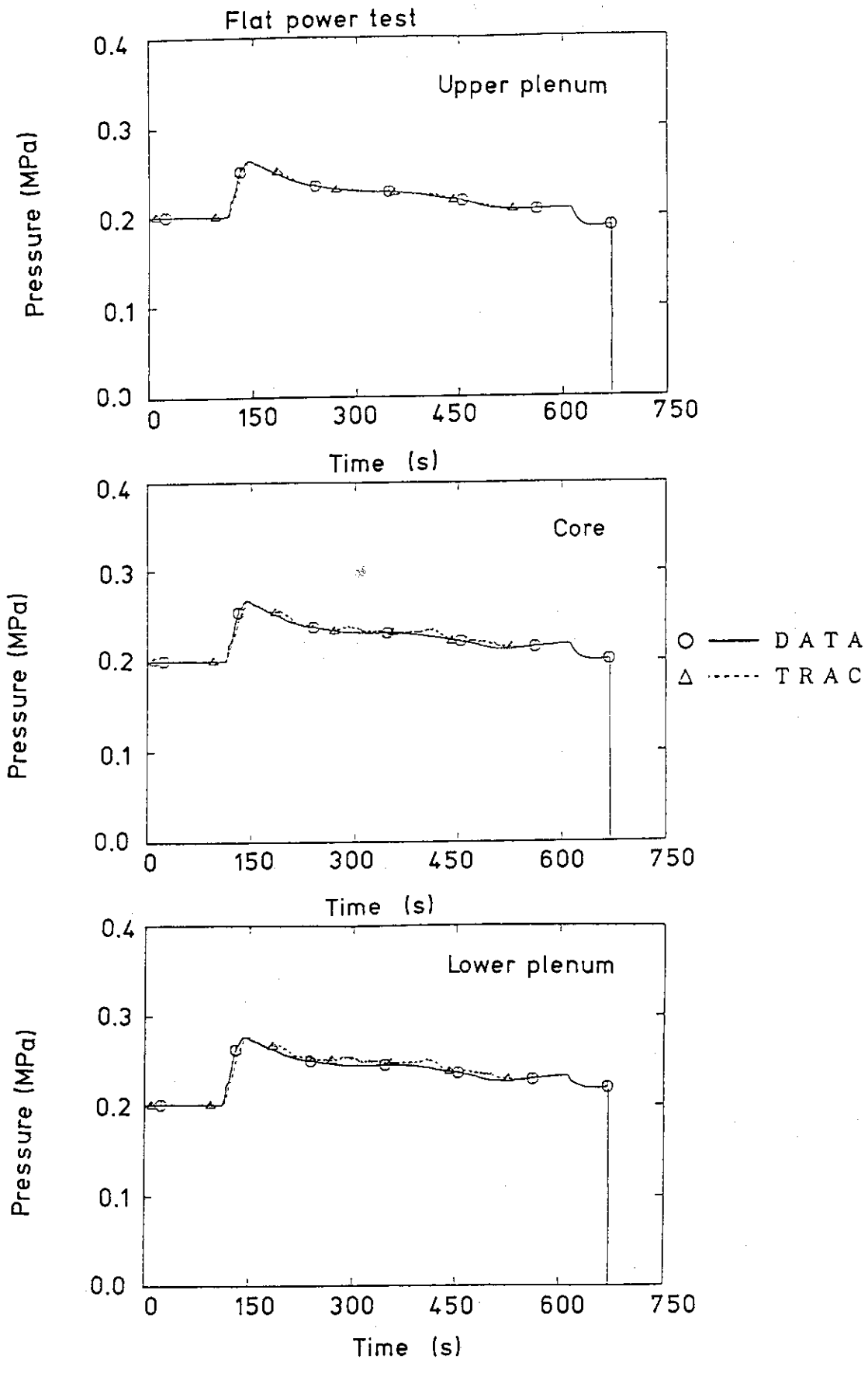

Fig.4.1.1 Comparison of pressure in pressure vessel for flat power test

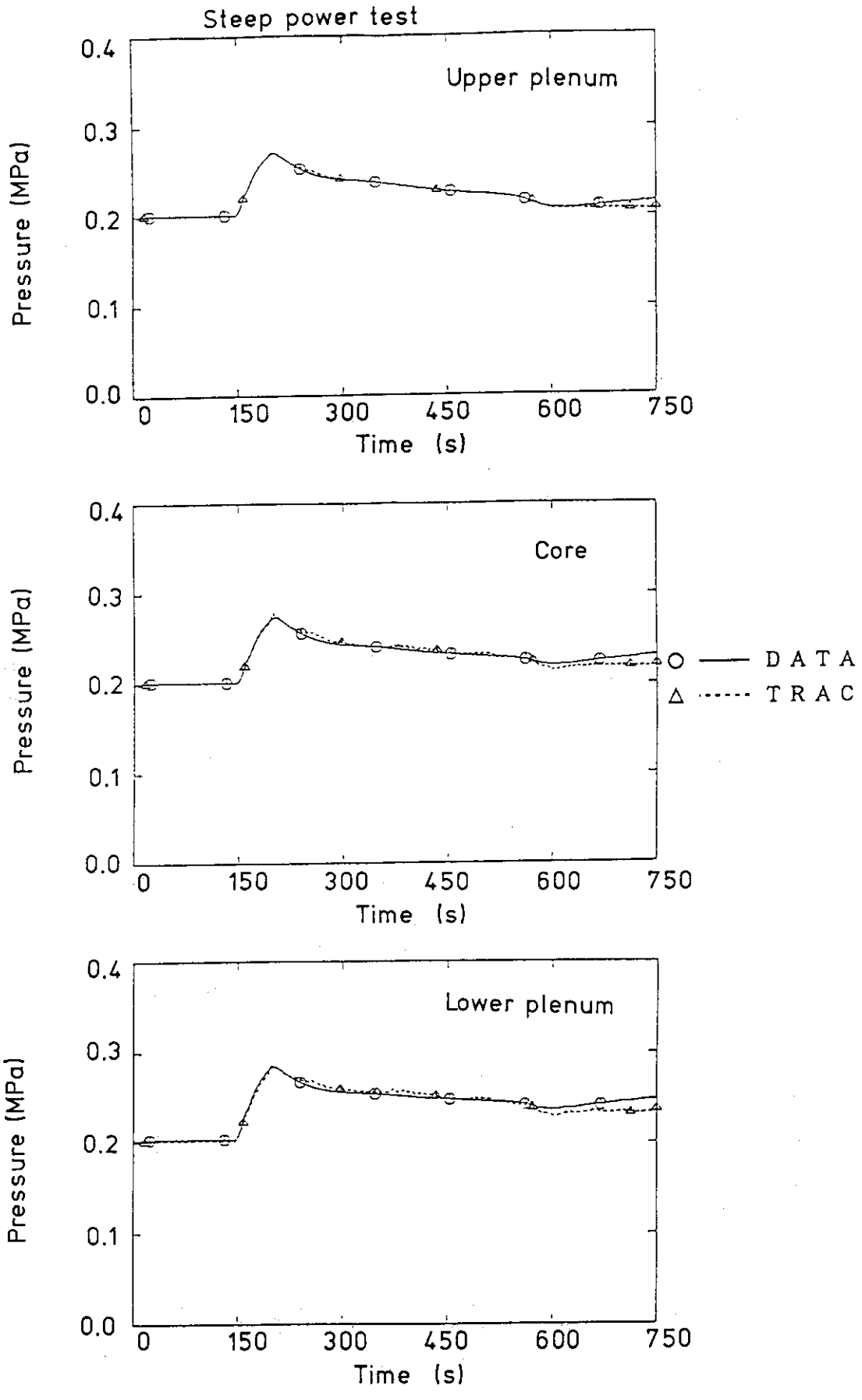

Fig.4.1.2 Comparison of pressure in pressure vessel for steep power test

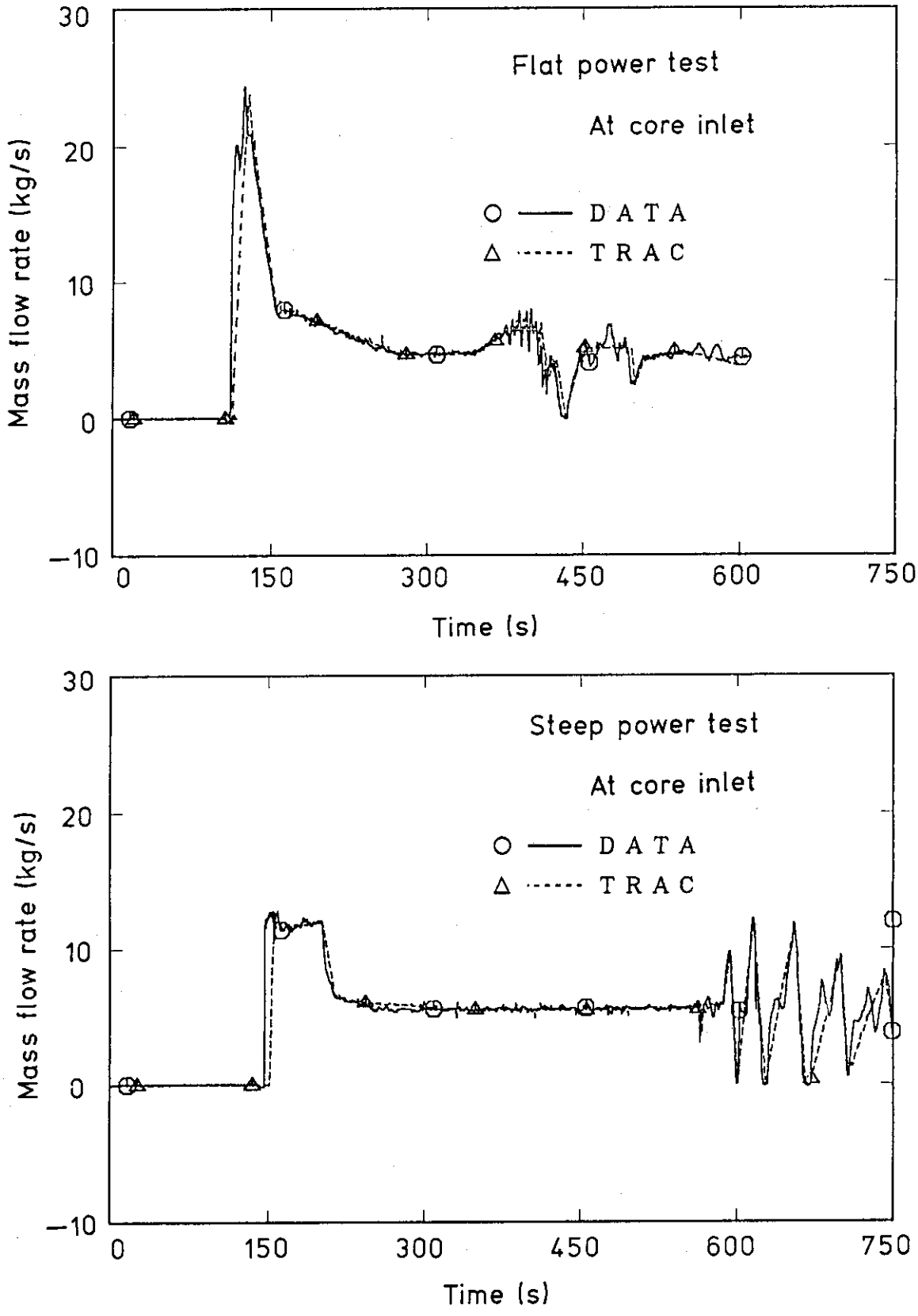

Fig.4.1.3 Comparison of core inlet mass flow rate

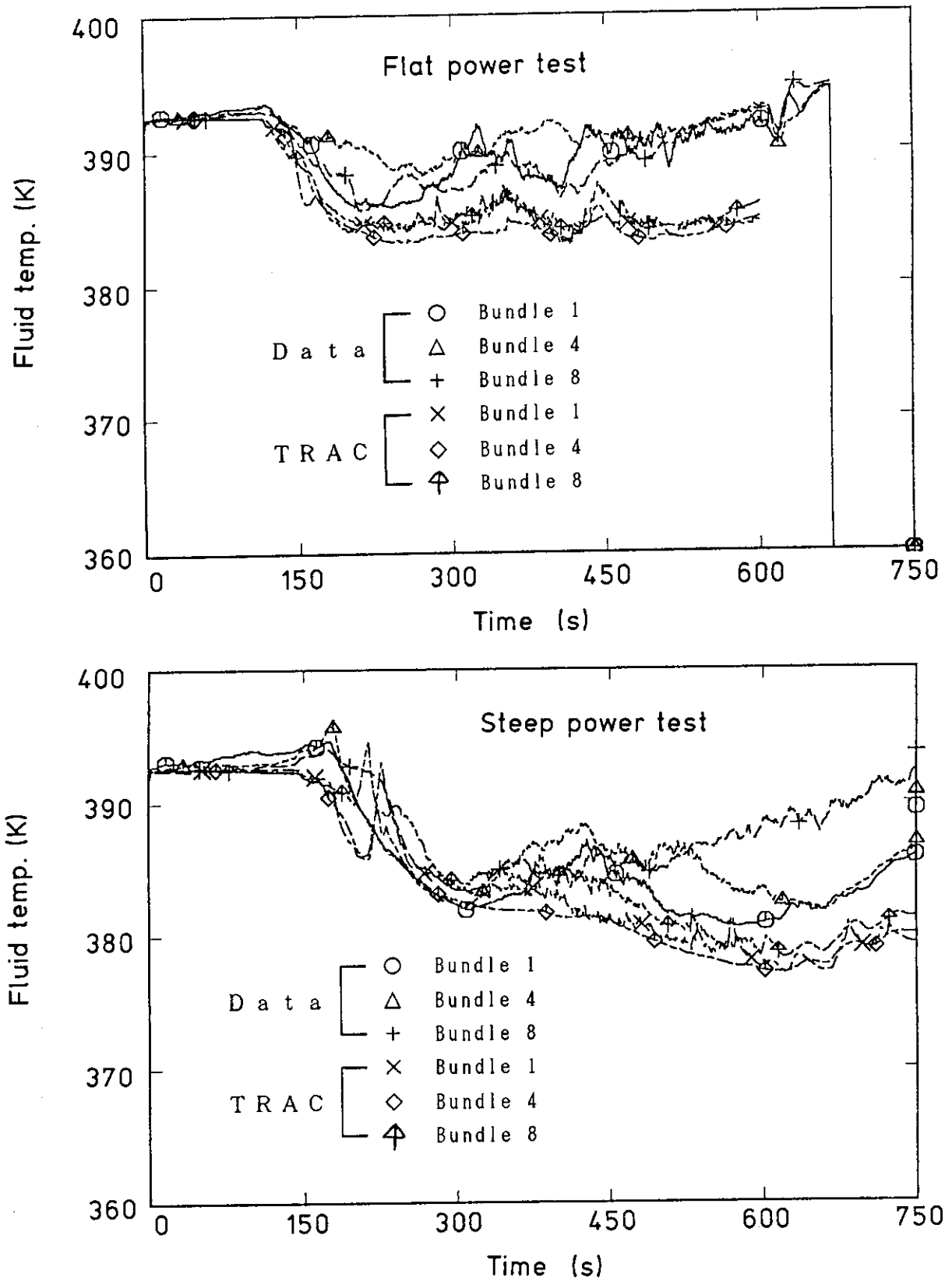

Fig.4.1.4 Comparison of fluid temperature at inlet of core

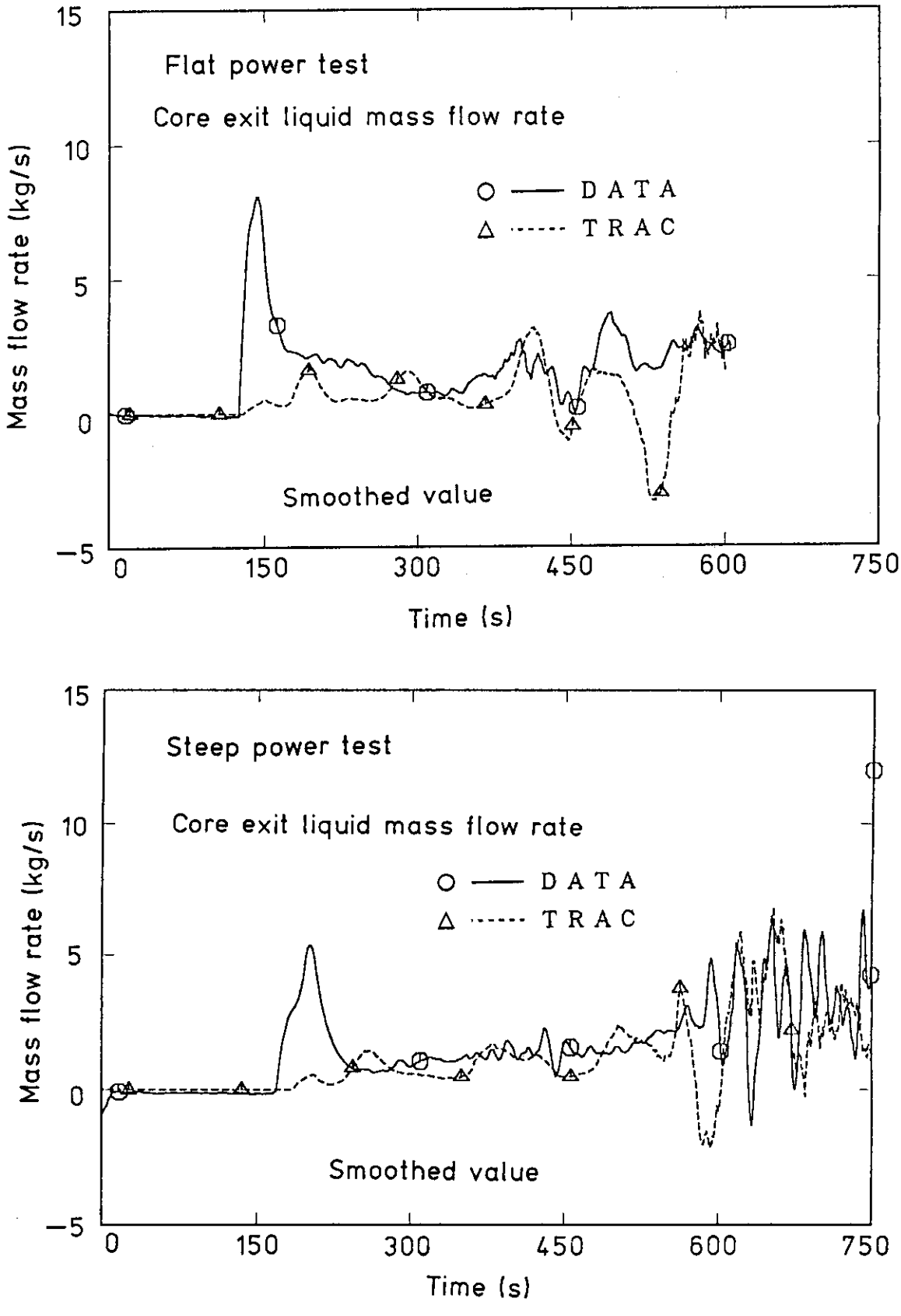

Fig.4.1.5 Comparison of core exit liquid mass flow rate

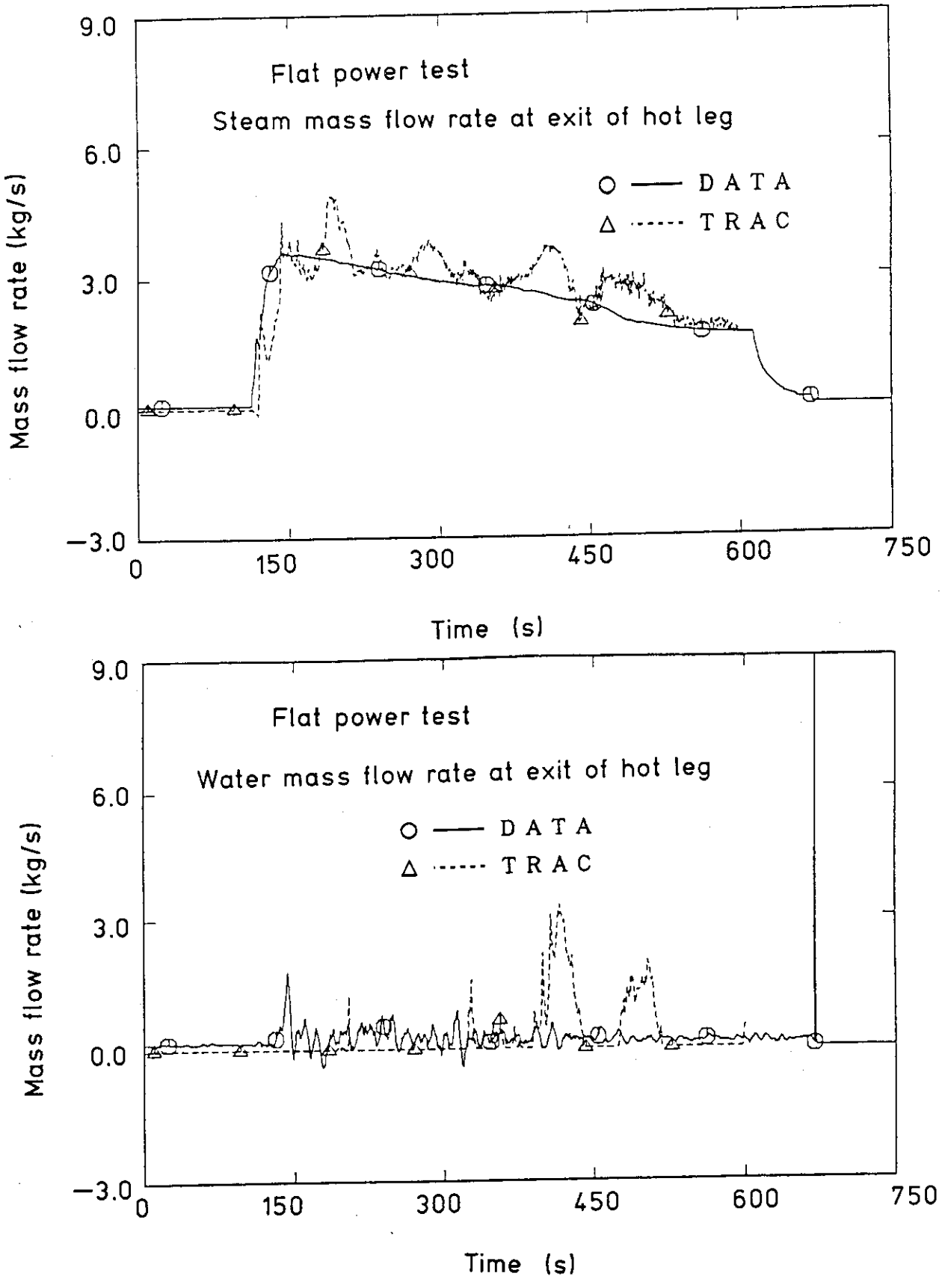

Fig.4.1.6 Comparison of steam and water mass flow rates at exit of hot leg for flat power test

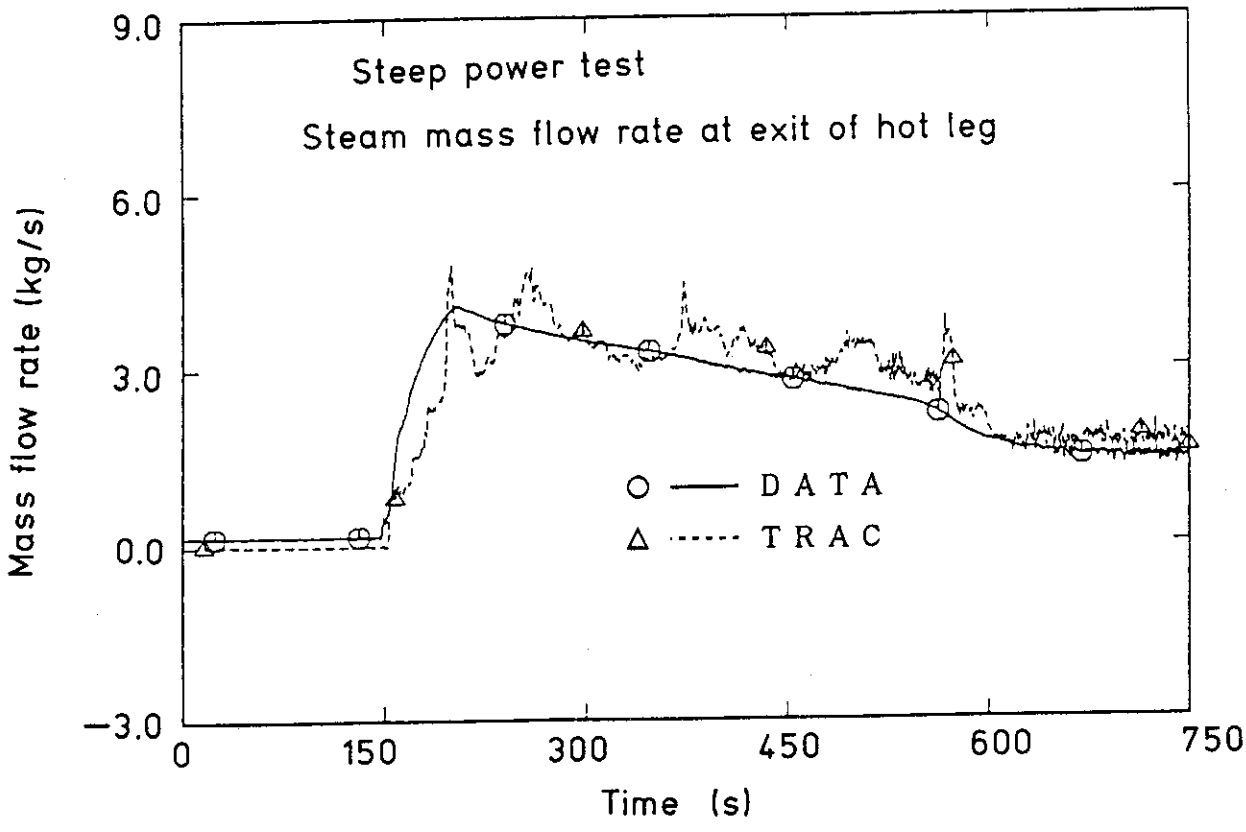

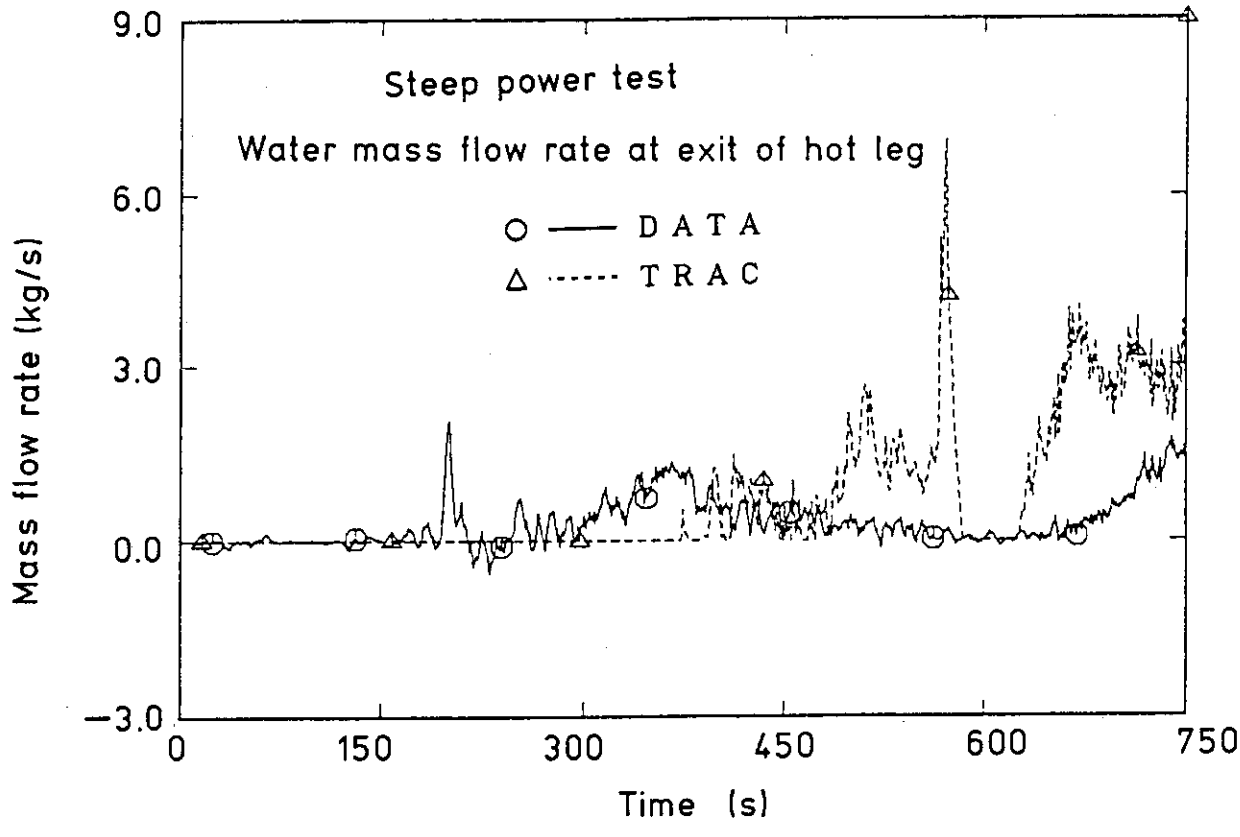

Fig.4.1.7 Comparison of steam and water mass flow rates at exit of hot leg for steep power test

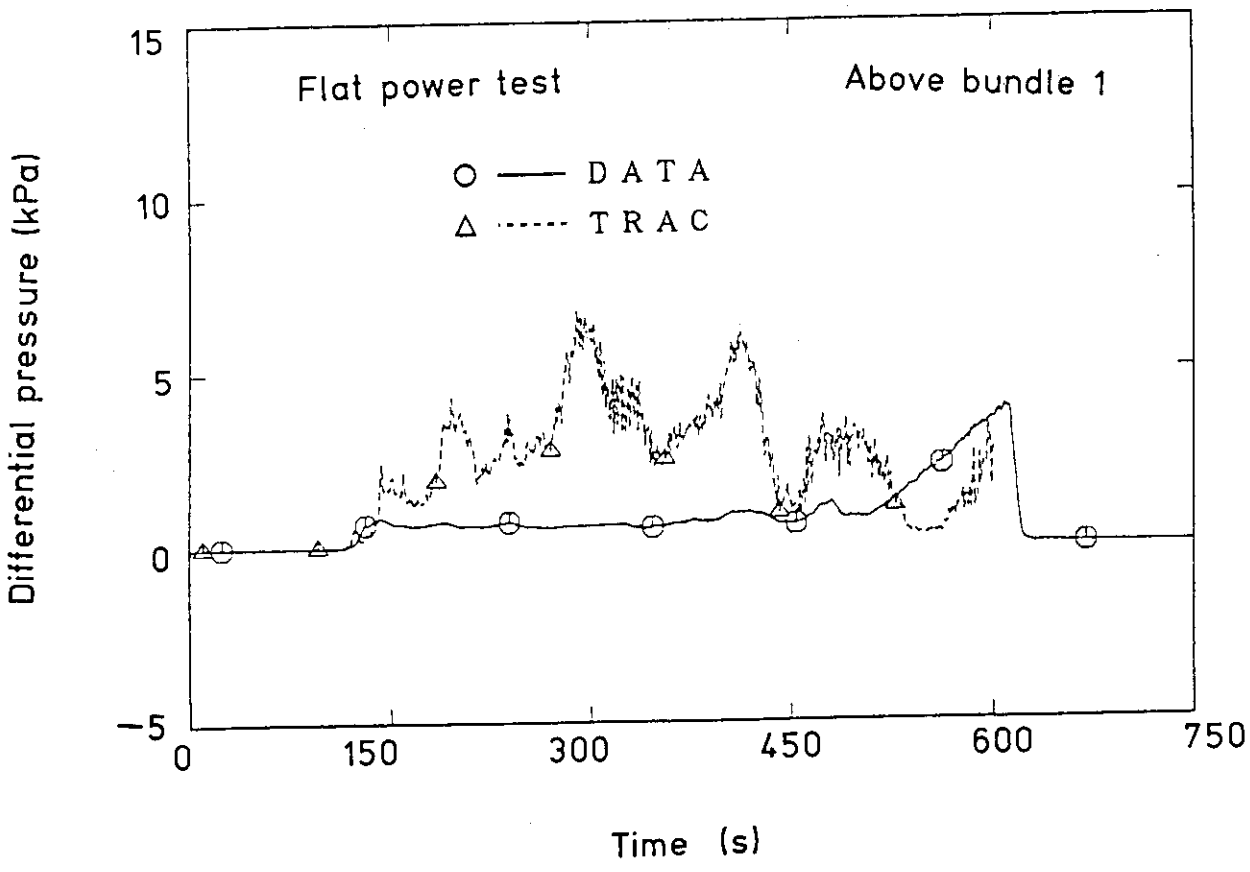

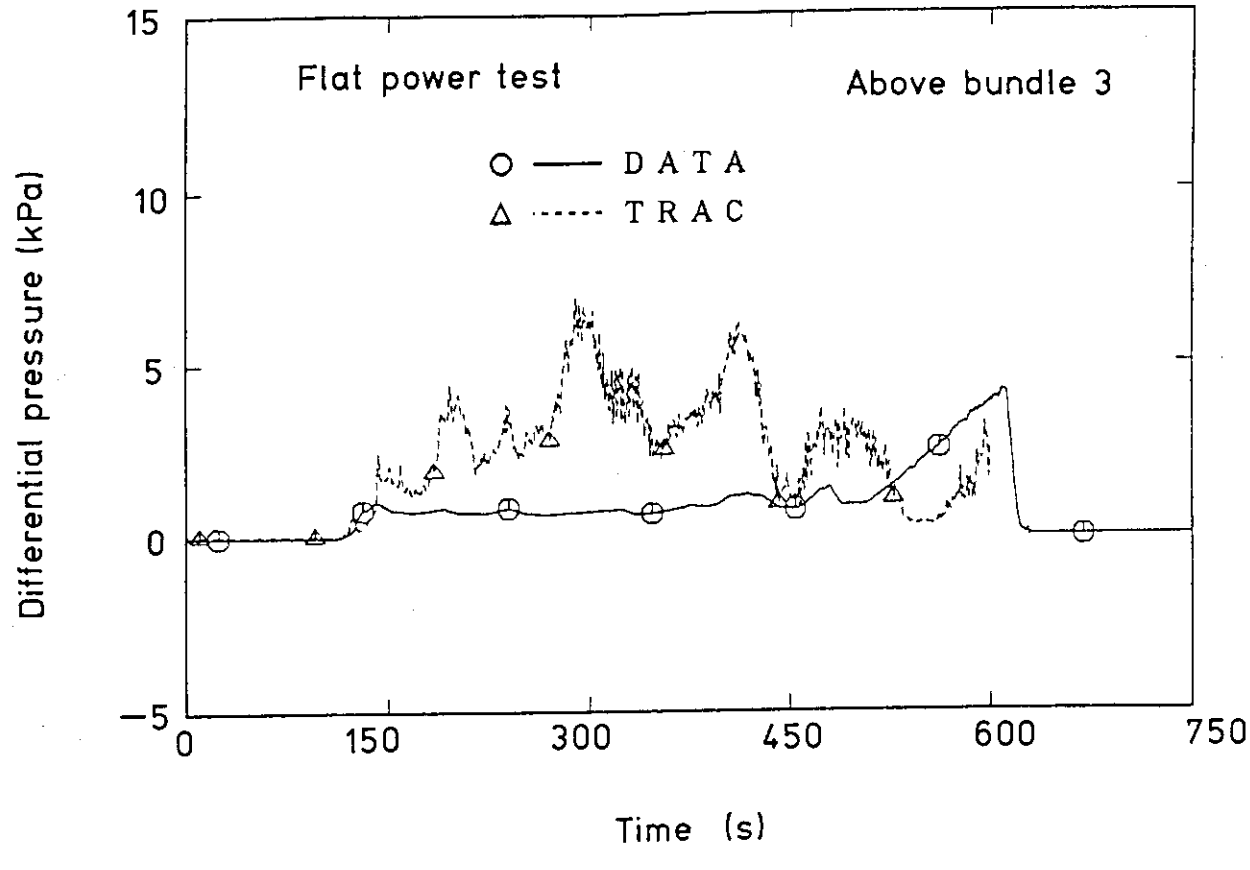

Fig.4.1.8(1) Comparison of differential pressure in upper plenum for flat power test

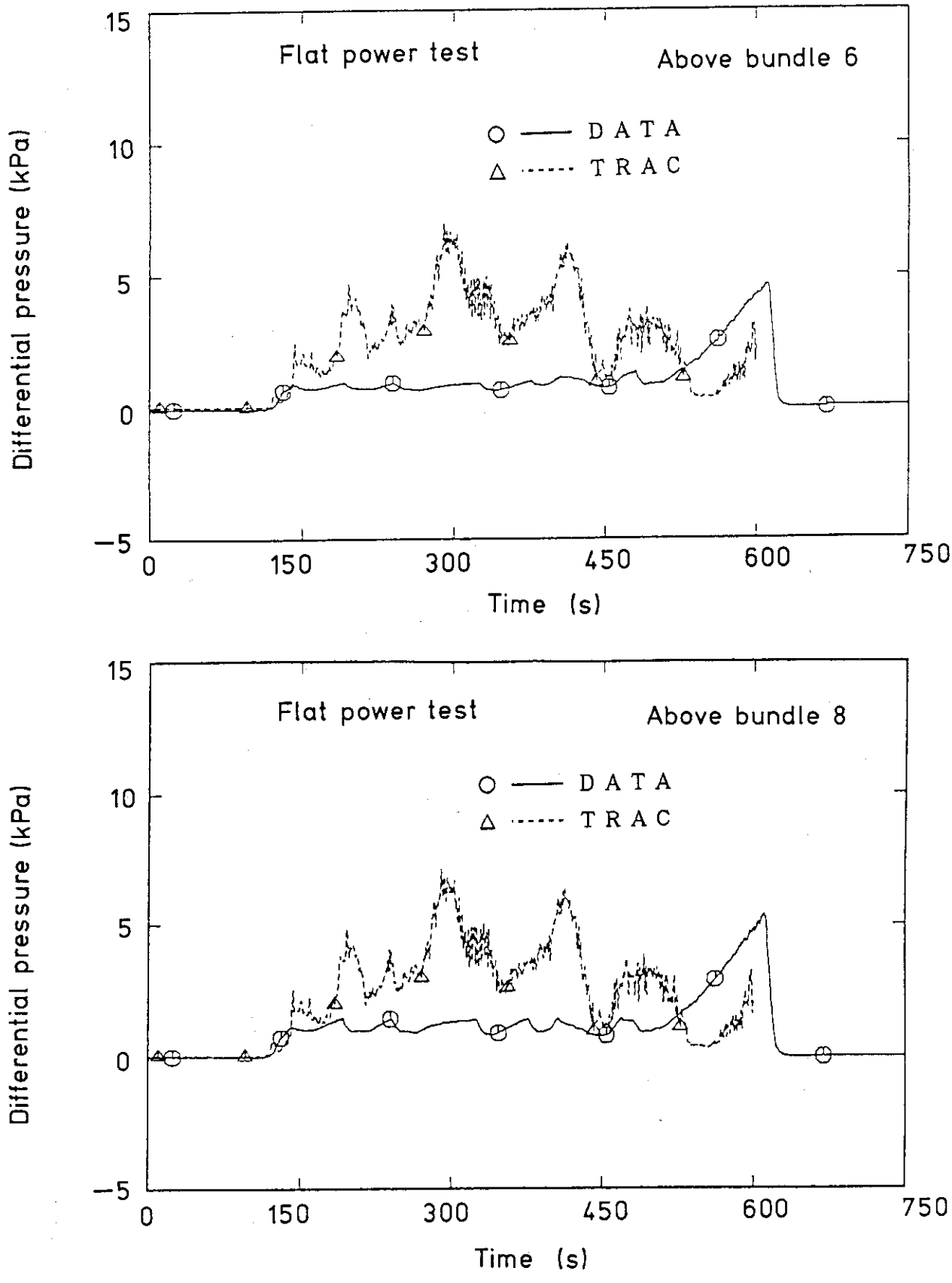

Fig.4.1.8(2) Comparison of differential pressure in upper plenum for flat power test

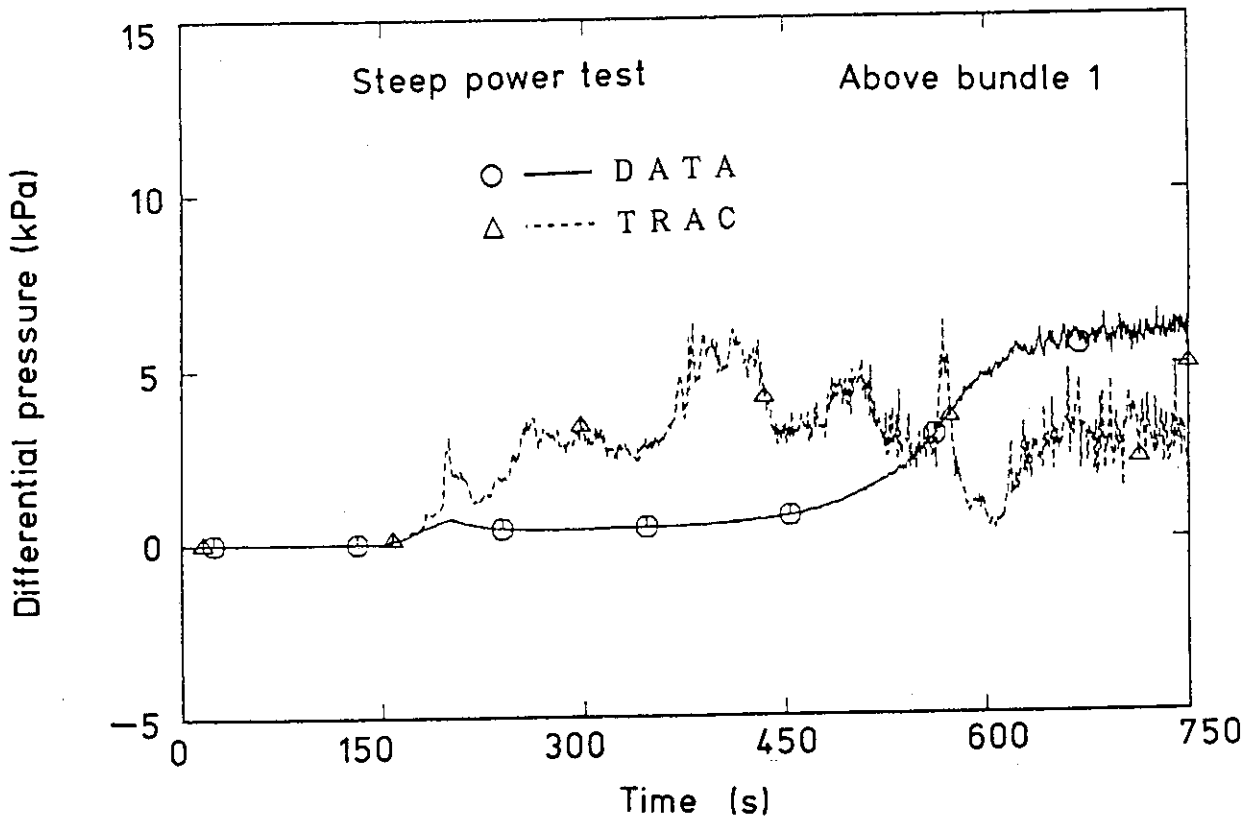

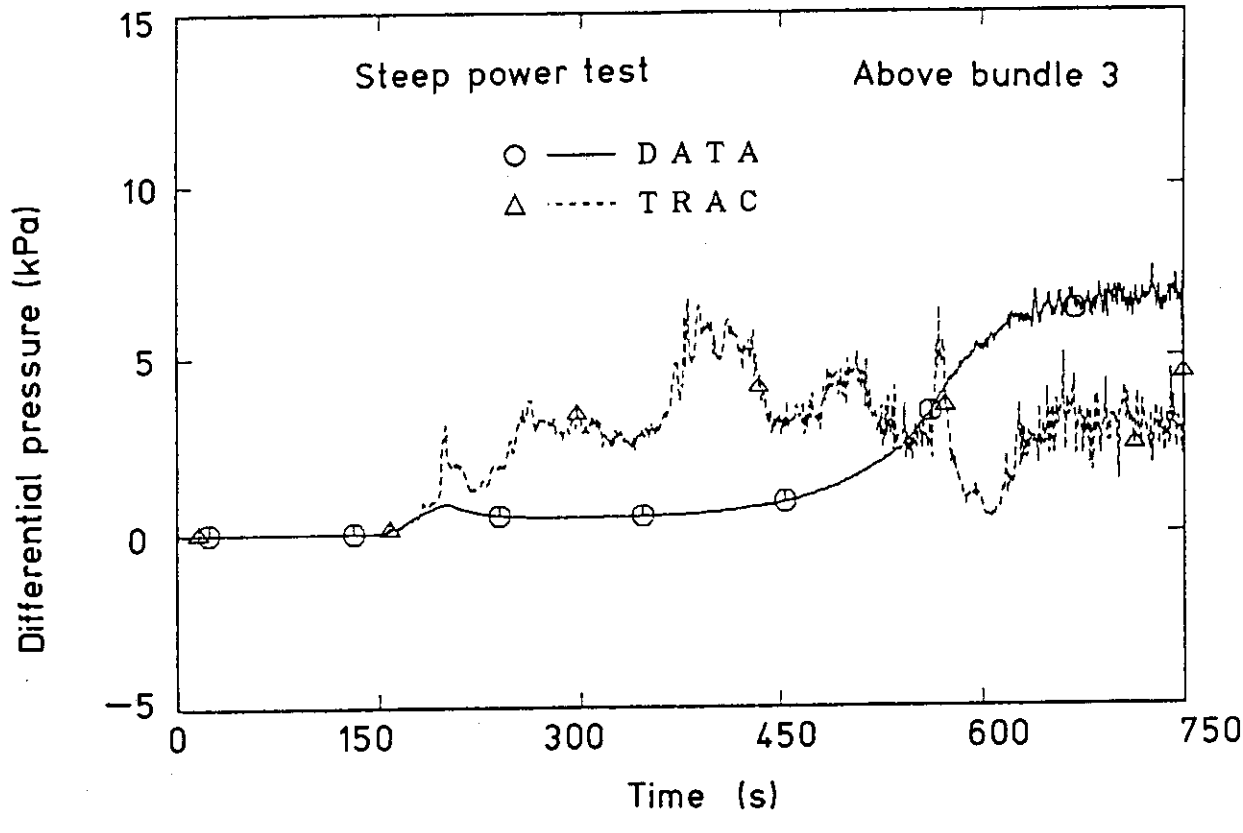

Fig.4.1.9(1) Comparison of differential pressure in upper plenum for steep power test

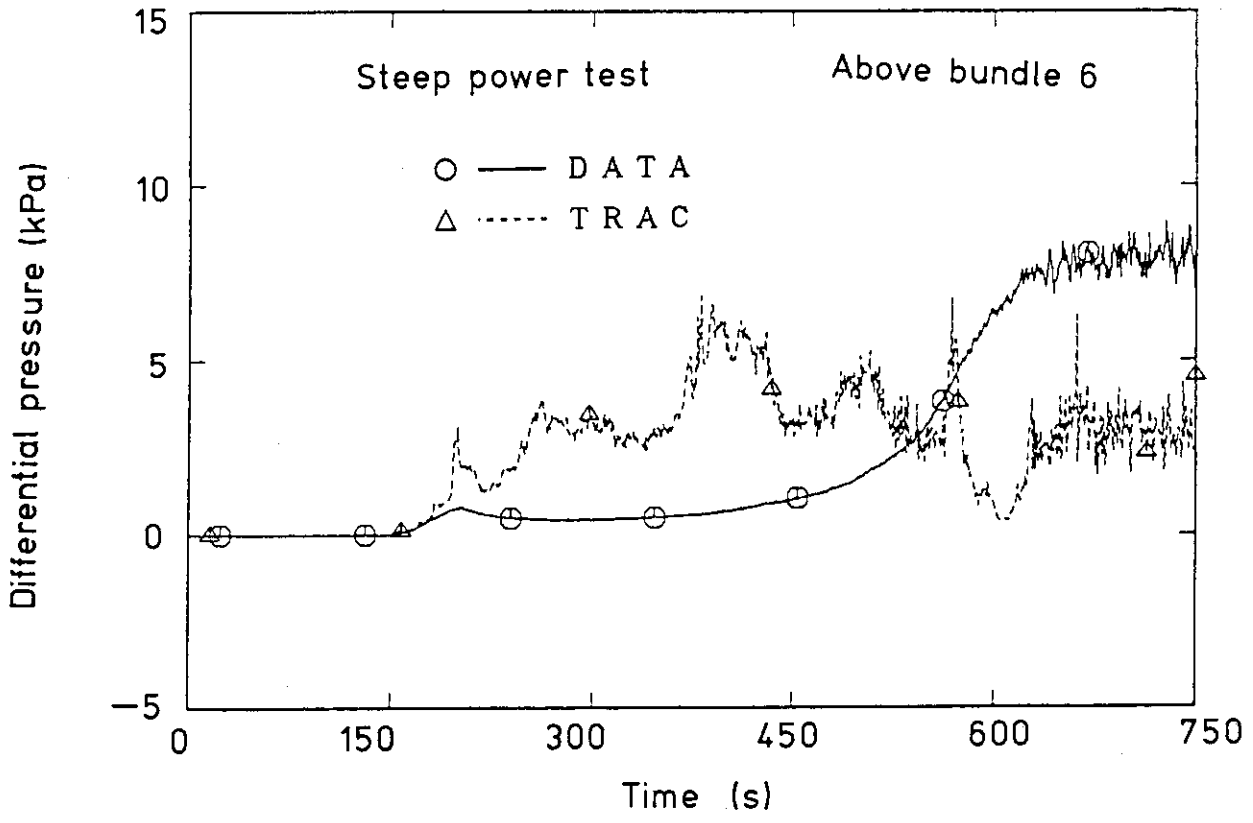

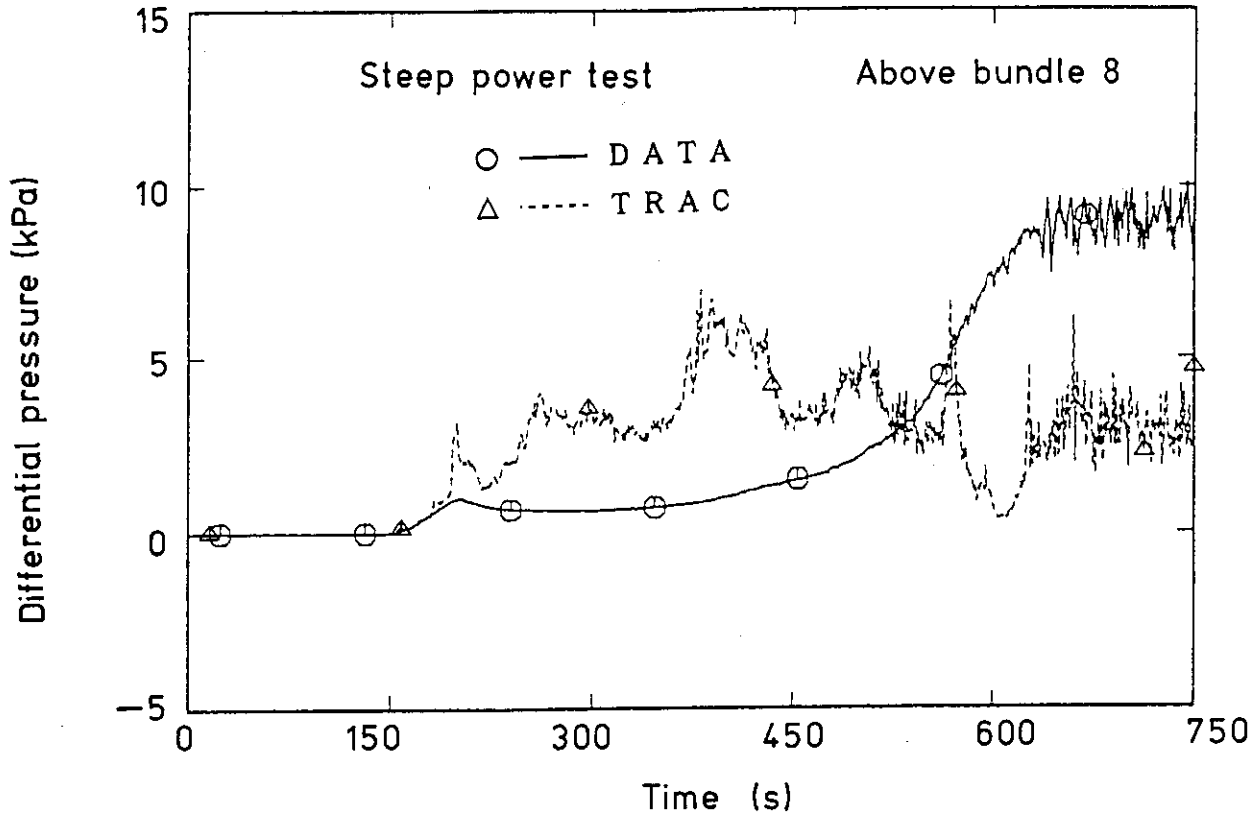

Fig.4.1.9(2) Comparison of differential pressure in upper plenum for steep power test

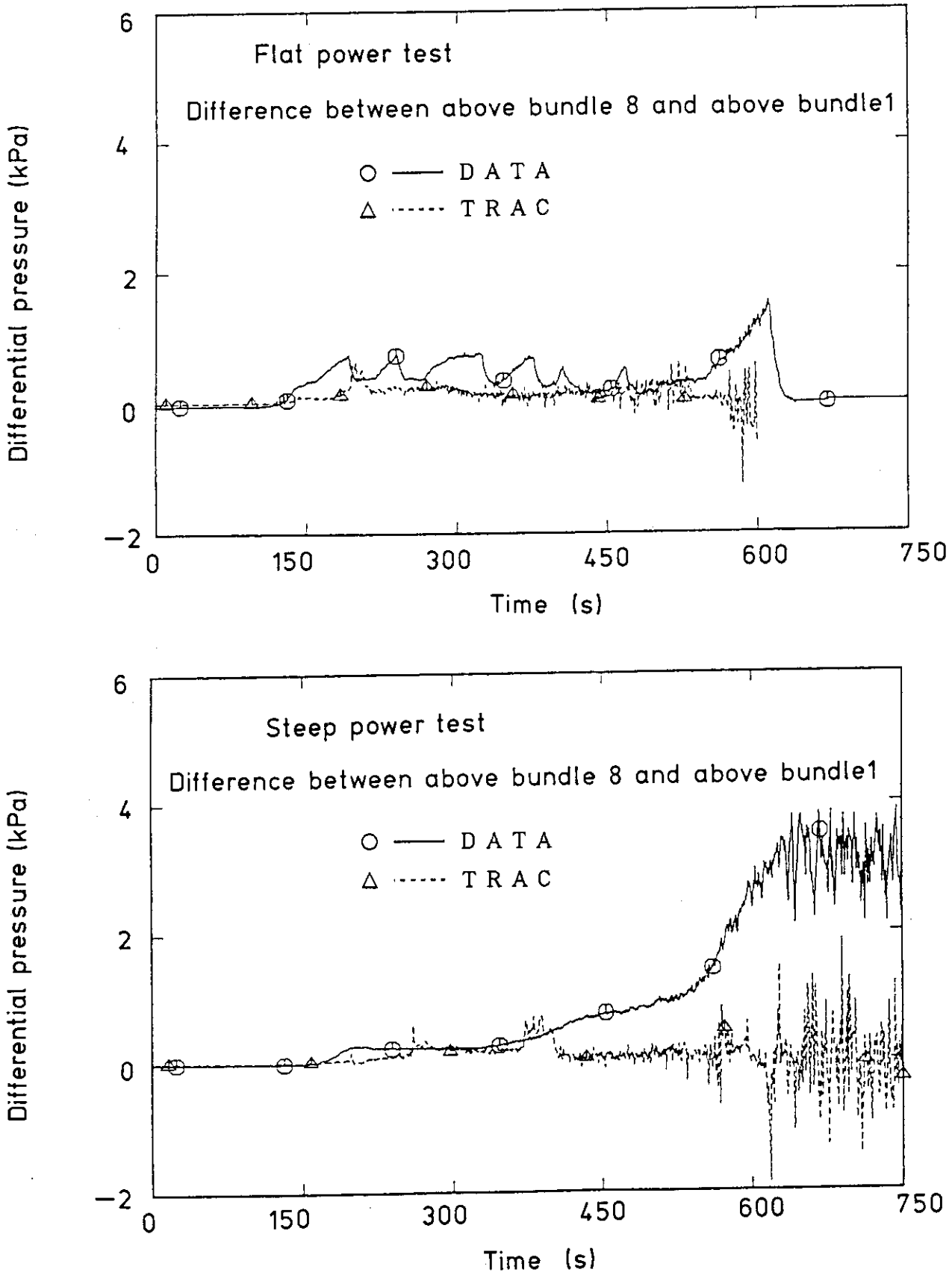

Fig.4.1.10 Comparison of difference of differential pressure in upper plenum between above bundle 8 and above bundle 1

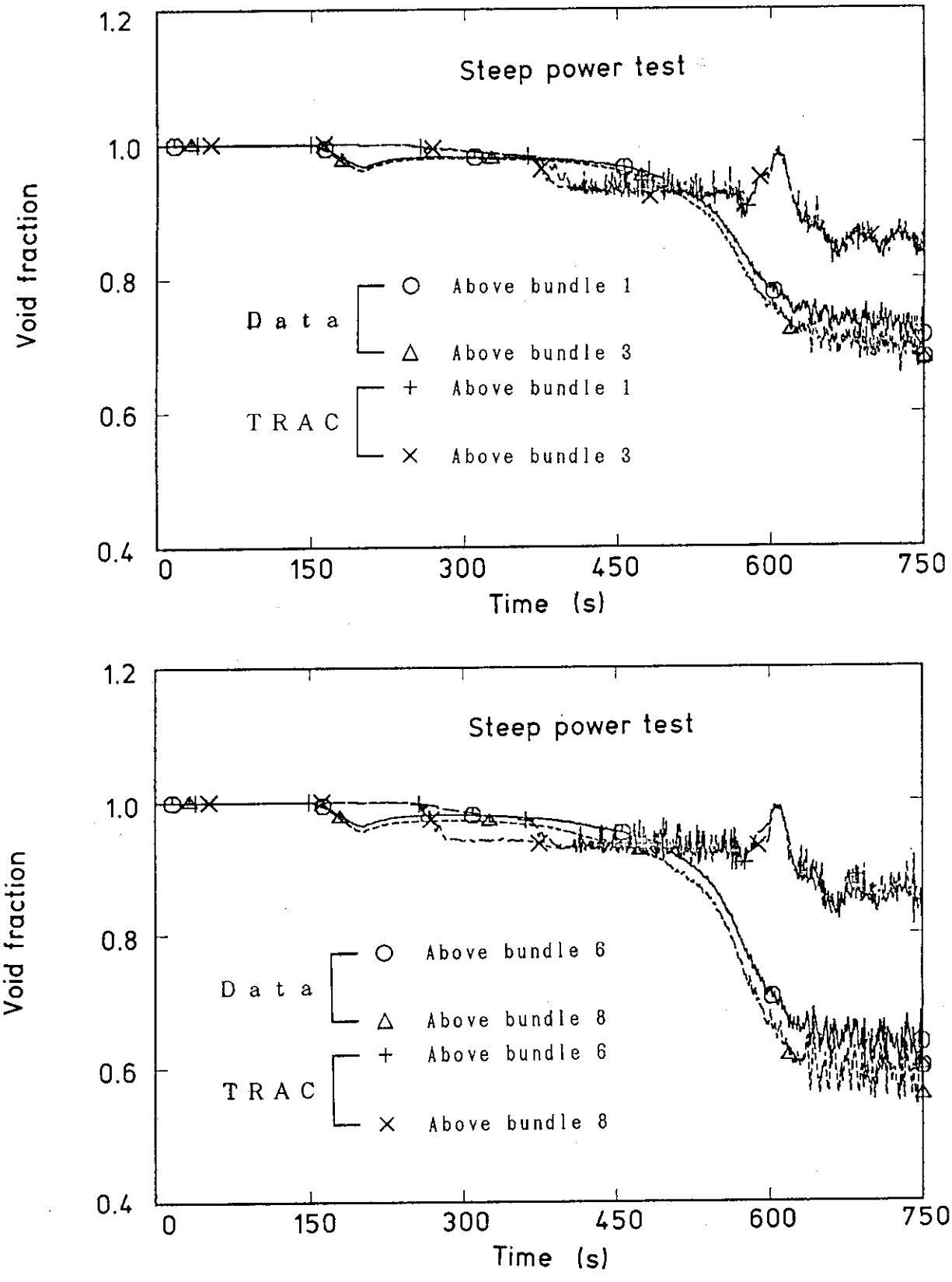

Fig.4.1.11 Comparison of void fraction in upper plenum for steep power test

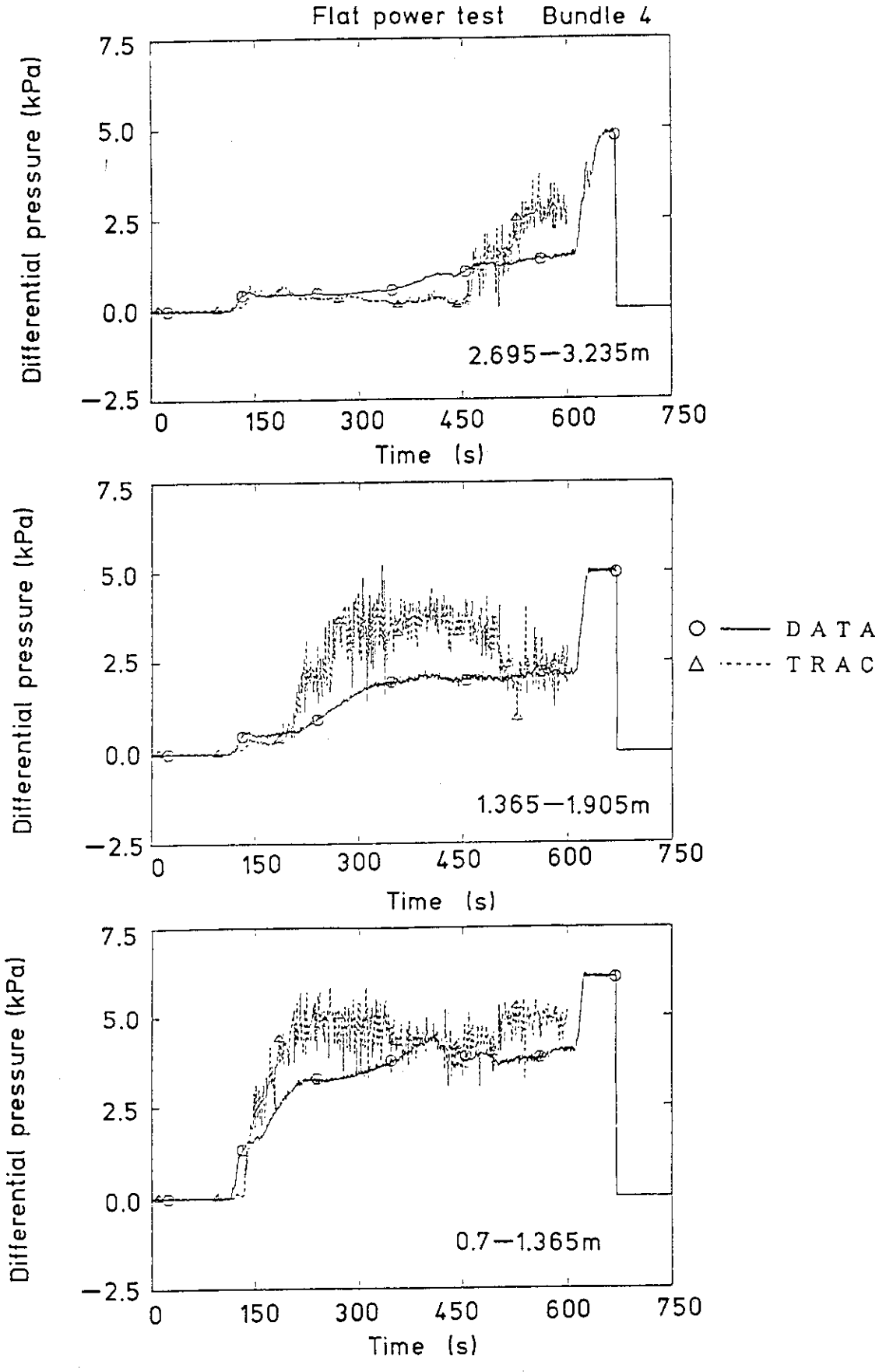

Fig.4.2.1 Comparison of sectional differential pressure in bundle 4 for flat power test

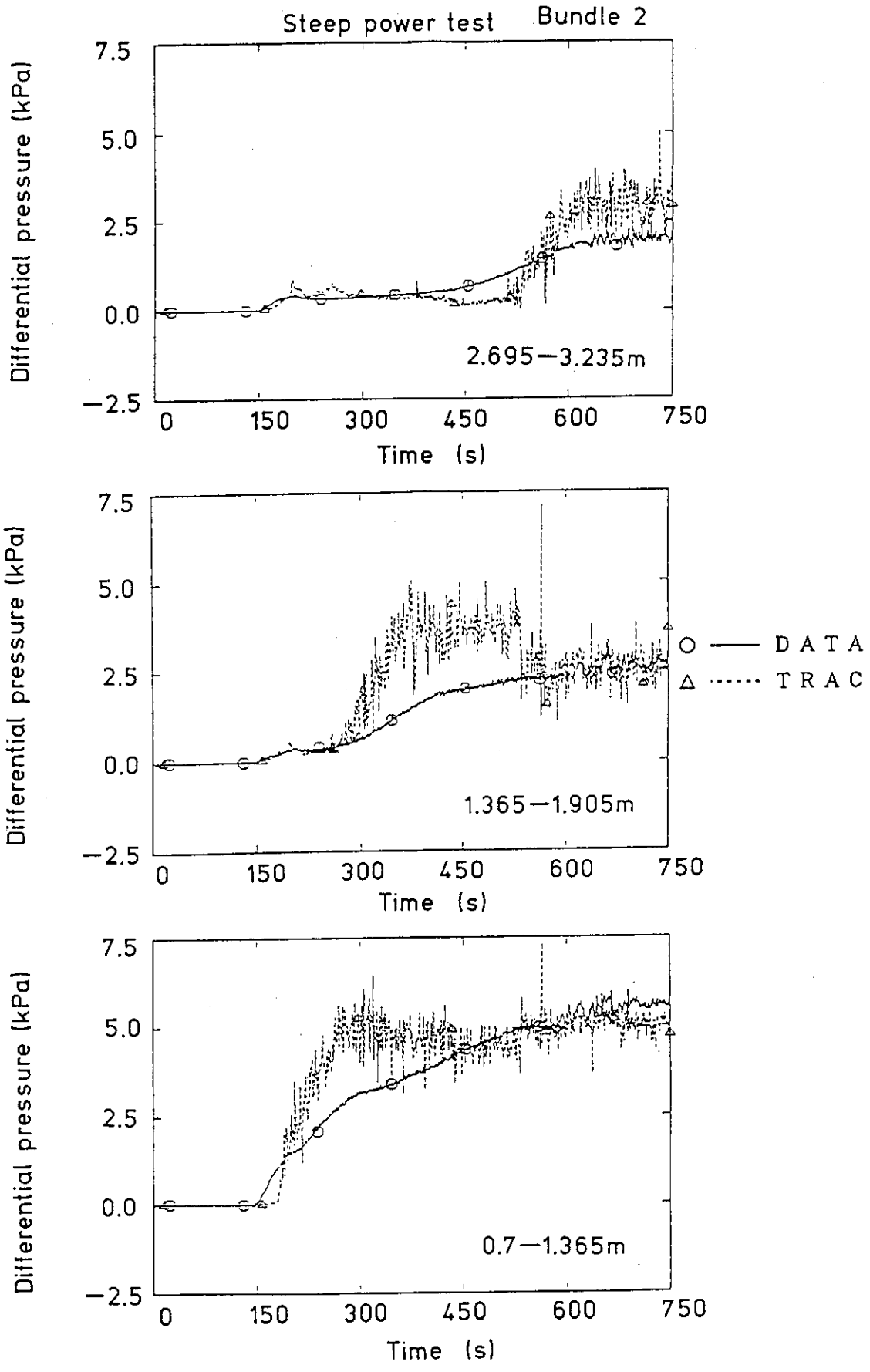

Fig.4.2.2(1) Comparison of sectional differential pressure in bundle 2 for steep power test

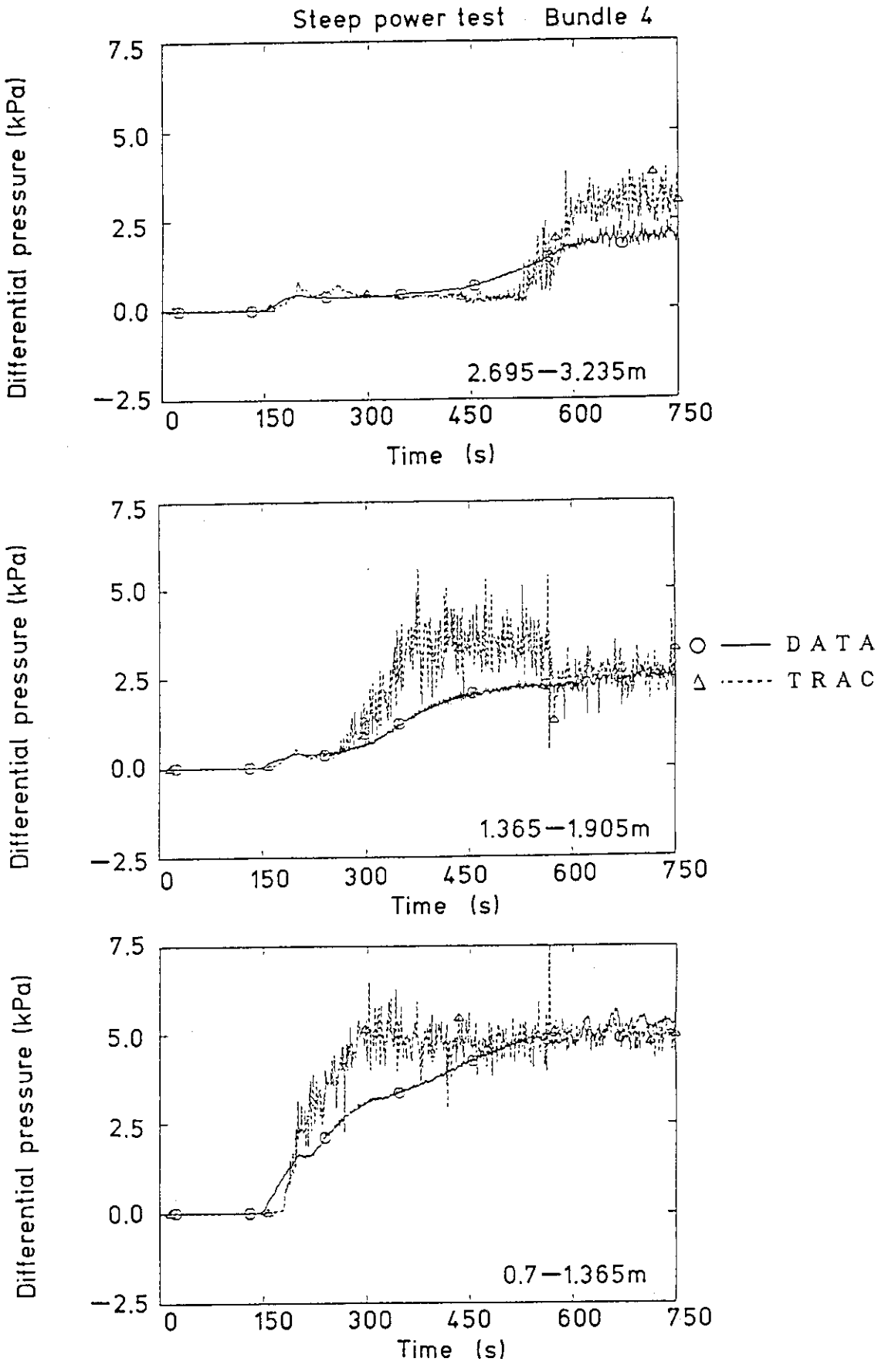

Fig.4.2.2(2) Comparison of sectional differential pressure in bundle 4 for steep power test

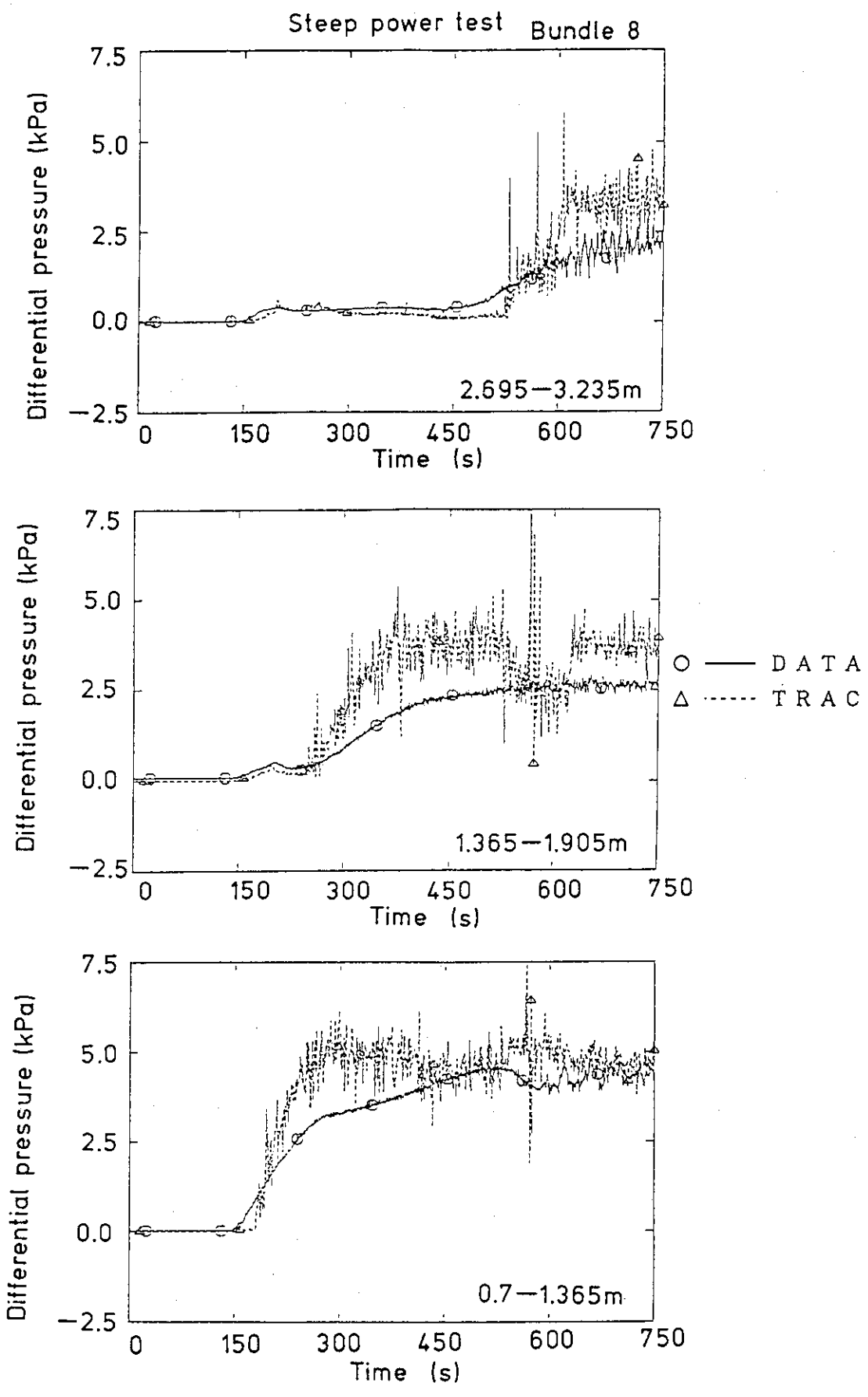

Fig.4.2.2(3) Comparison of sectional differential pressure in bundle 8 for steep power test

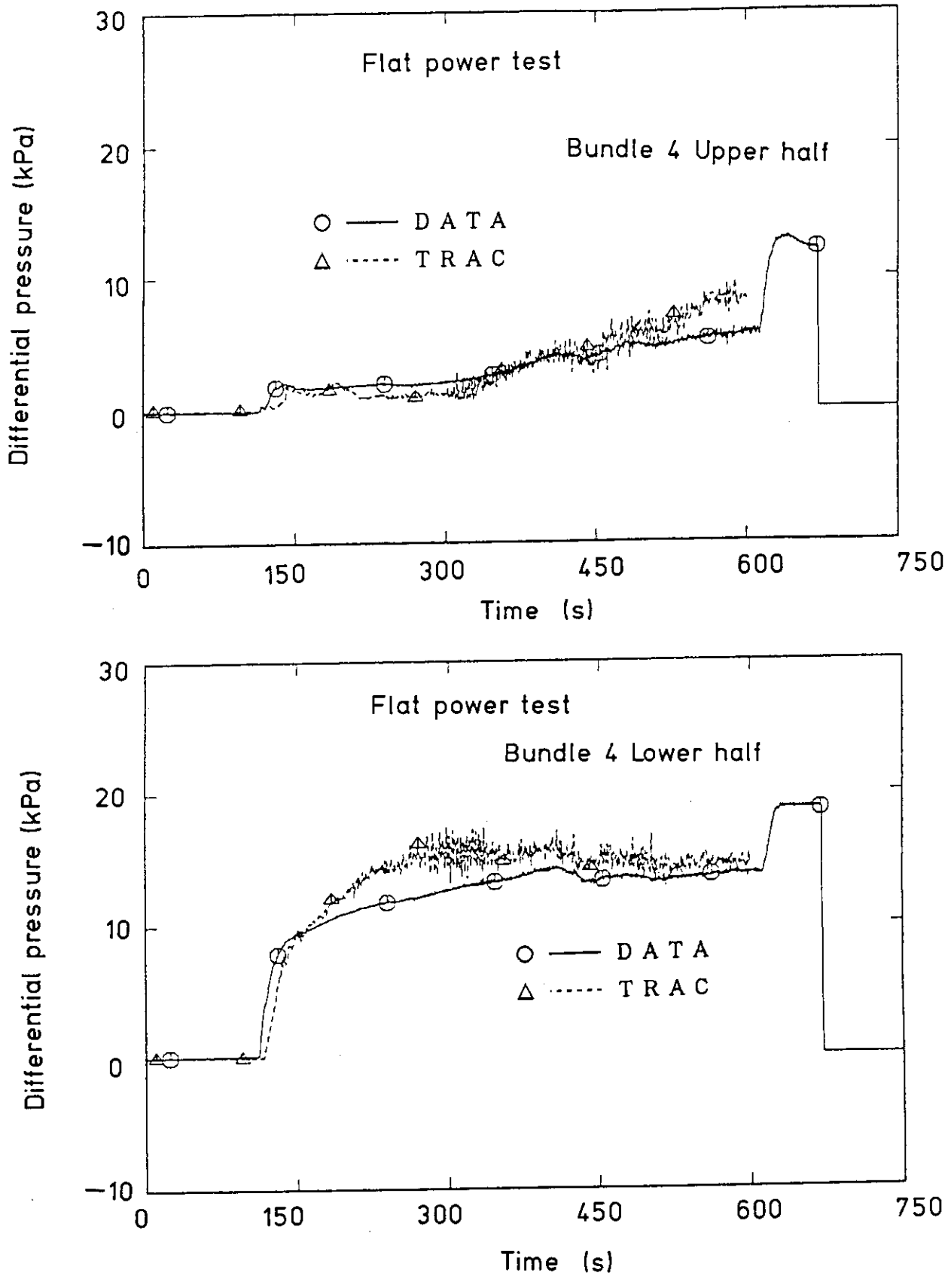

Fig.4.2.3 Comparison of upper and lower half differential pressures in bundle 4 for flat power test

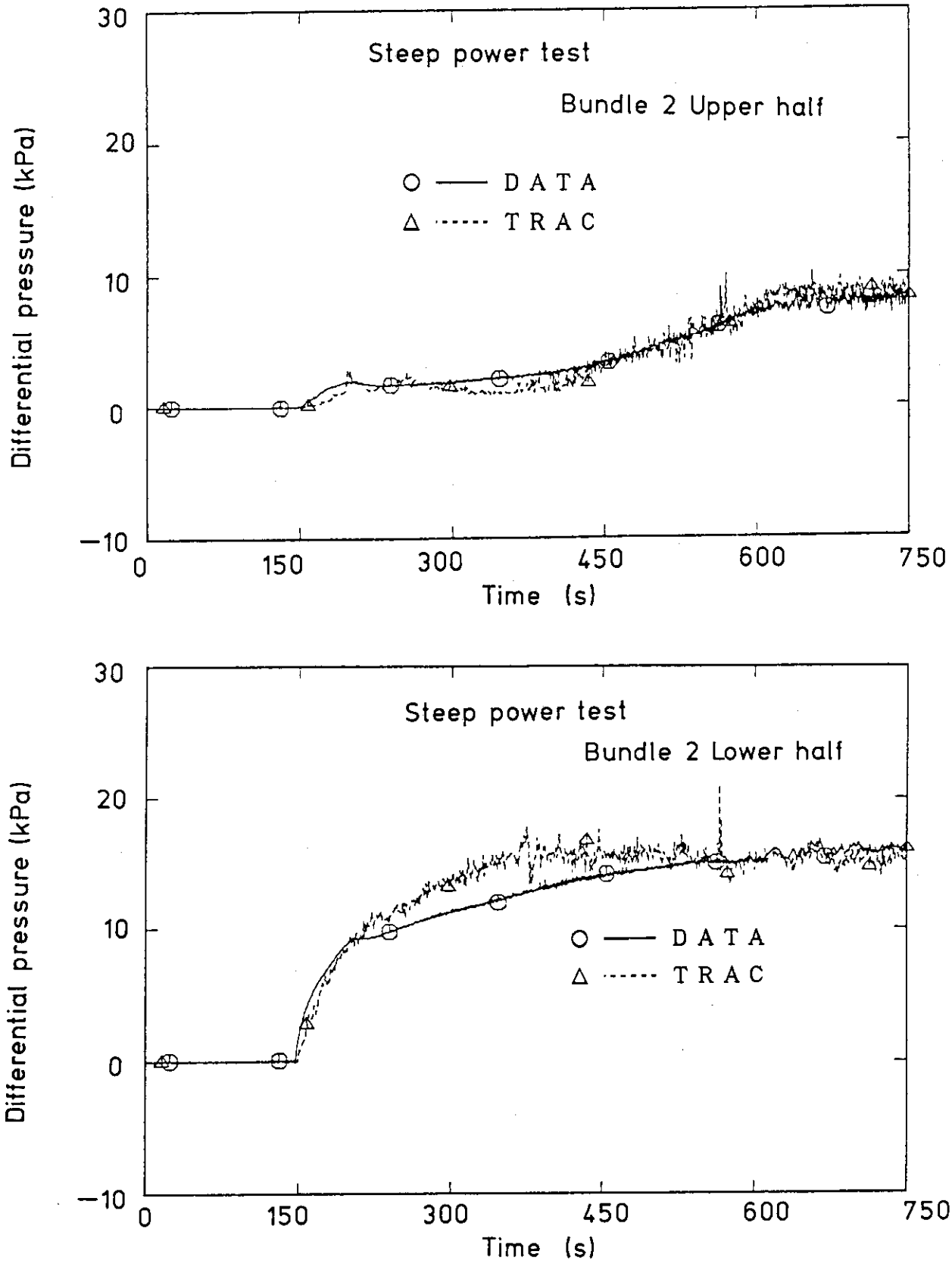

Fig.4.2.4(1) Comparison of upper and lower half differential pressures in bundle 2 for steep power test

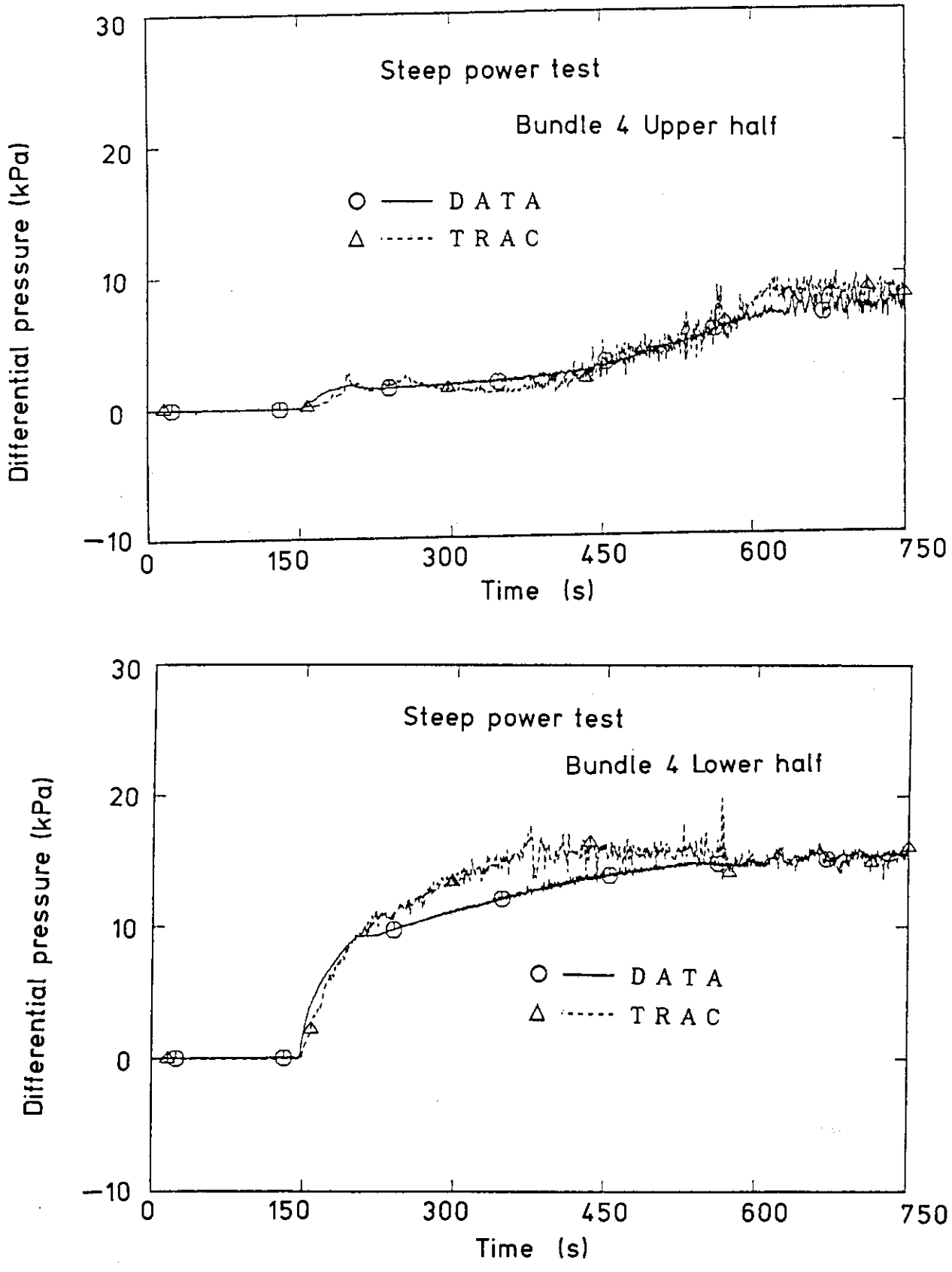

Fig.4.2.4(2) Comparison of upper and lower half differential pressures in bundle 4 for steep power test

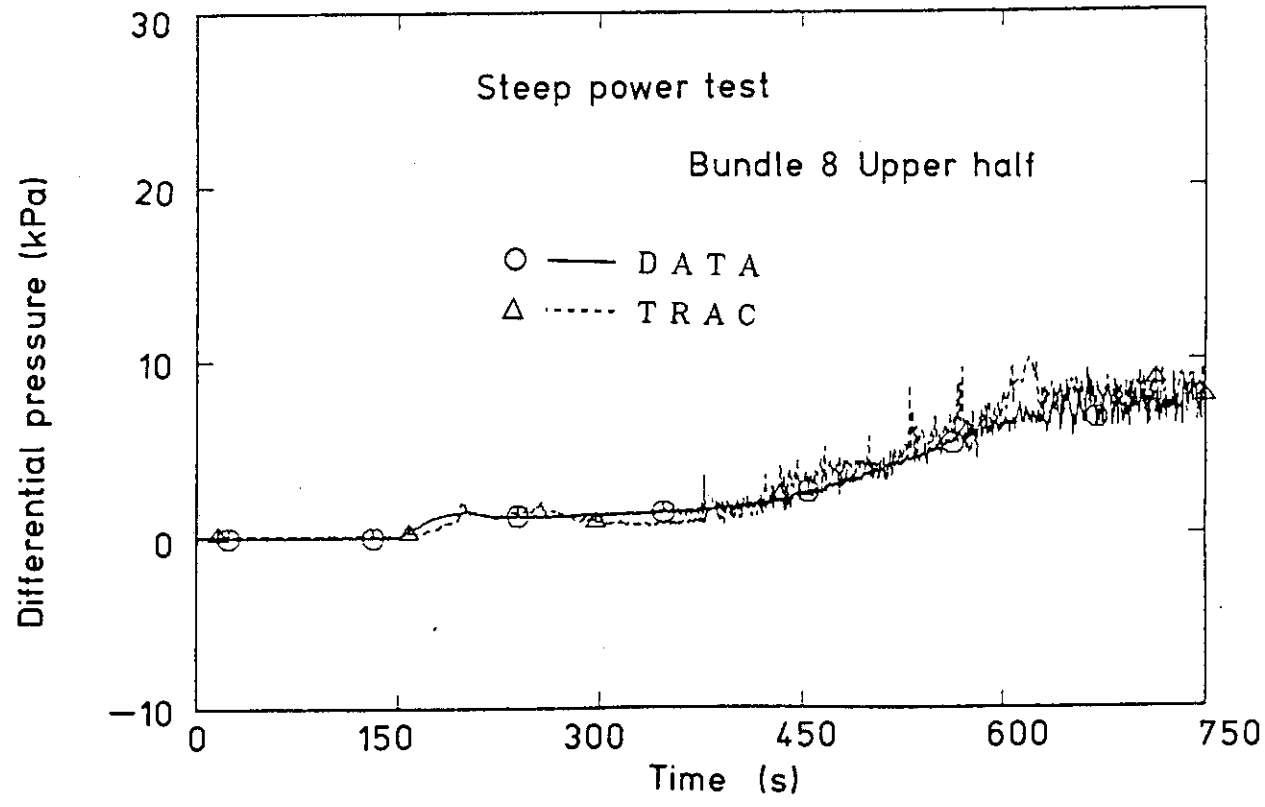

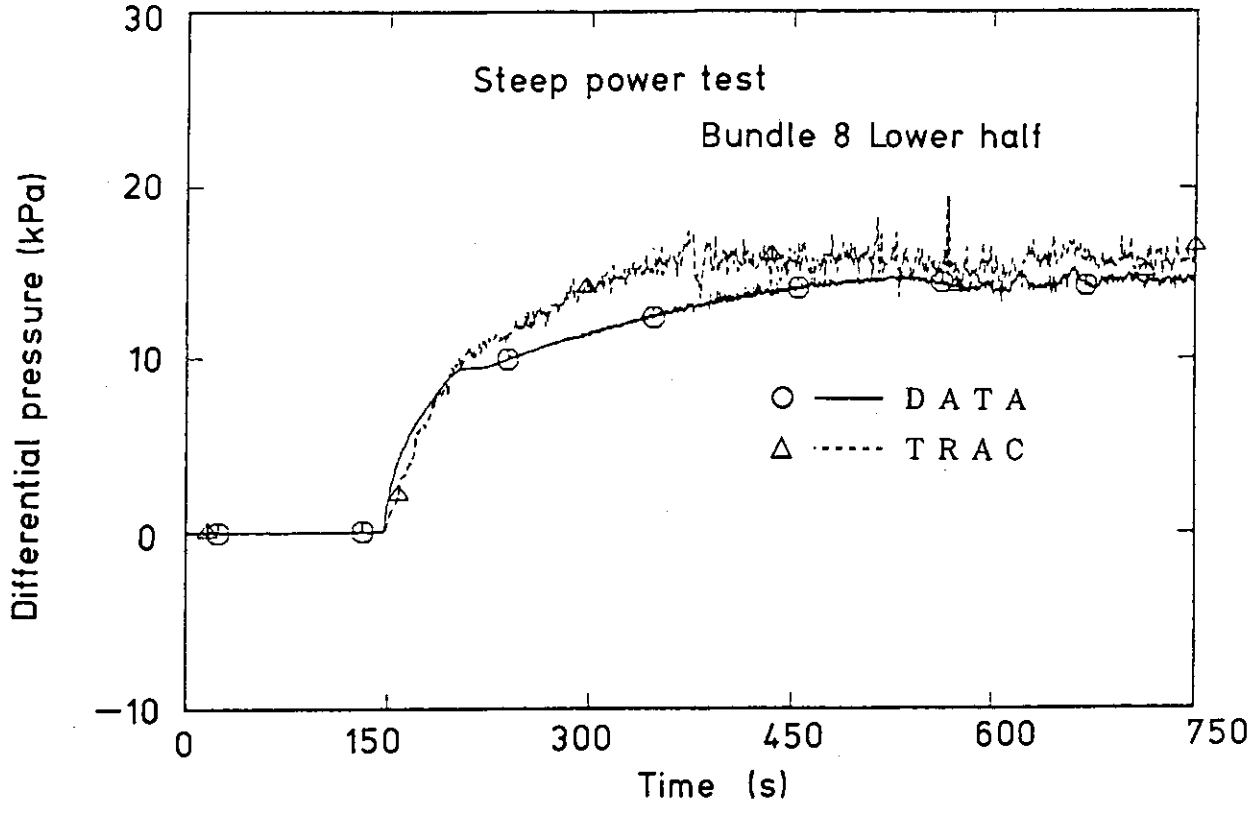

Fig.4.2.4(3) Comparison of upper and lower half differential pressures in bundle 8 for steep power test

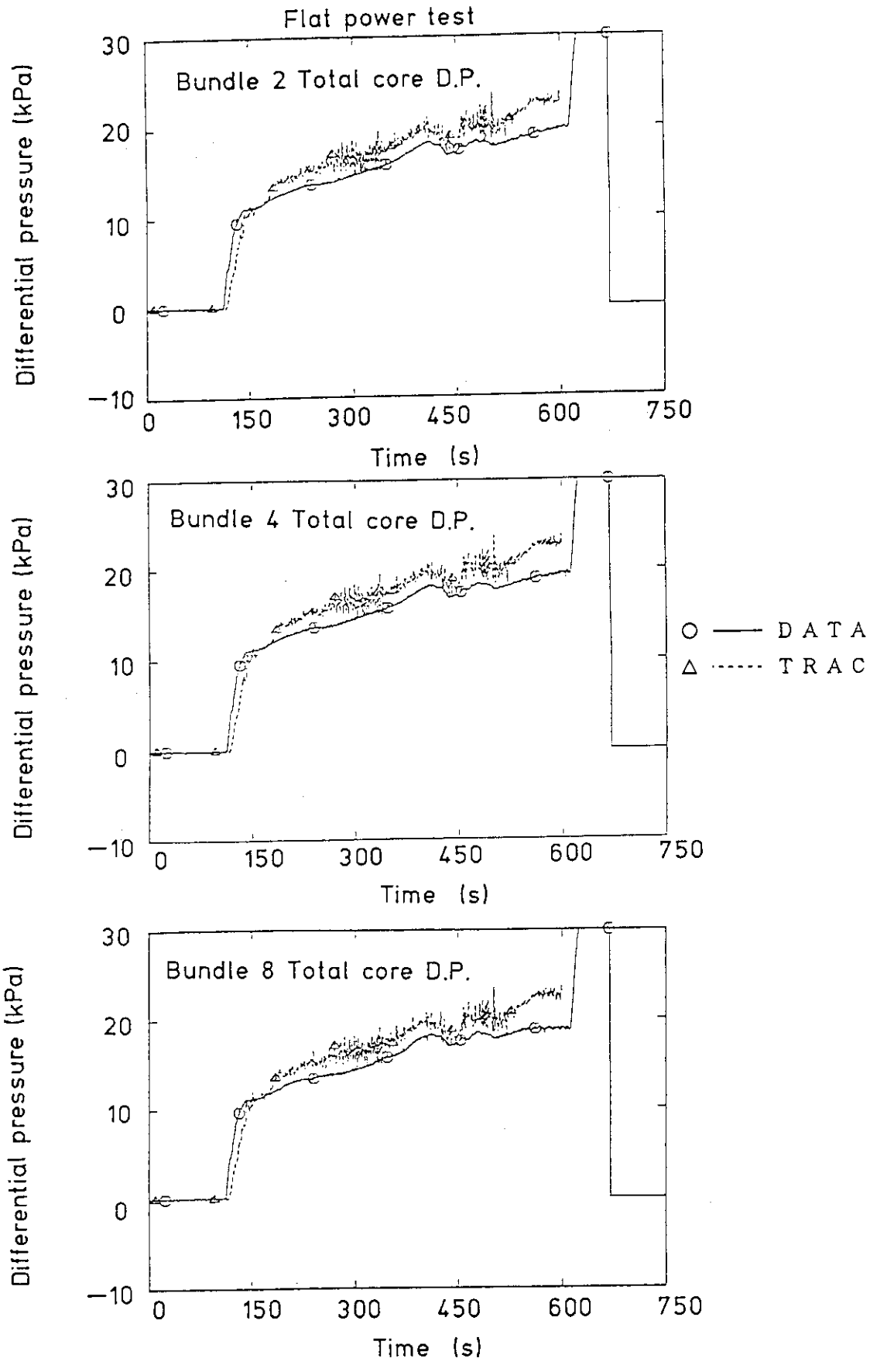

Fig.4.2.5 Comparison of total core differential pressure for flat power test

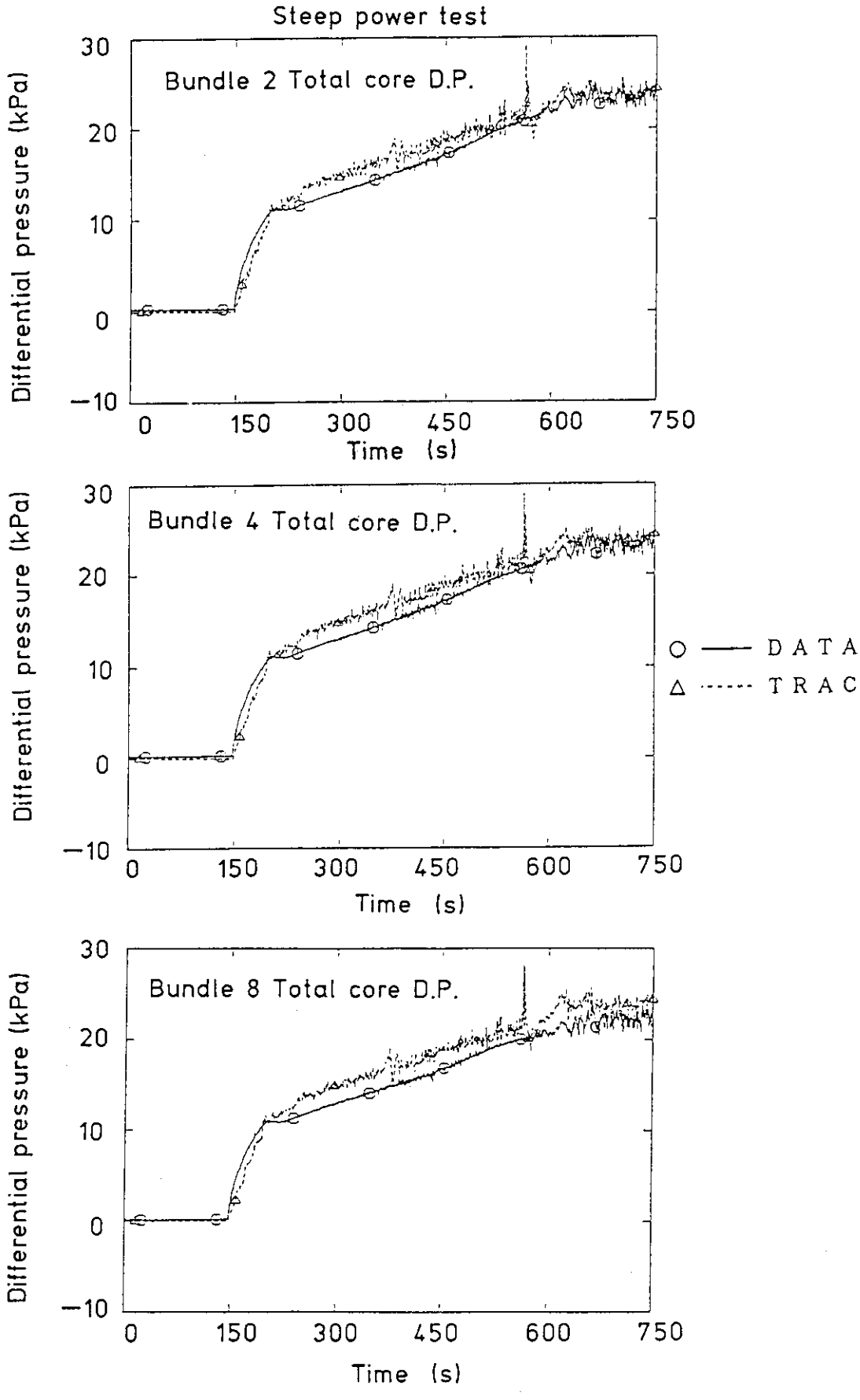

Fig.4.2.6 Comparison of total core differential pressure for steep power test

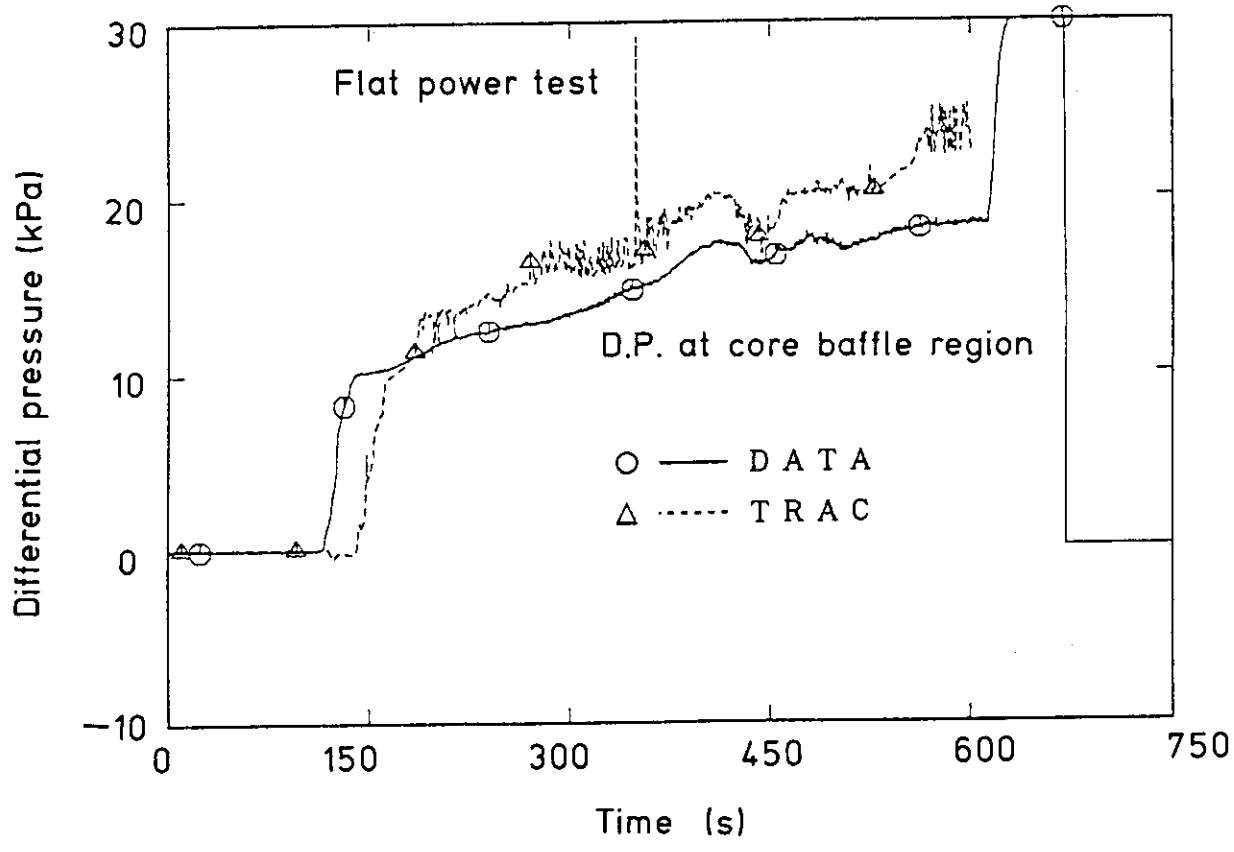

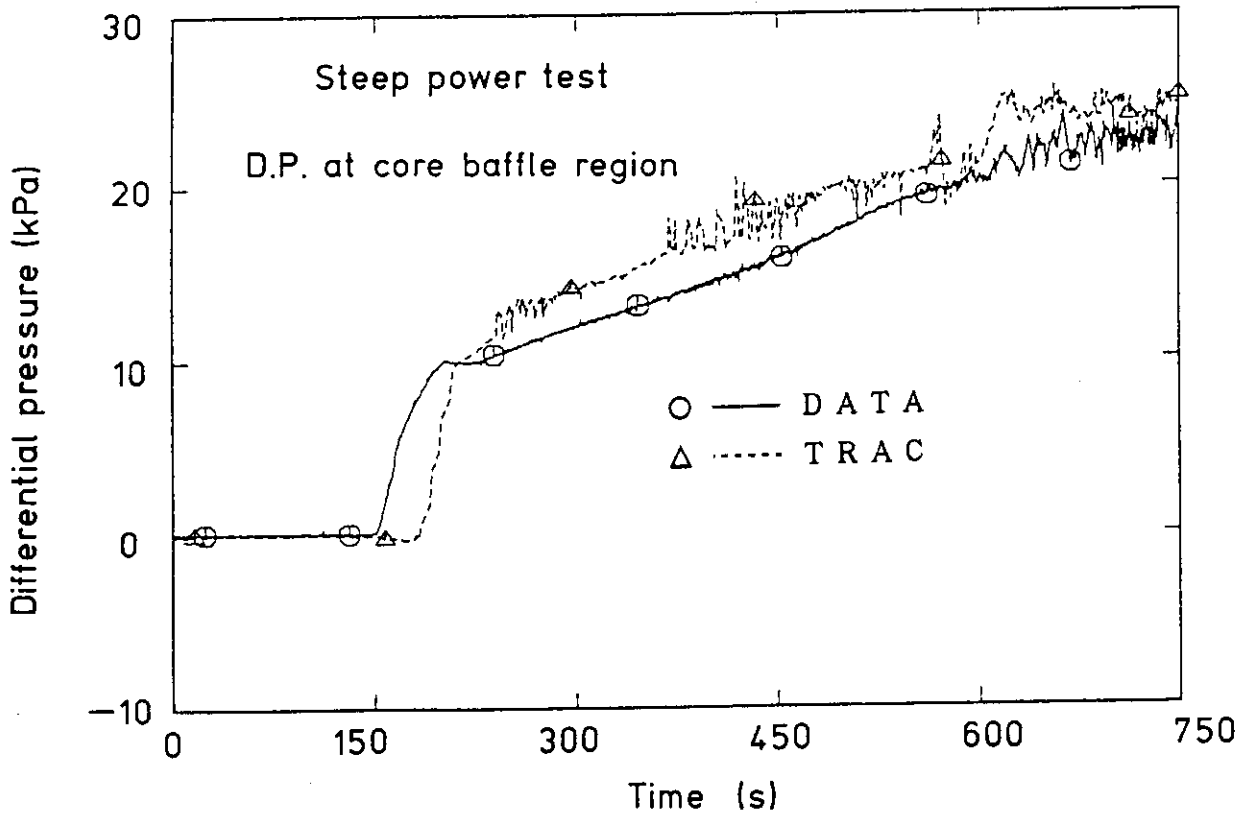

Fig.4.2.7 Comparison of differential pressure in core baffle region

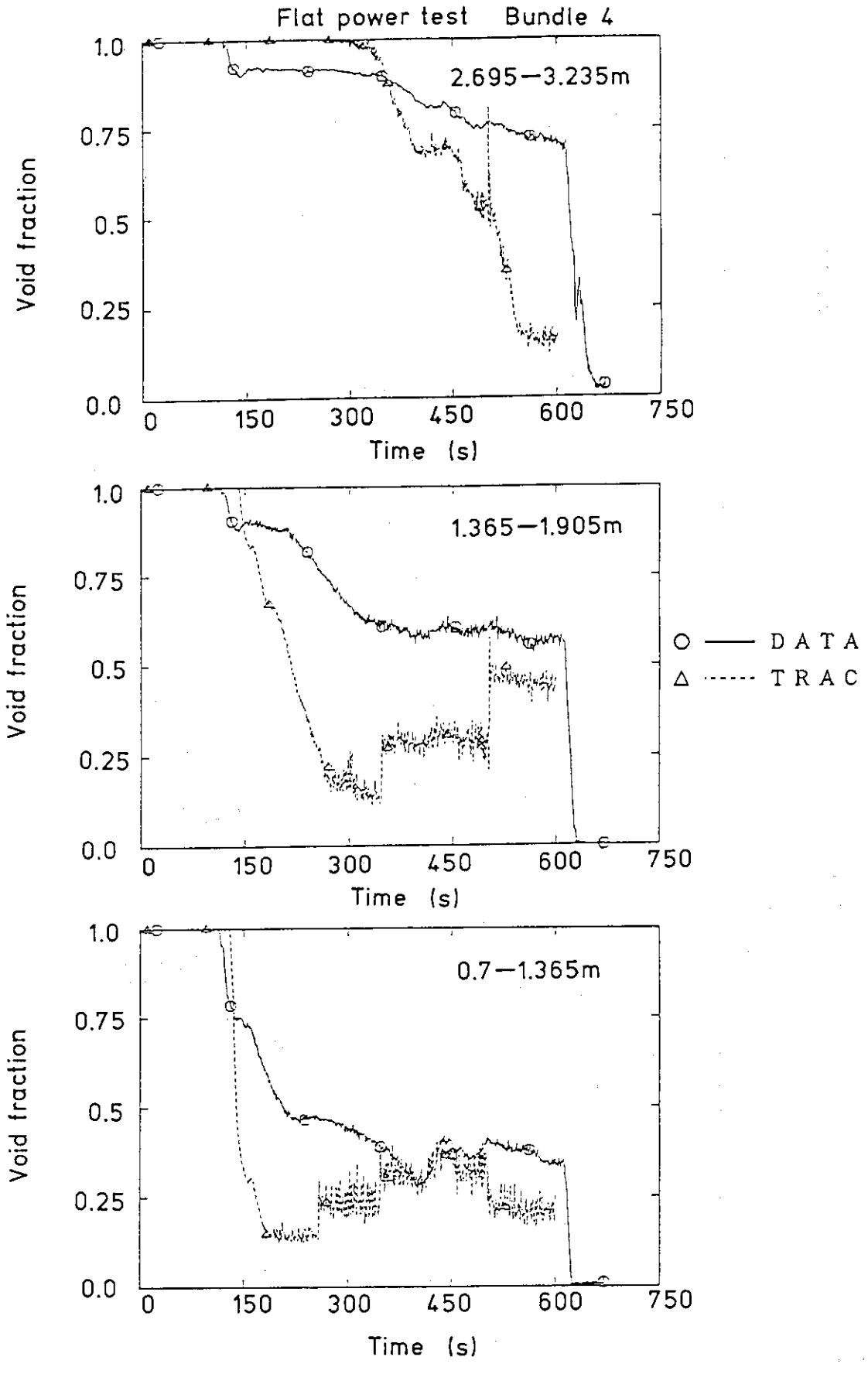

Fig.4.2.8 Comparison of sectional void fraction in bundle 4 for flat power test

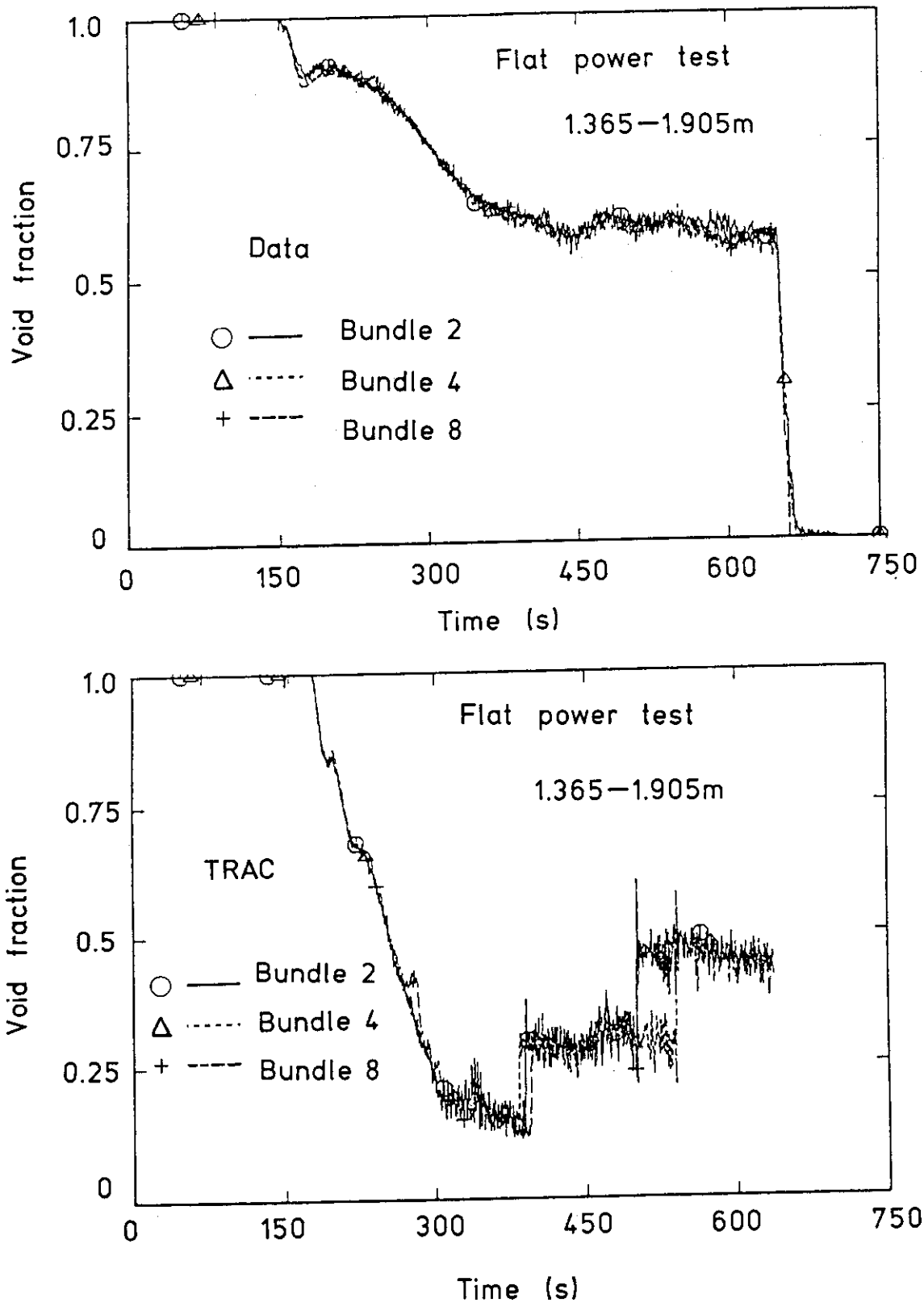

Fig.4.2.9 Comparison of radial distribution of sectional void fraction for flat power test

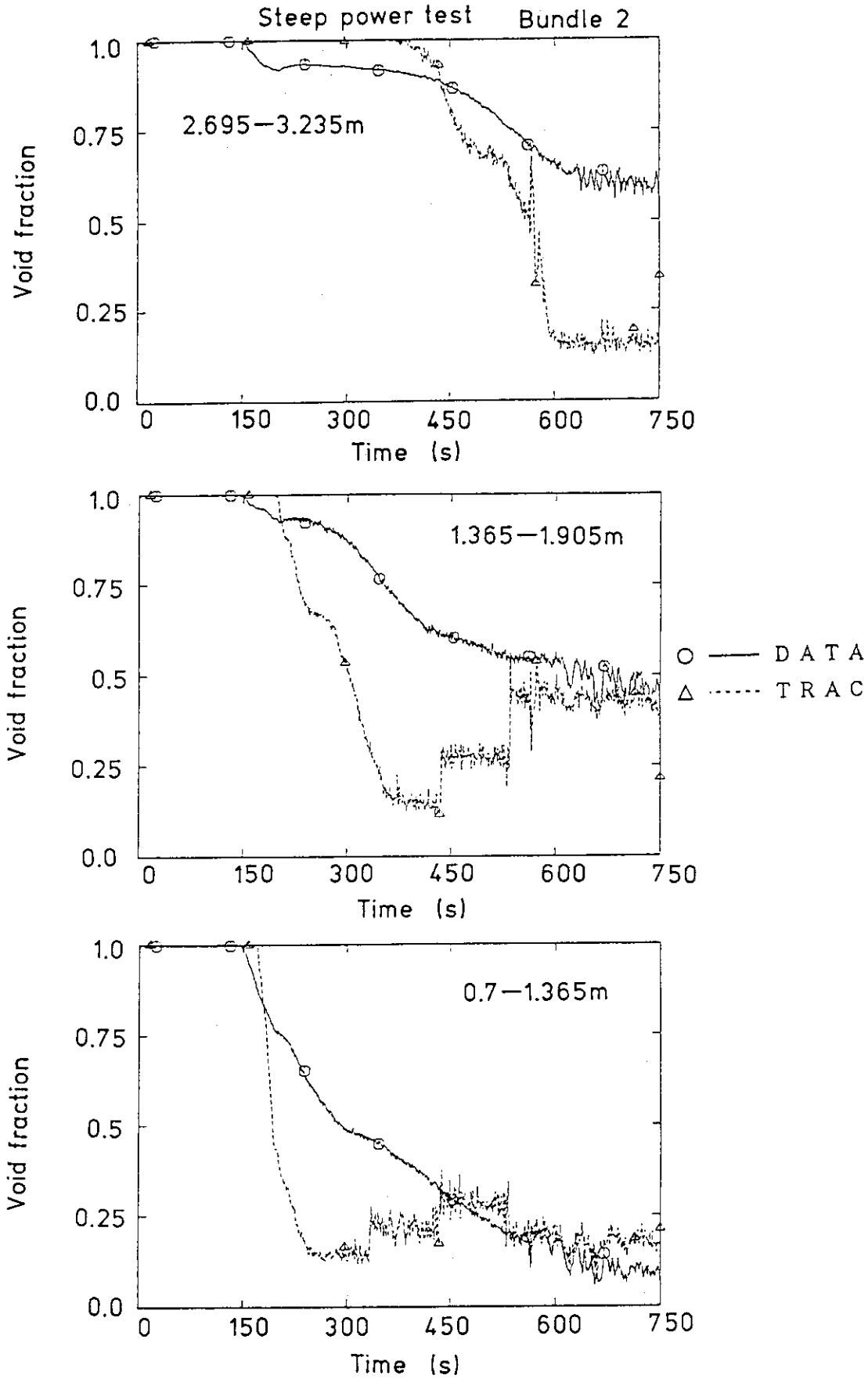

Fig.4.2.10(1) Comparison of sectional void fraction in bundle 2 for steep power test

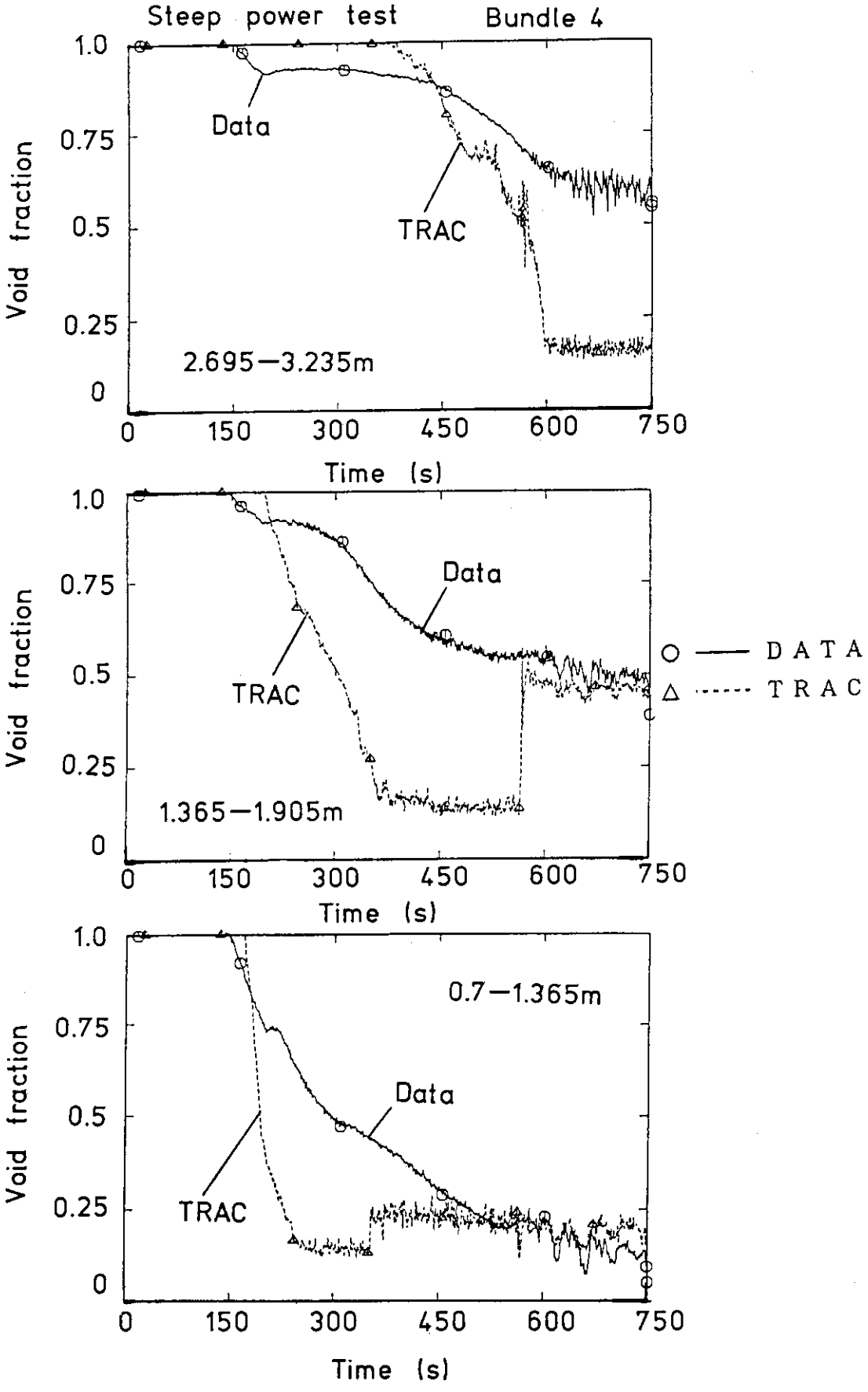

Fig.4.2.10(2) Comparison of sectional void fraction in bundle 4 for steep power test

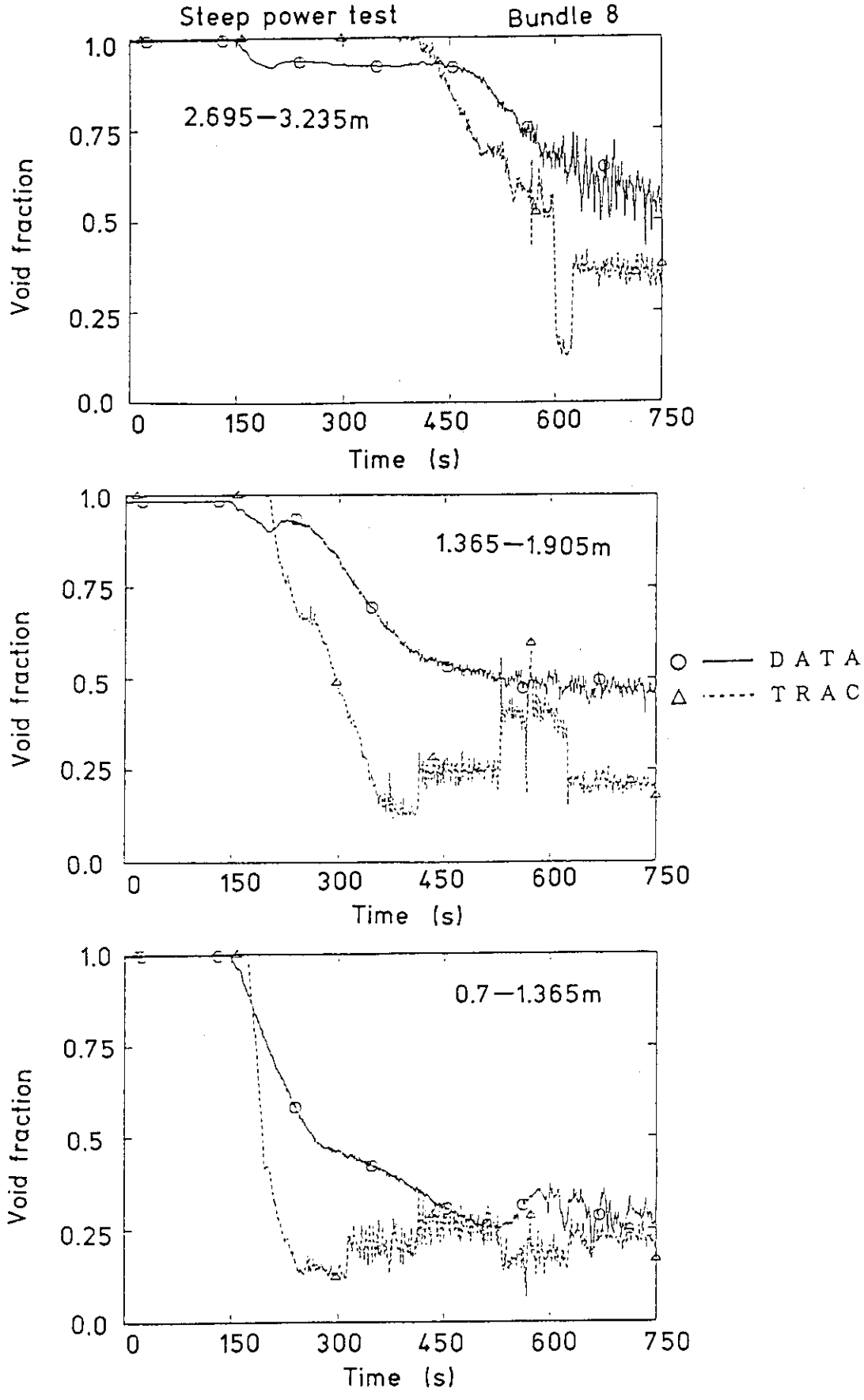

Fig.4.2.10(3) Comparison of sectional void fraction in bundle 8 for steep power test

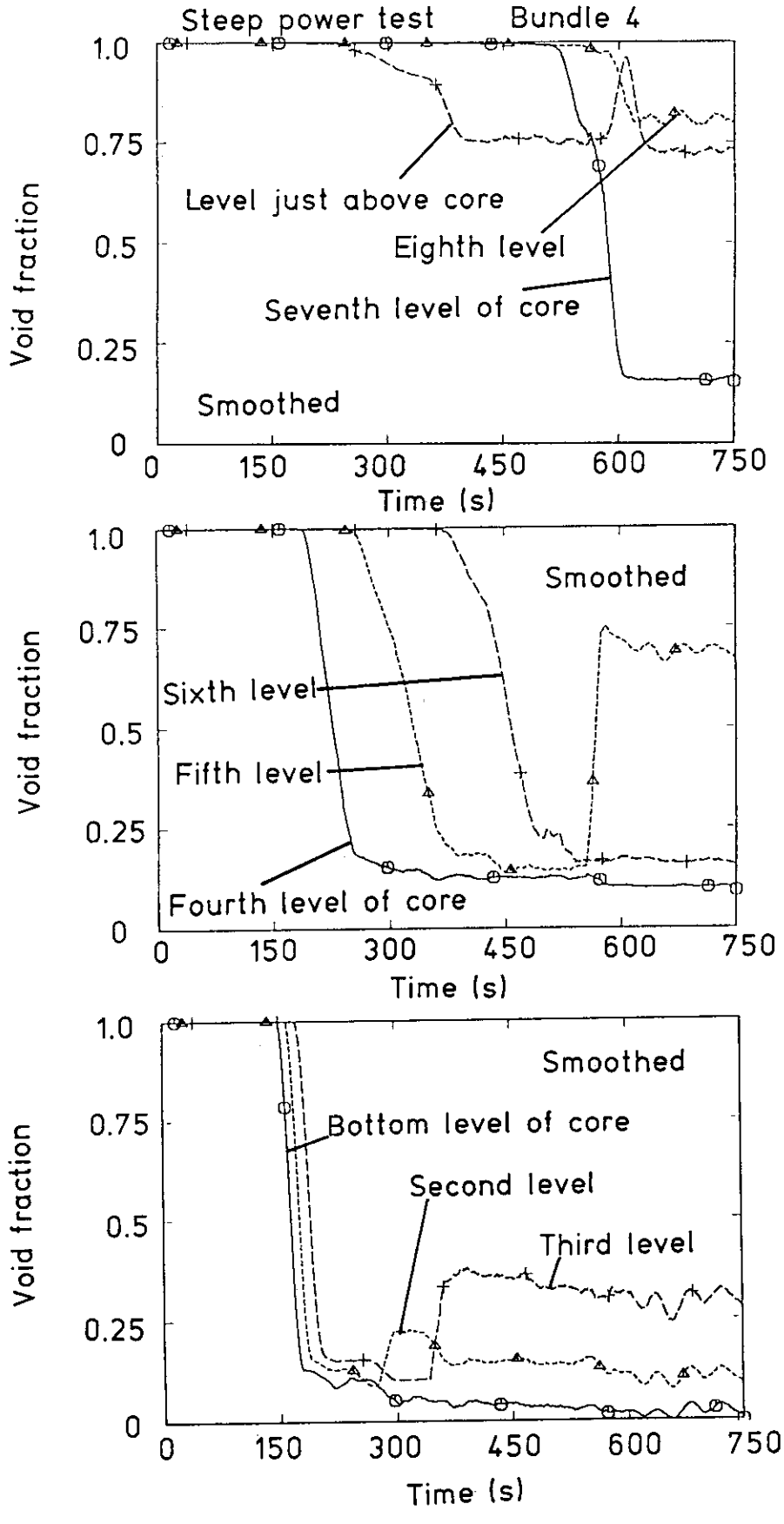

Fig.4.2.11 Comparison of void fraction in each computational cell in bundle 4 for steep power test

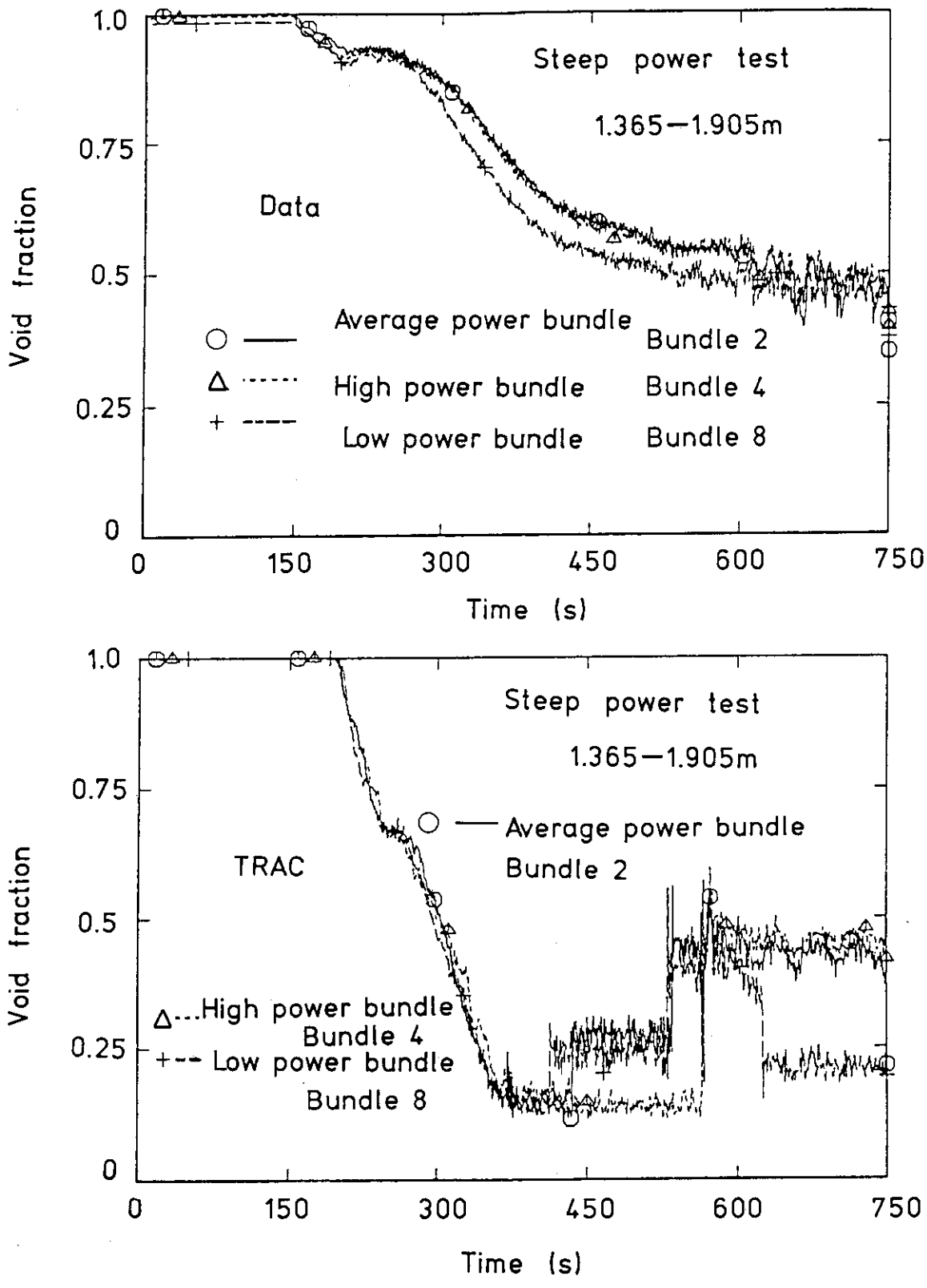

Fig.4.2.12(1) Comparison of radial distribution of sectional void fraction for steep power test

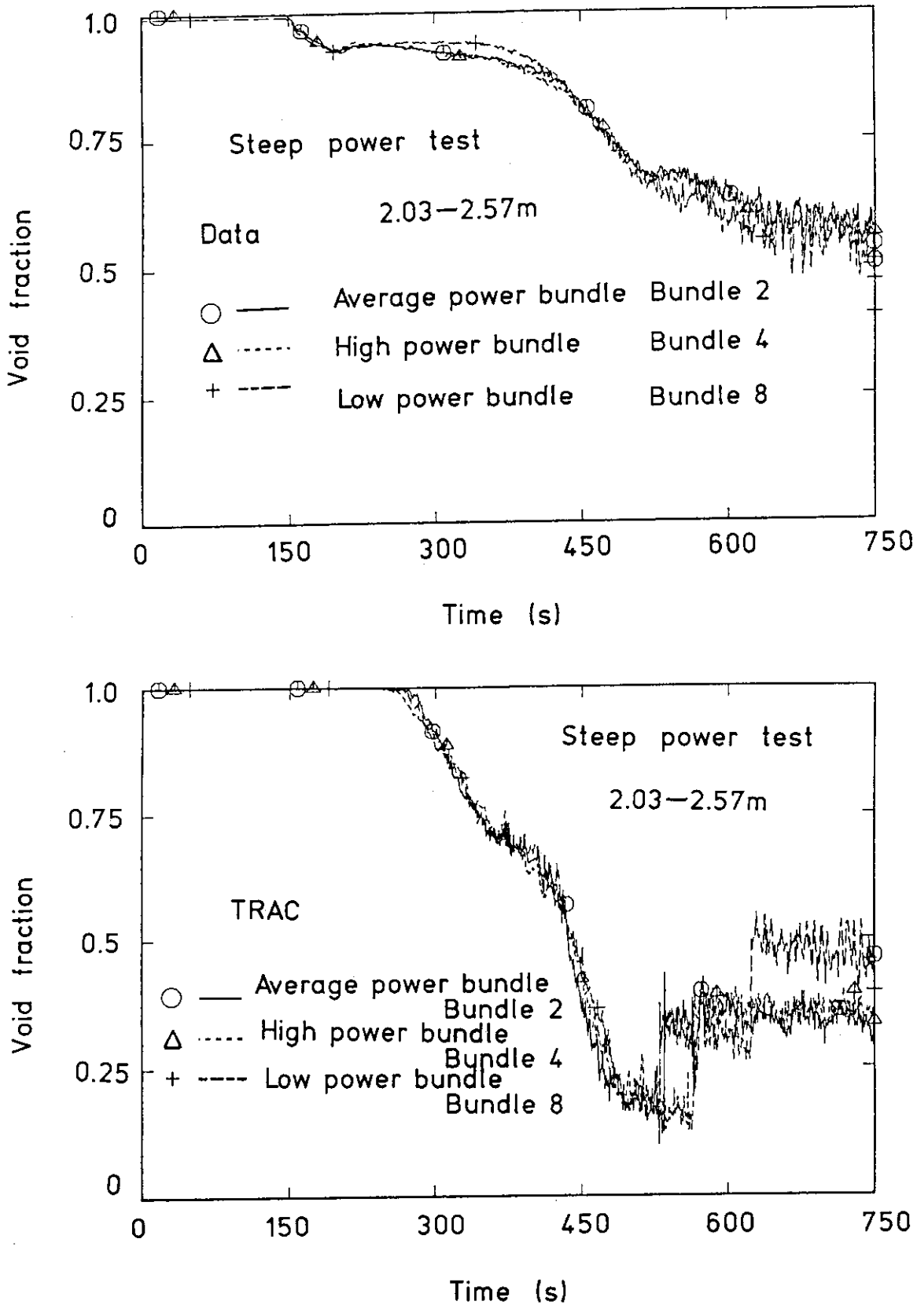

Fig.4.2.12(2) Comparison of radial distribution of sectional void fraction for steep power test

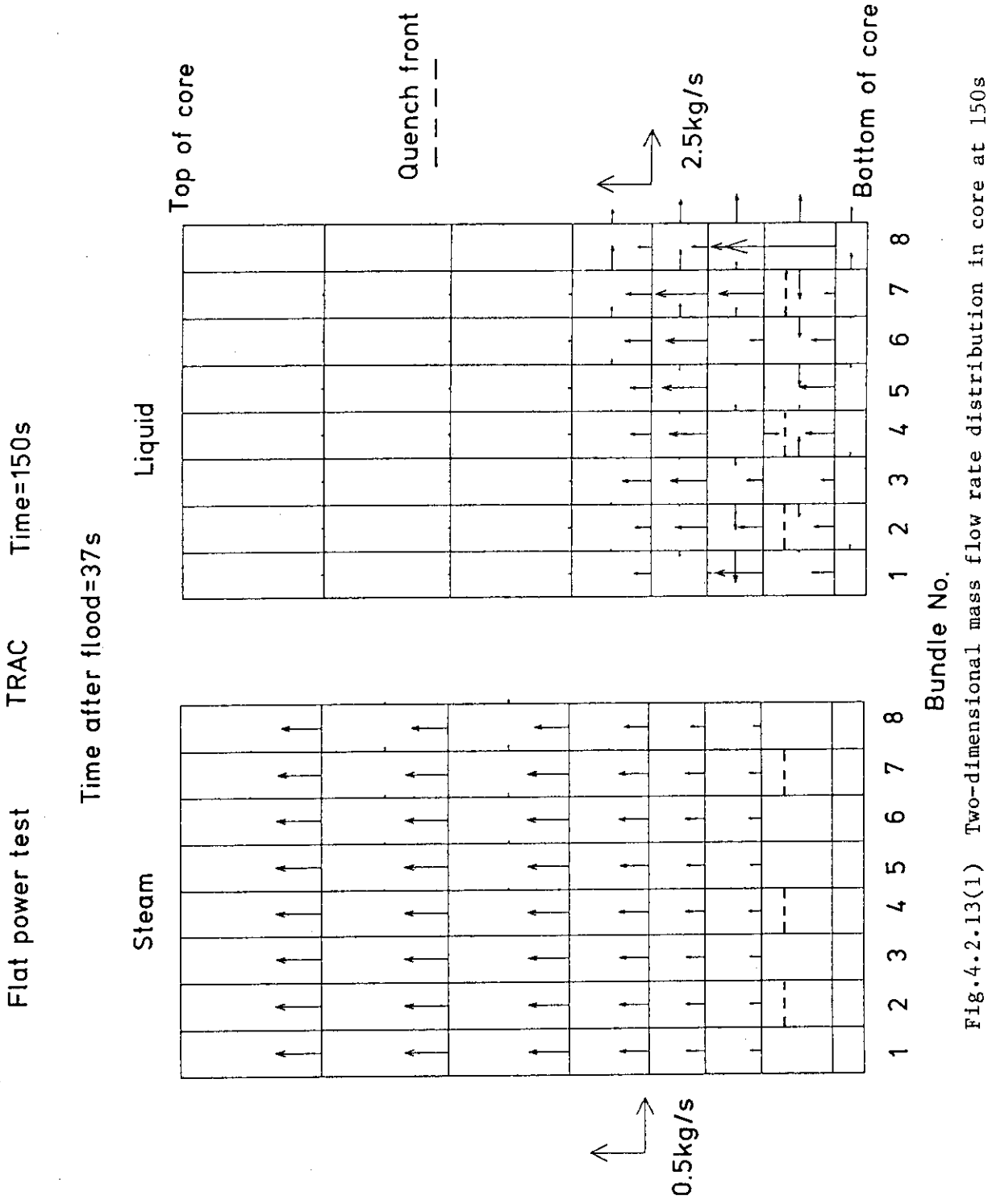

Fig.4.2.13(1) Two-dimensional mass flow rate distribution in core at 150s for flat power test

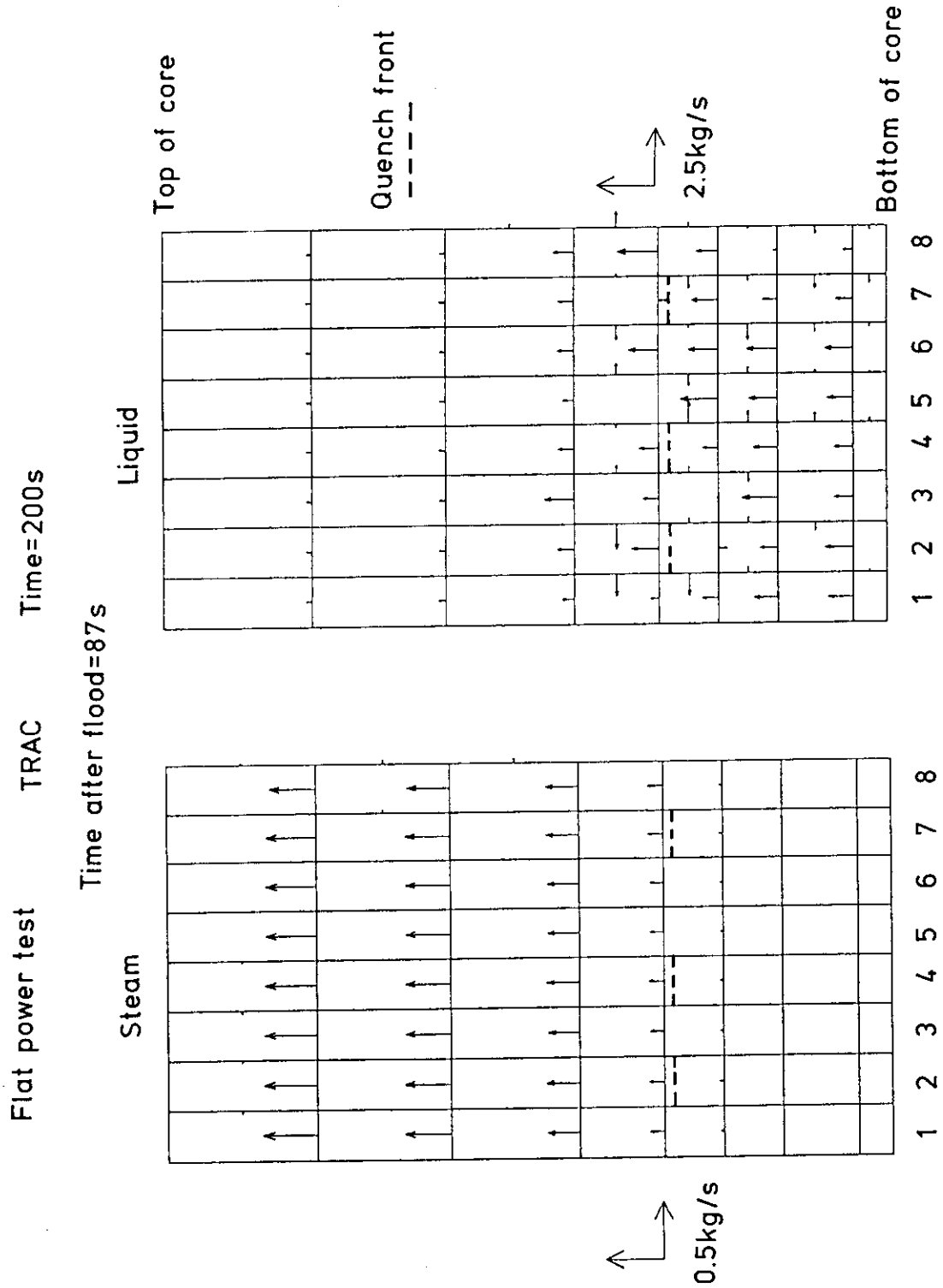

Fig.4.2.13(2) Two-dimensional mass flow rate distribution in core at 200s for flat power test

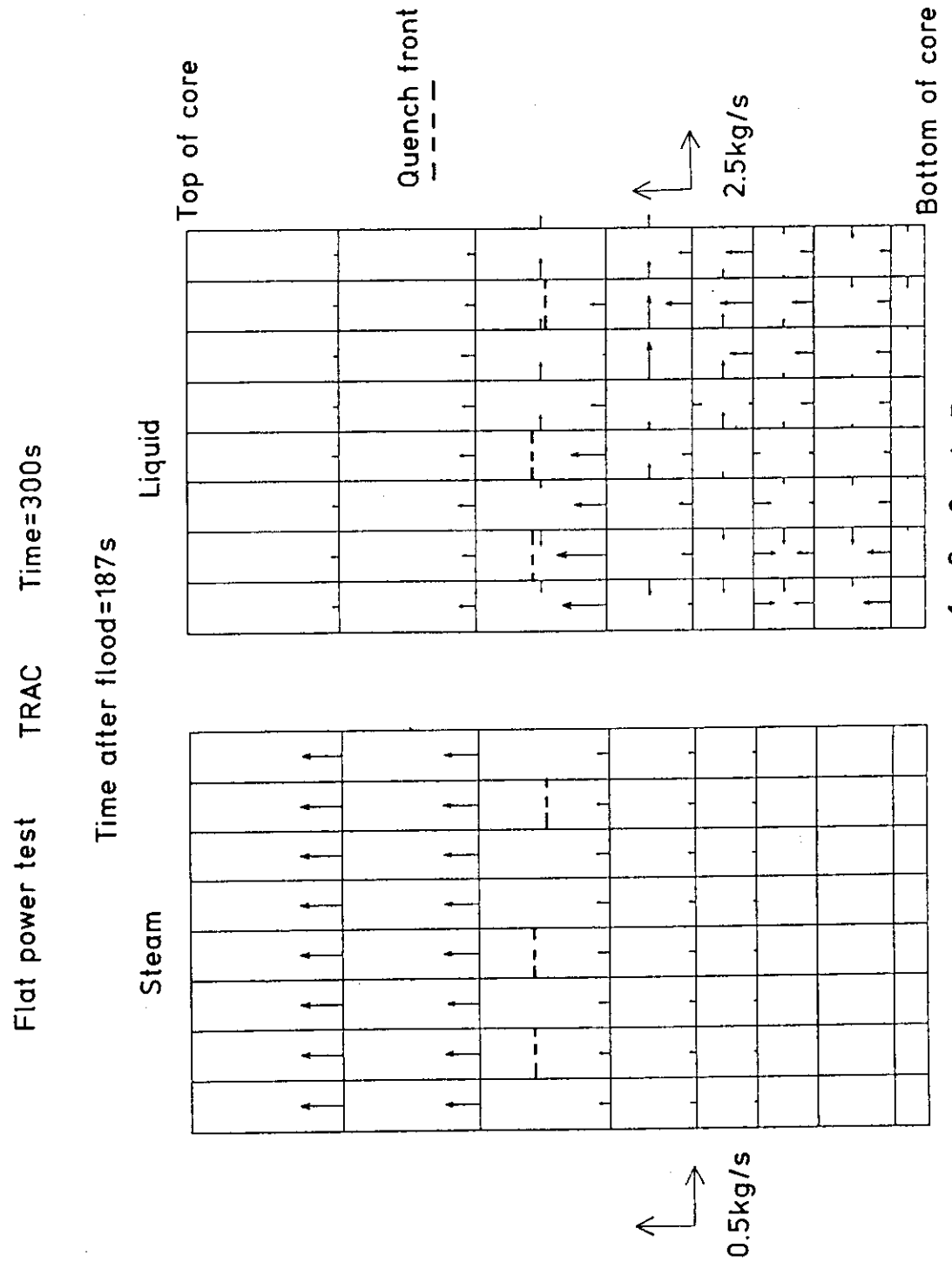

Fig.4.2.13(3) Two-dimensional mass flow rate distribution in core at 300s for flat power test

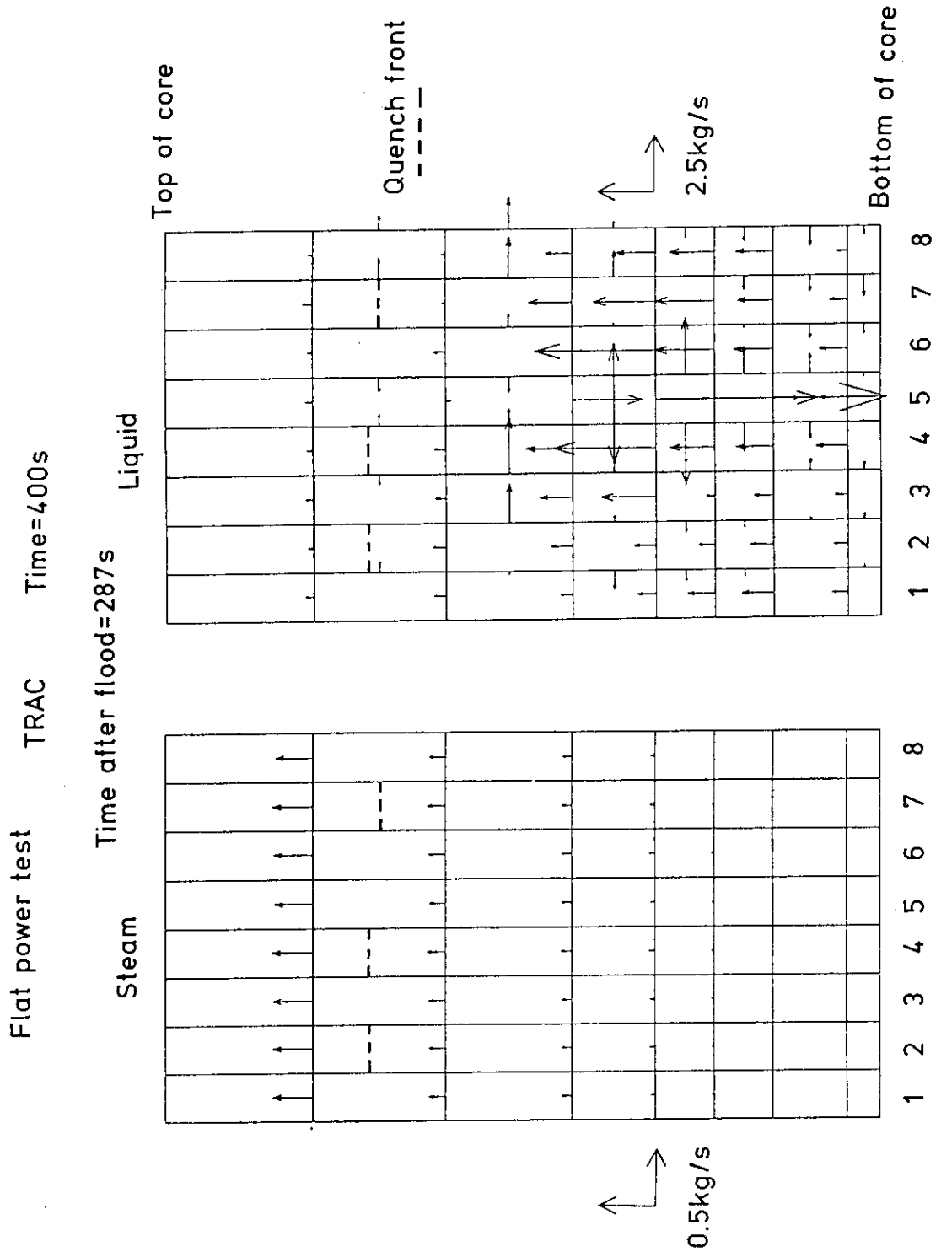

Fig.4.2.13(4) Two-dimensional mass flow rate distribution in core at 400s for flat power test

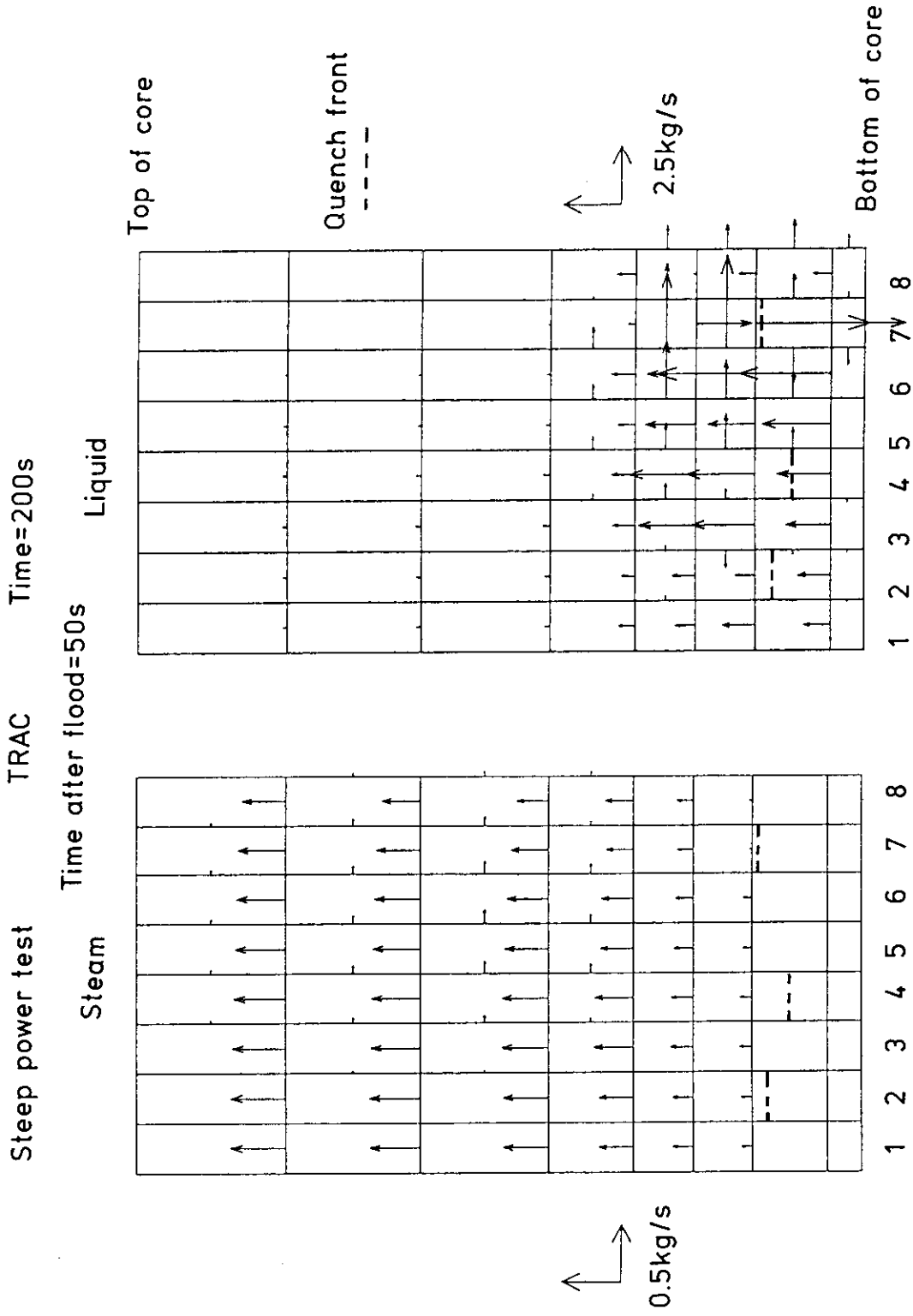

Fig.4.2.14(1) Two-dimensional mass flow rate distribution in core at 200s for steep power test

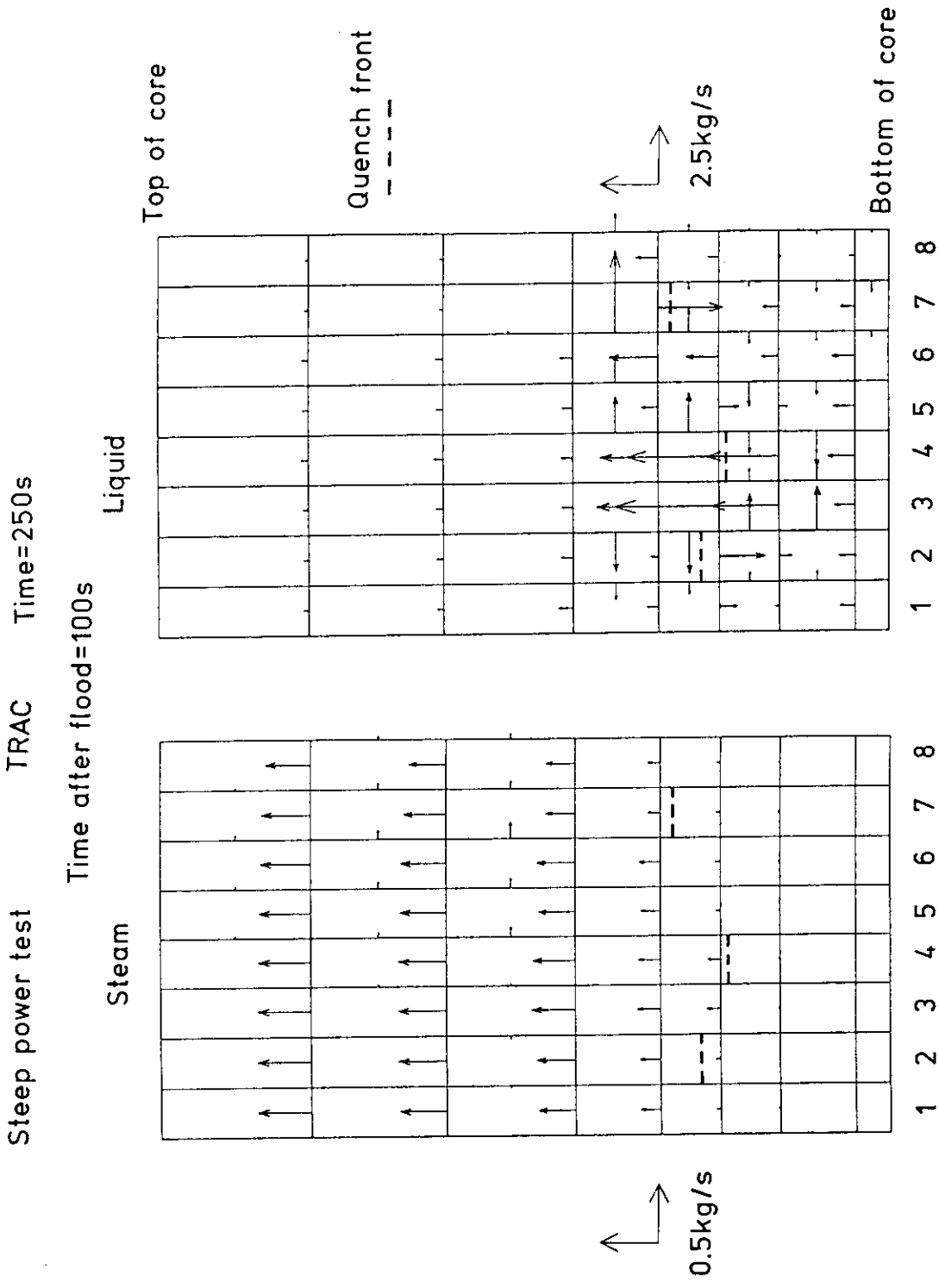

Fig.4.2.14(2) Two-dimensional mass flow rate distribution in core at 250s for steep power test

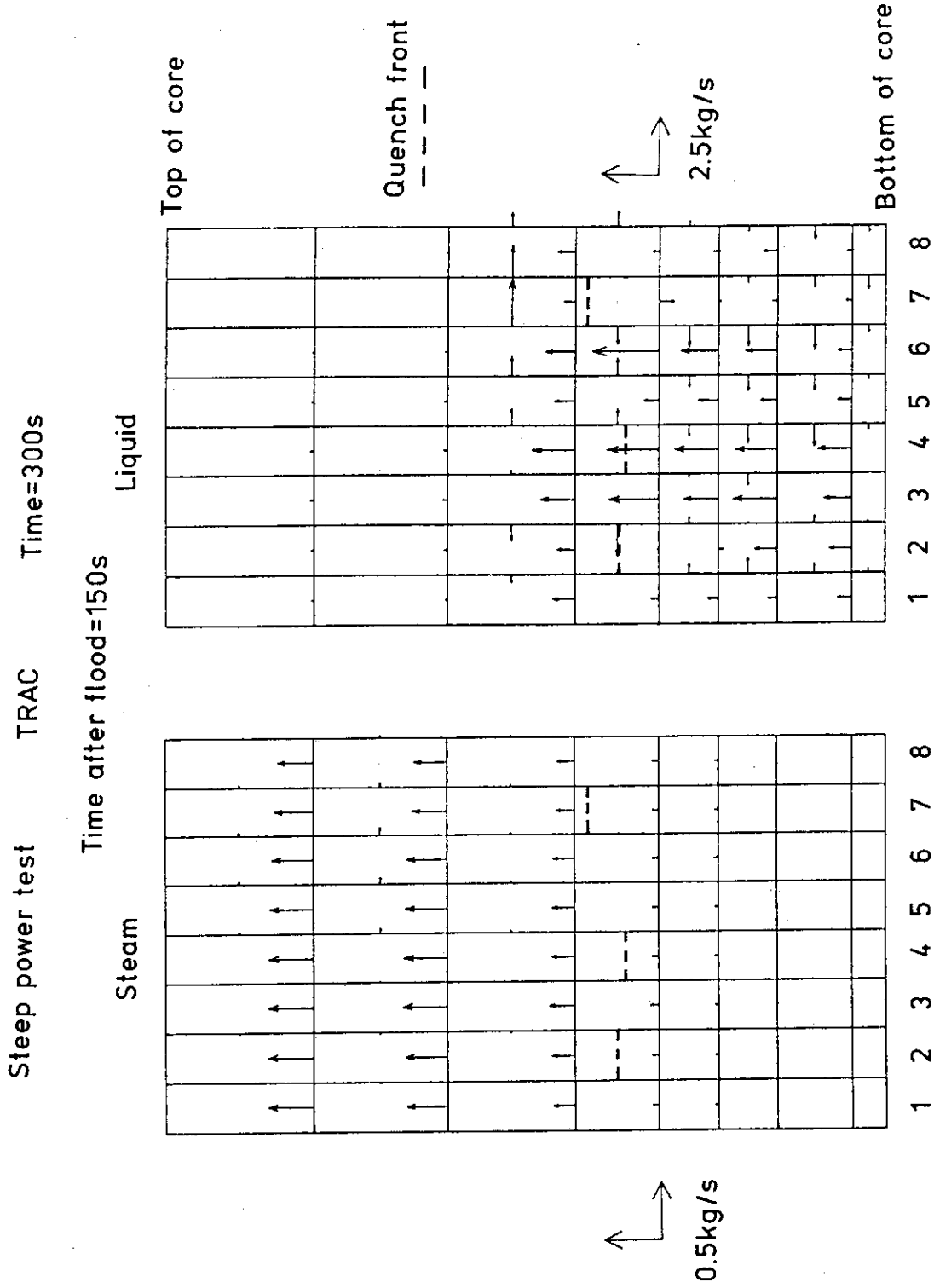

Fig.4.2.14(3) Two-dimensional mass flow rate distribution in core at 300s for steep power test

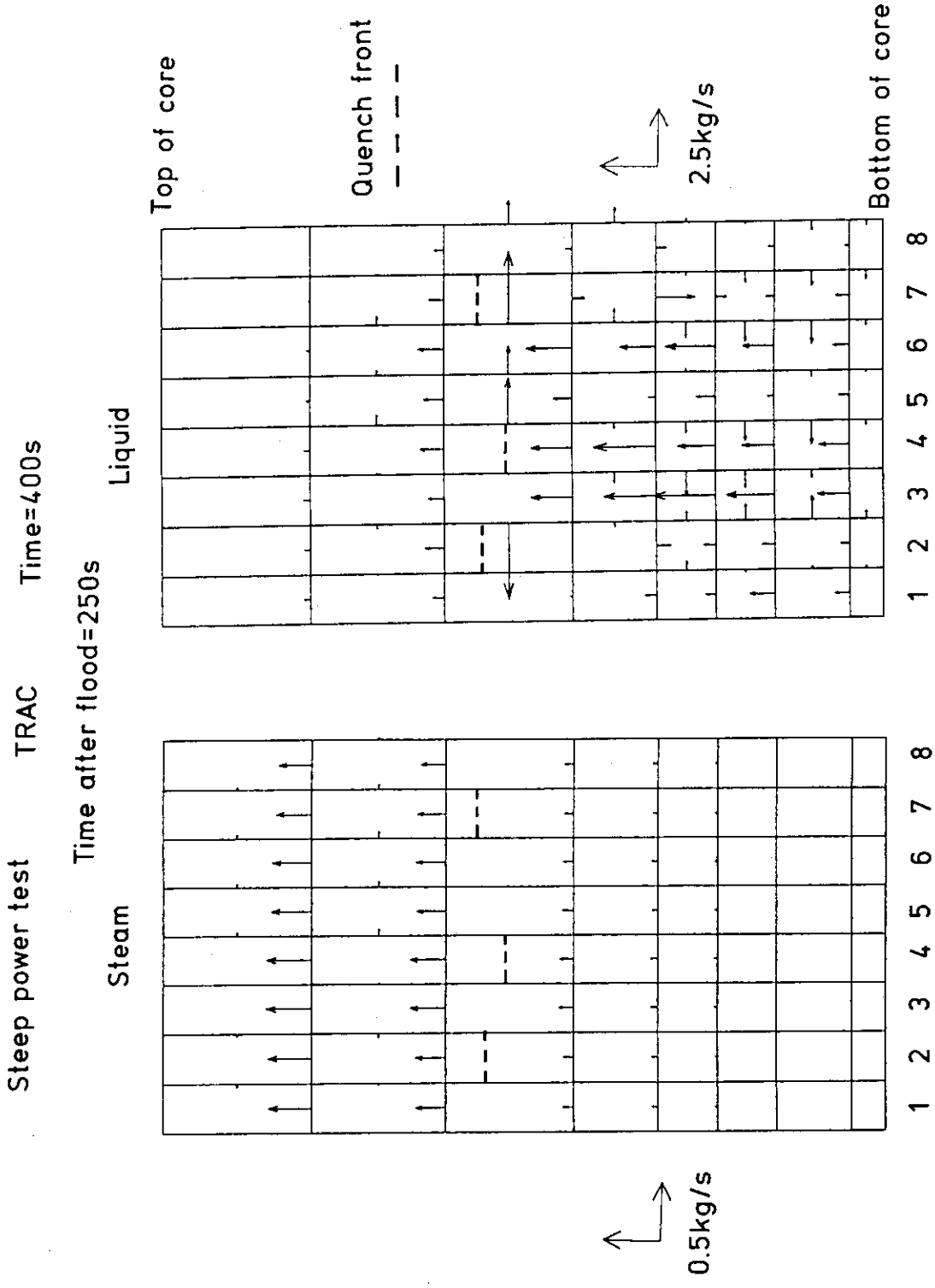

Fig.4.2.14(4) Two-dimensional mass flow rate distribution in core at 400s for steep power test

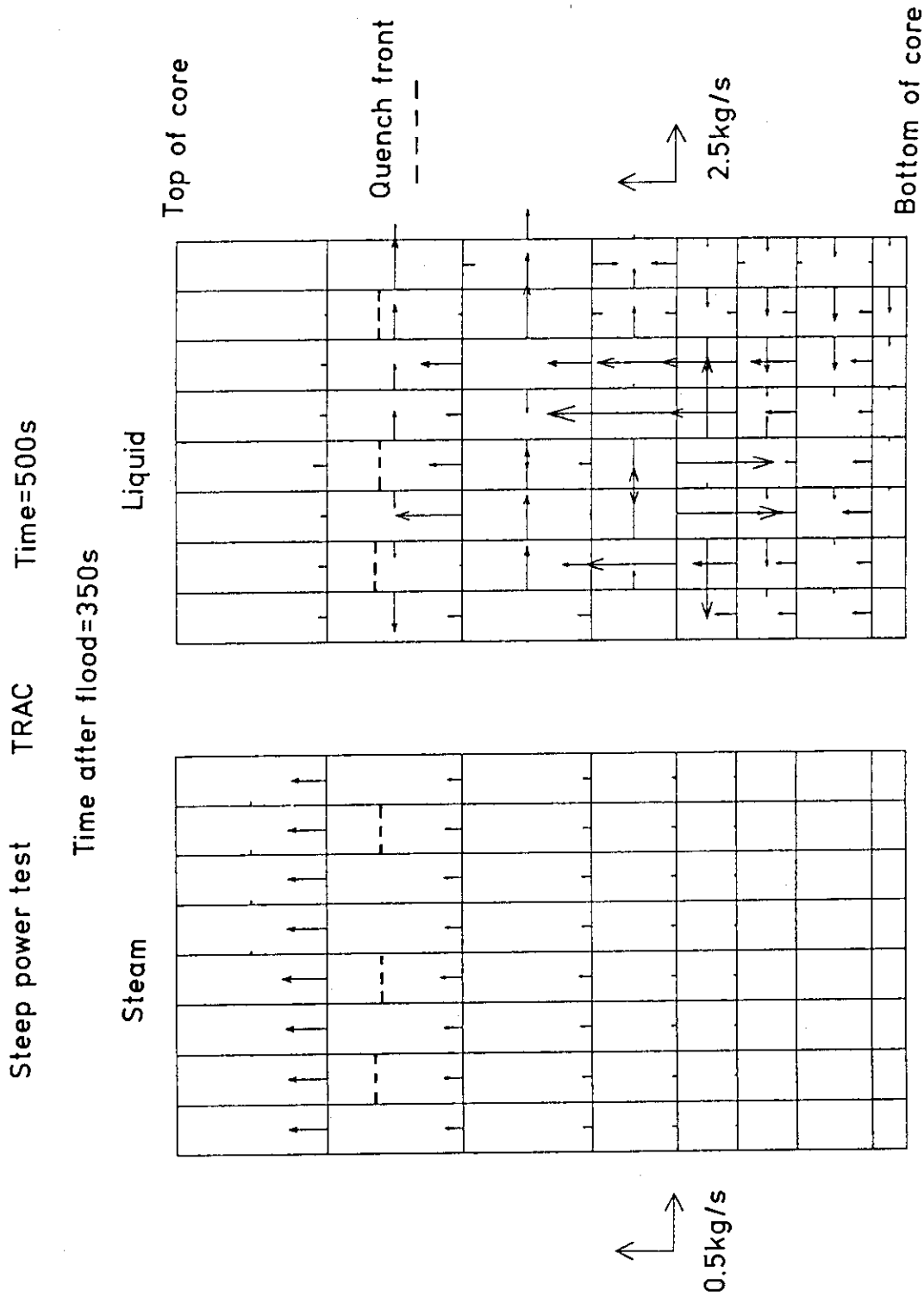

Fig.4.2.14(5) Two-dimensional mass flow rate distribution in core at 500s for steep power test

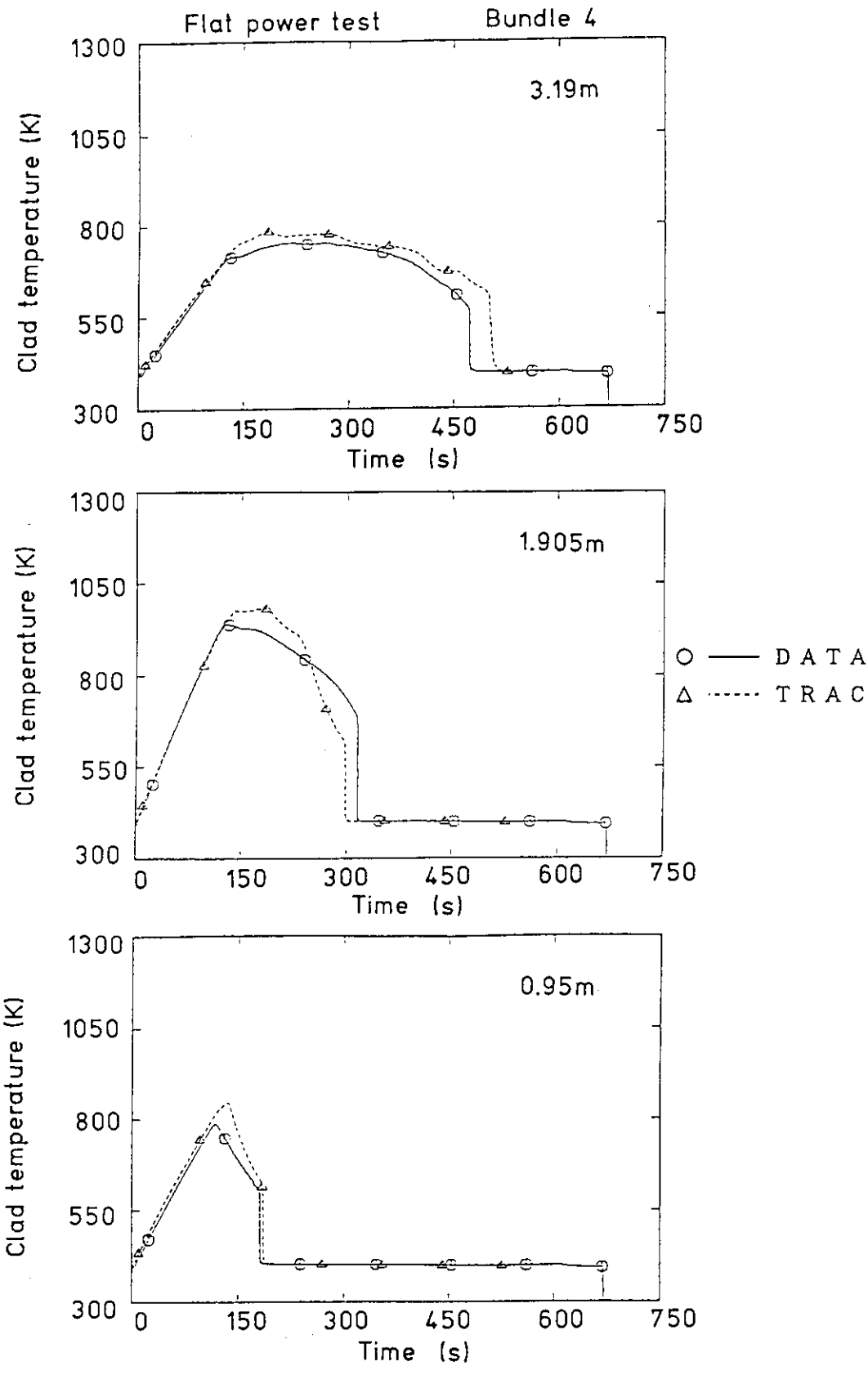

Fig.4.3.1 Comparison of clad surface temperature in bundle 4 for flat power test

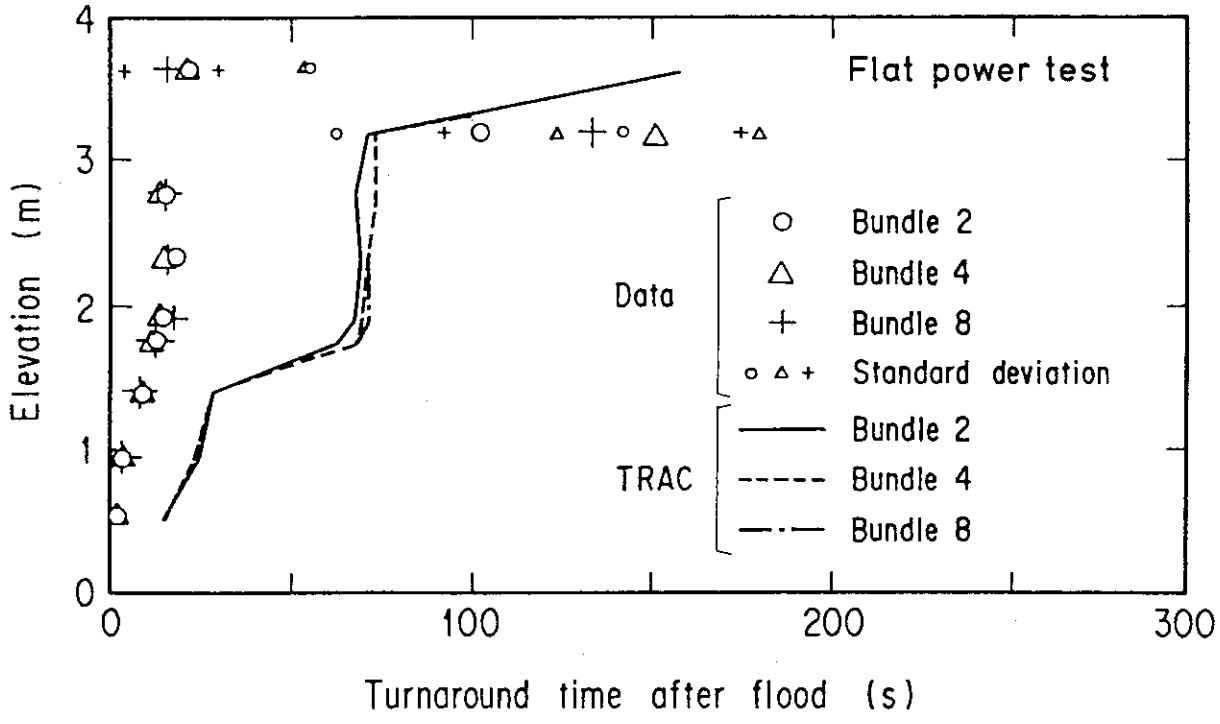

Fig.4.3.2 Comparison of turnaround time after flood for flat power test

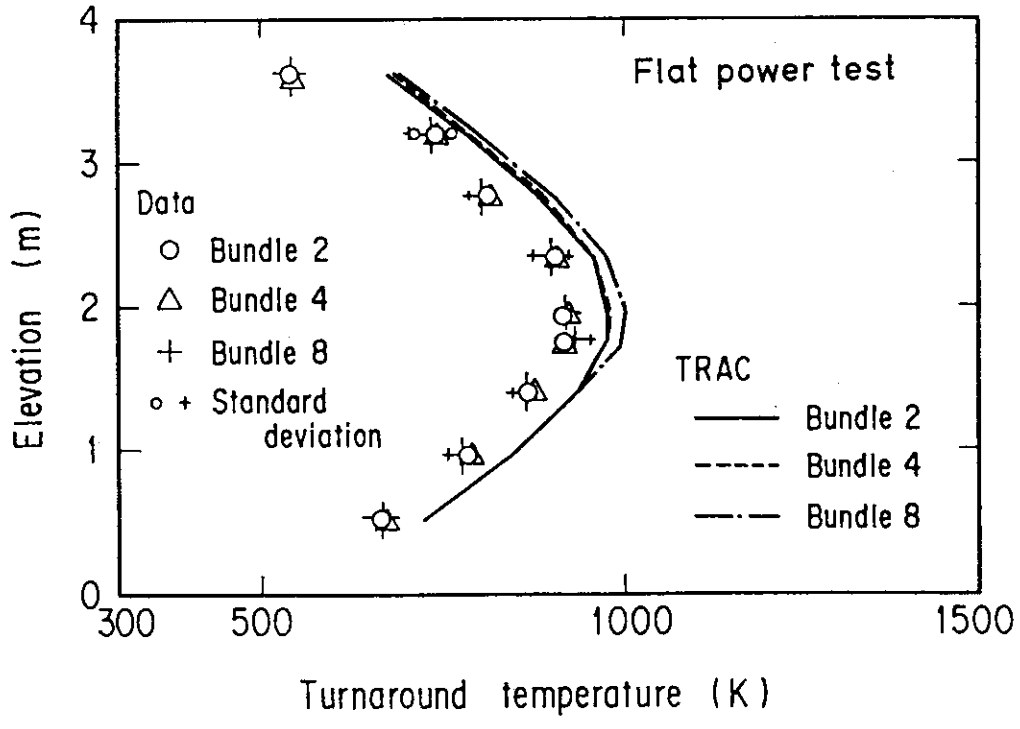

Fig.4.3.3 Comparison of turnaround temperature for flat power test

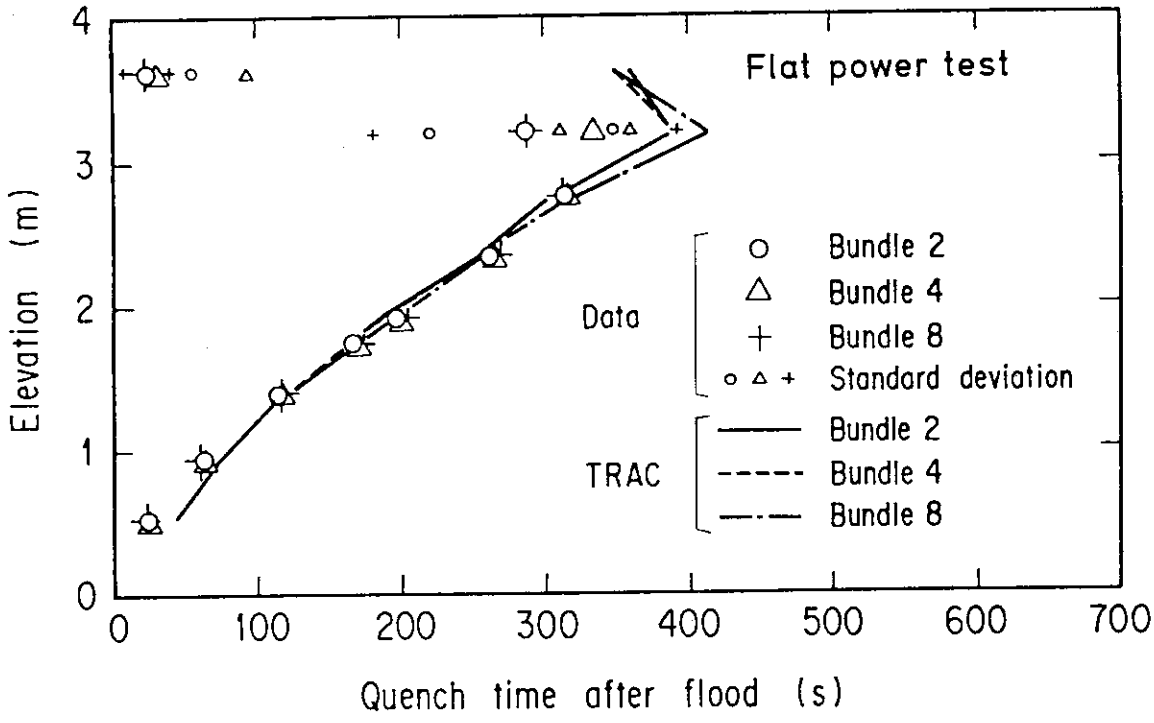

Fig.4.3.4 Comparison of quench time after flood for flat power test

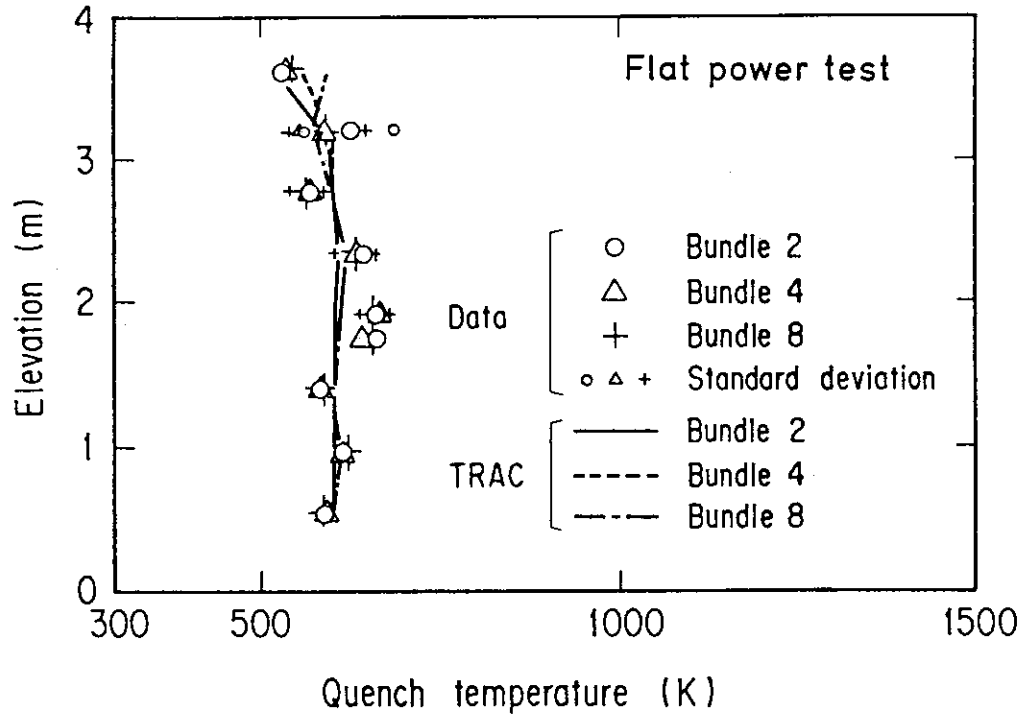

Fig.4.3.5 Comparison of quench temperature for flat power test

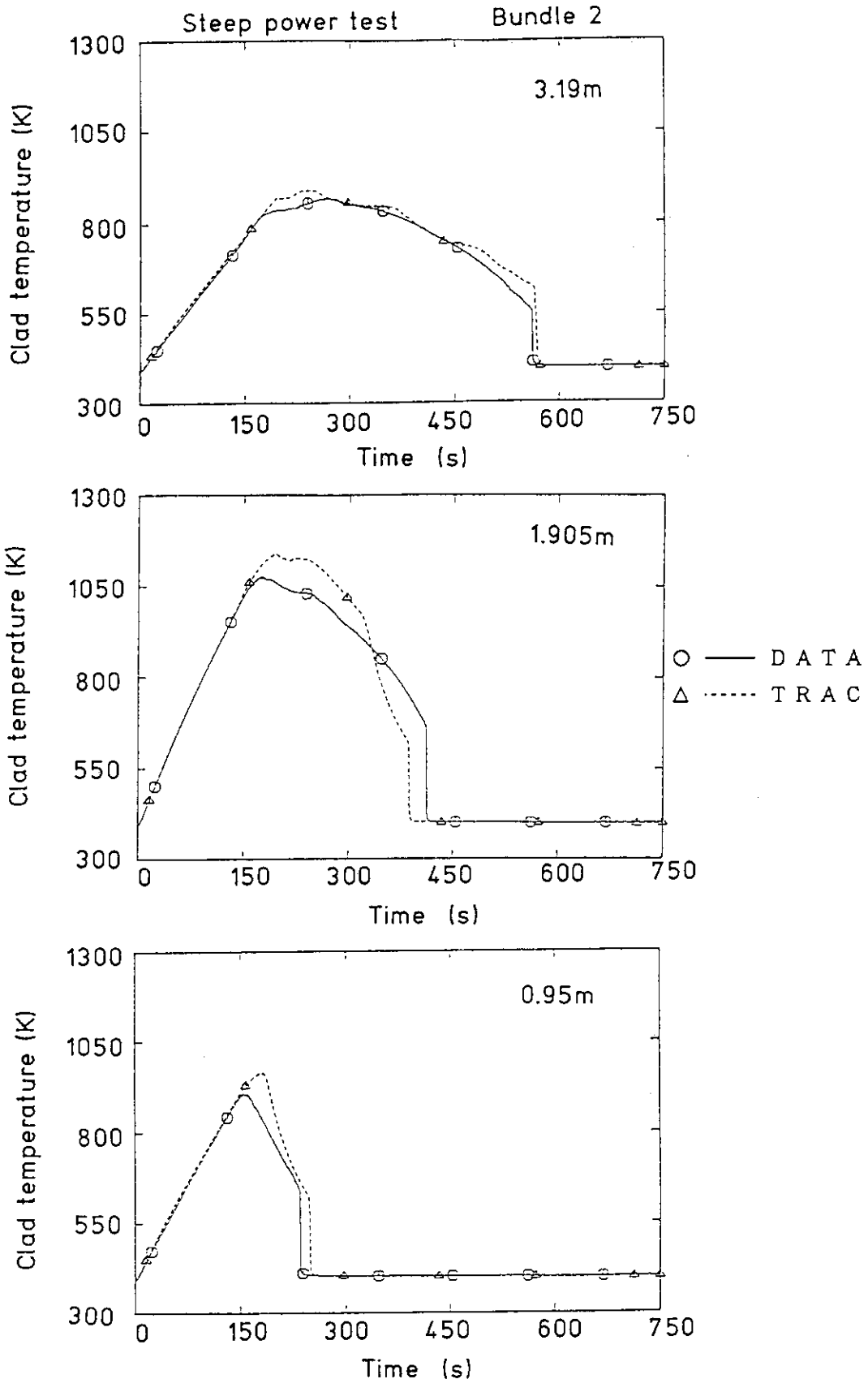

Fig.4.3.6(1) Comparison of clad surface temperature in bundle 2 for steep power test

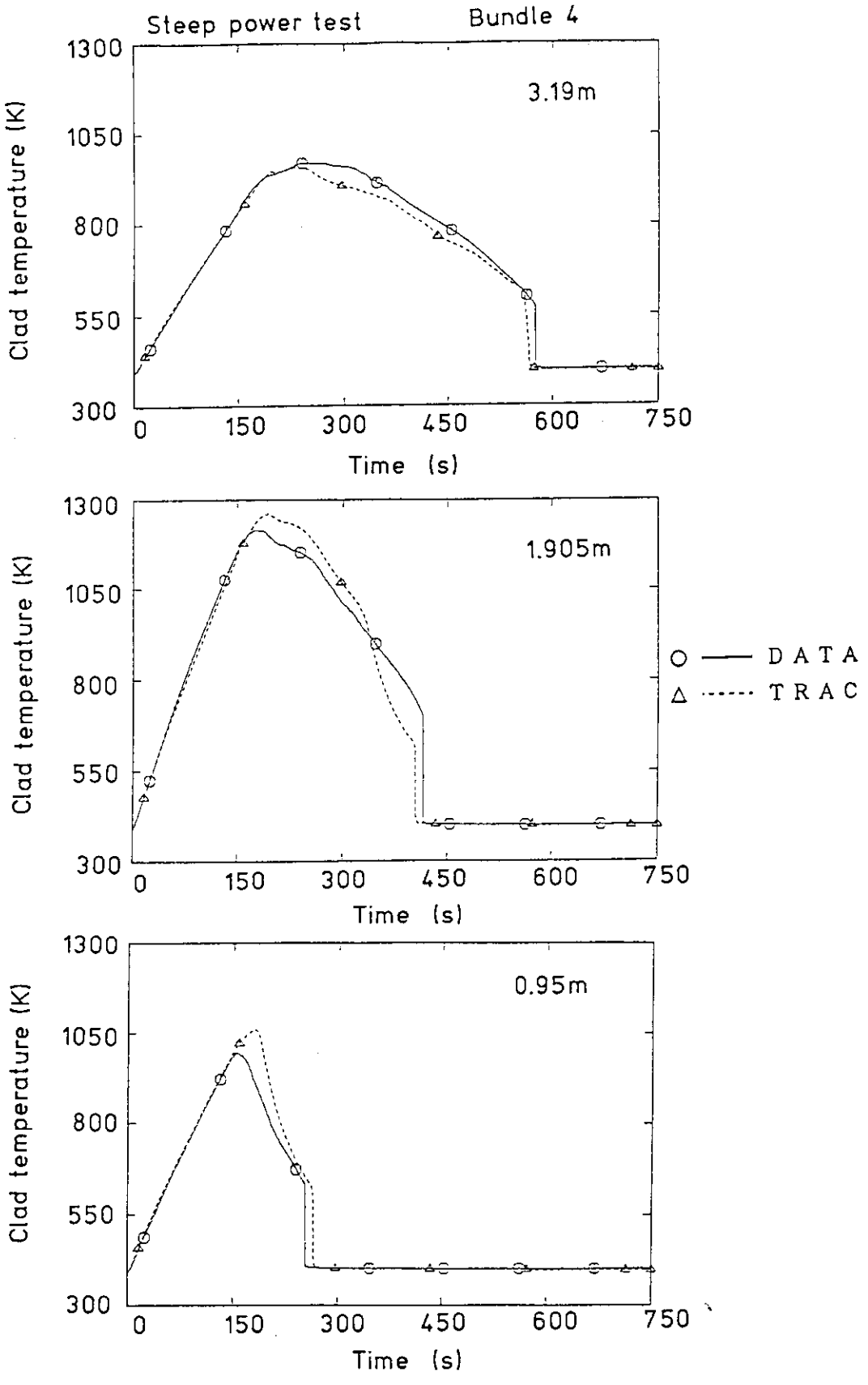

Fig.4.3.6(2) Comparison of clad surface temperature in bundle 4 for steep power test

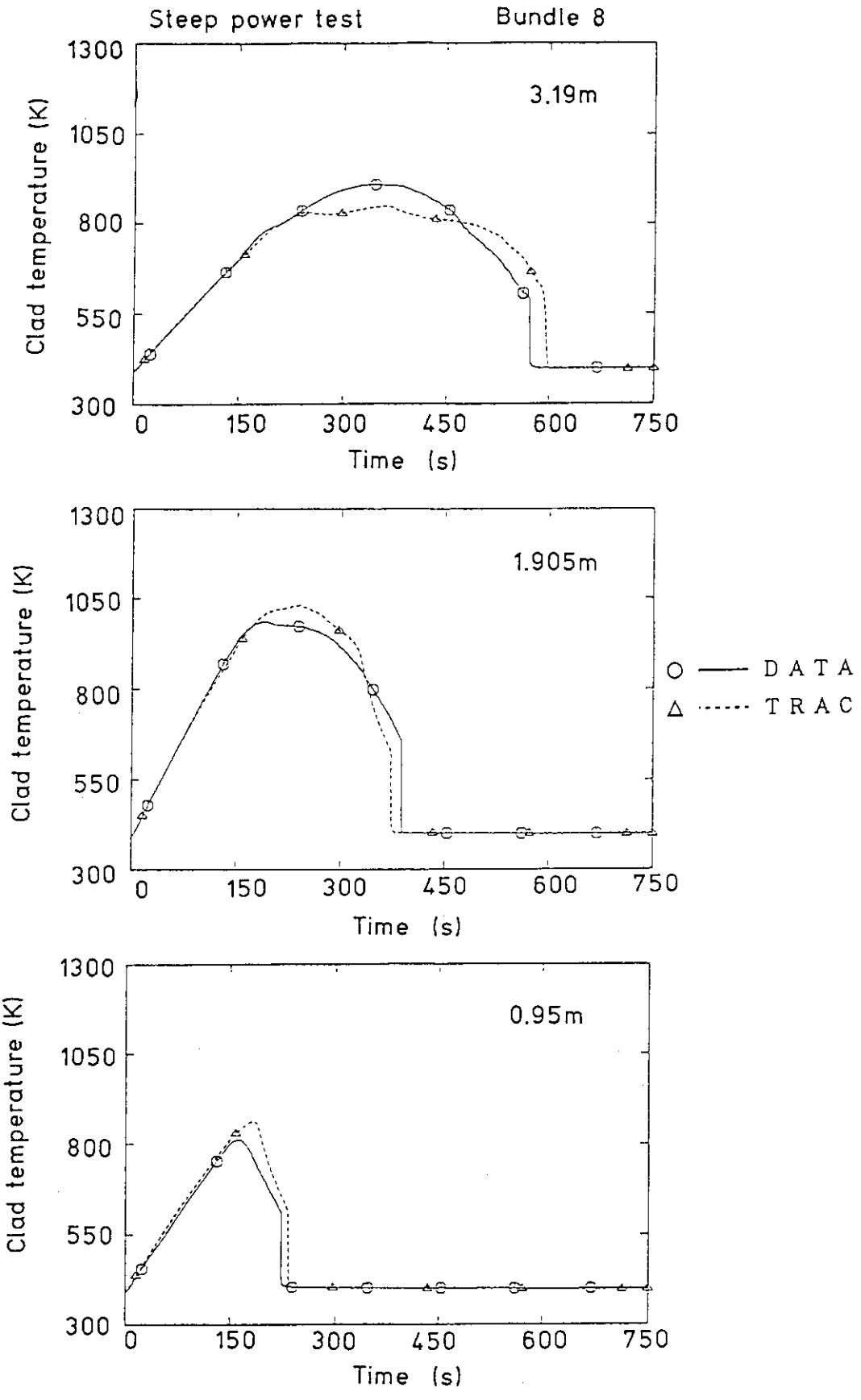

Fig.4.3.6(3) Comparison of clad surface temperature in bundle 8 for steep power test

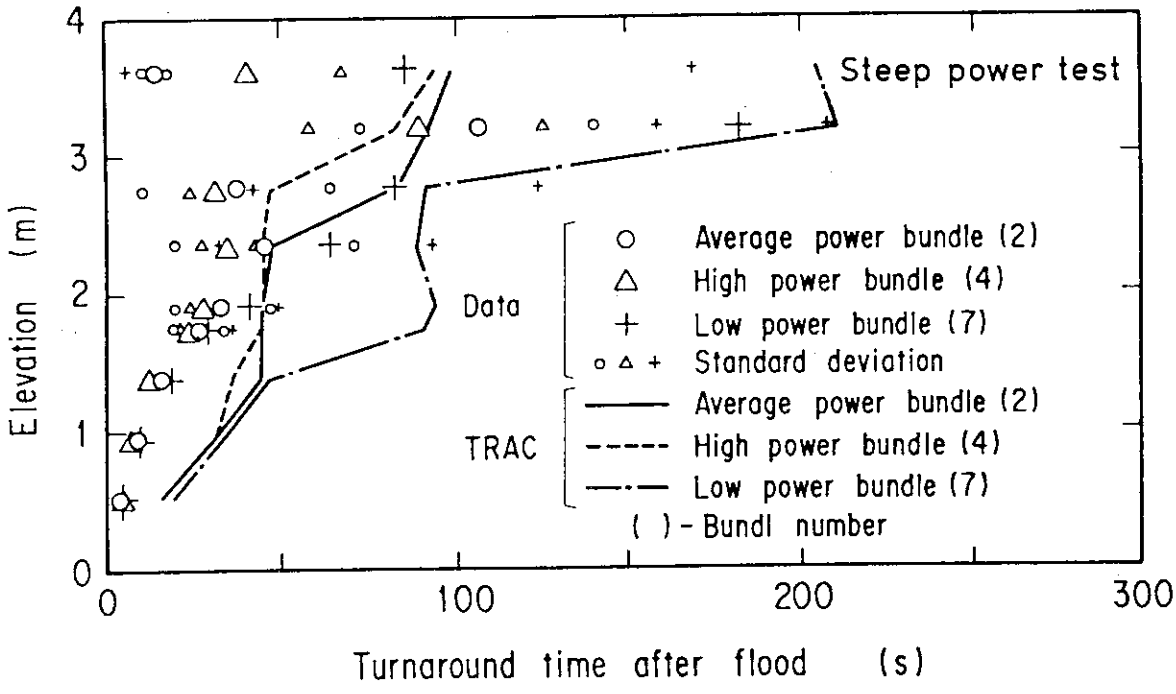

Fig.4.3.7 Comparison of turnaround time after flood for steep power test

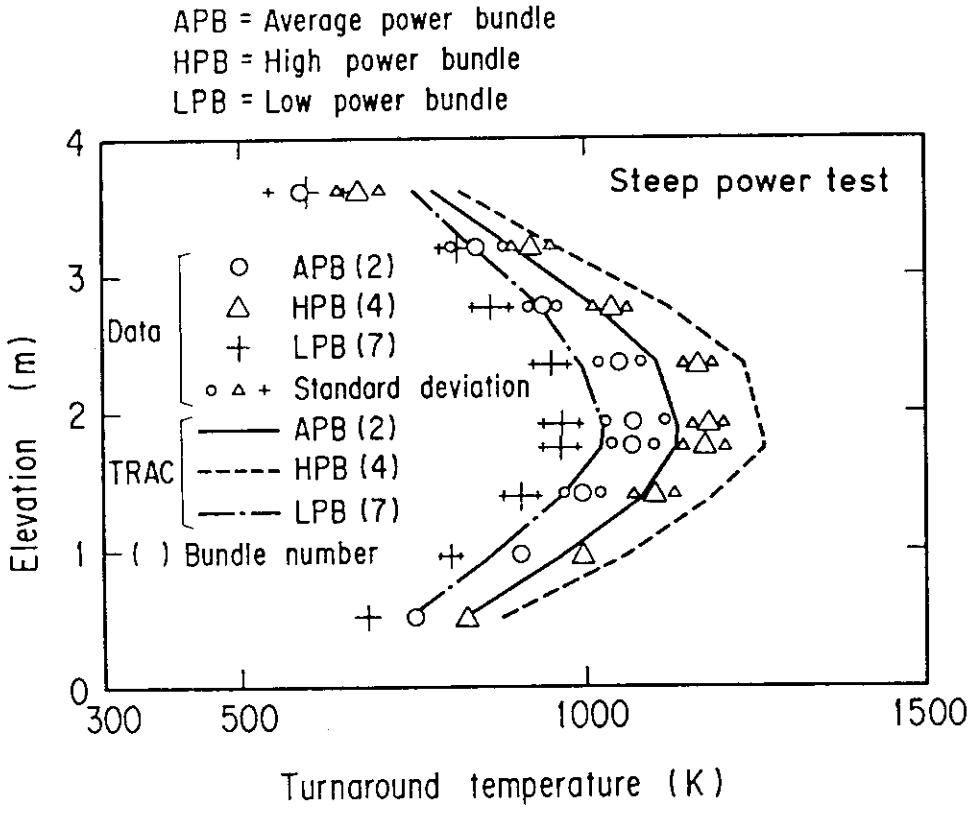

Fig.4.3.8 Comparison of turnaround temperature for steep power test

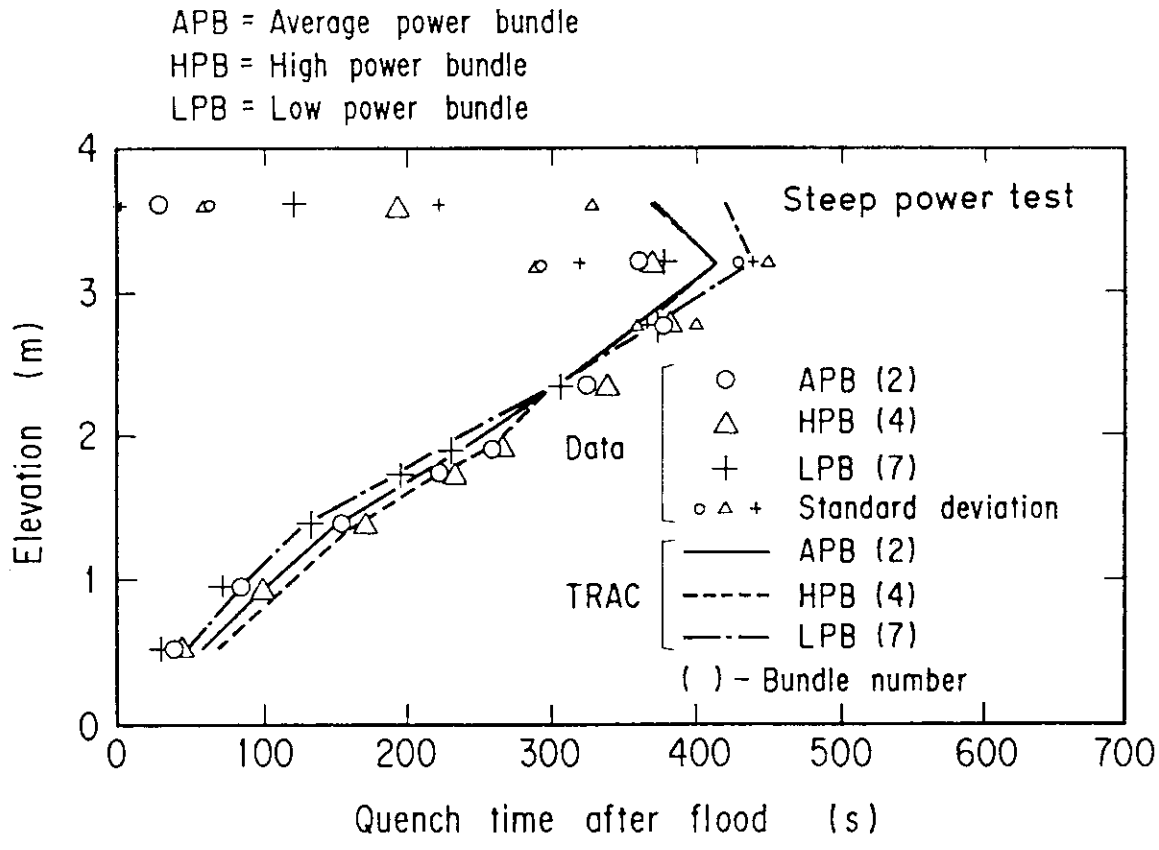

Fig.4.3.9 Comparison of quench time after flood for steep power test

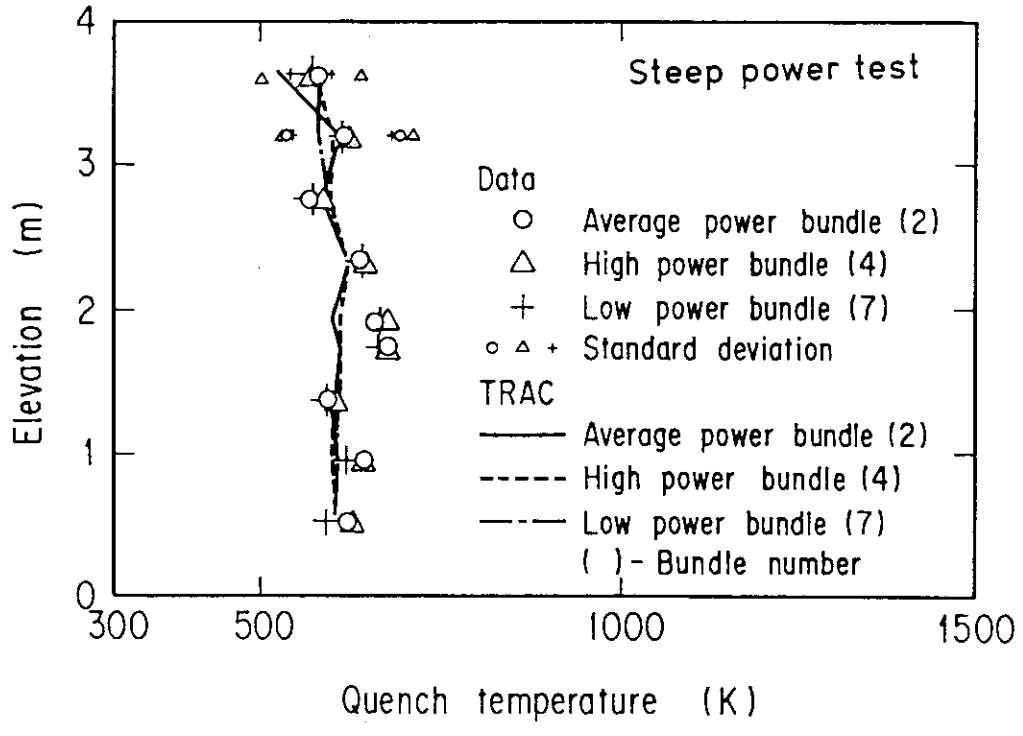

Fig.4.3.10 Comparison of quench temperature for steep power test

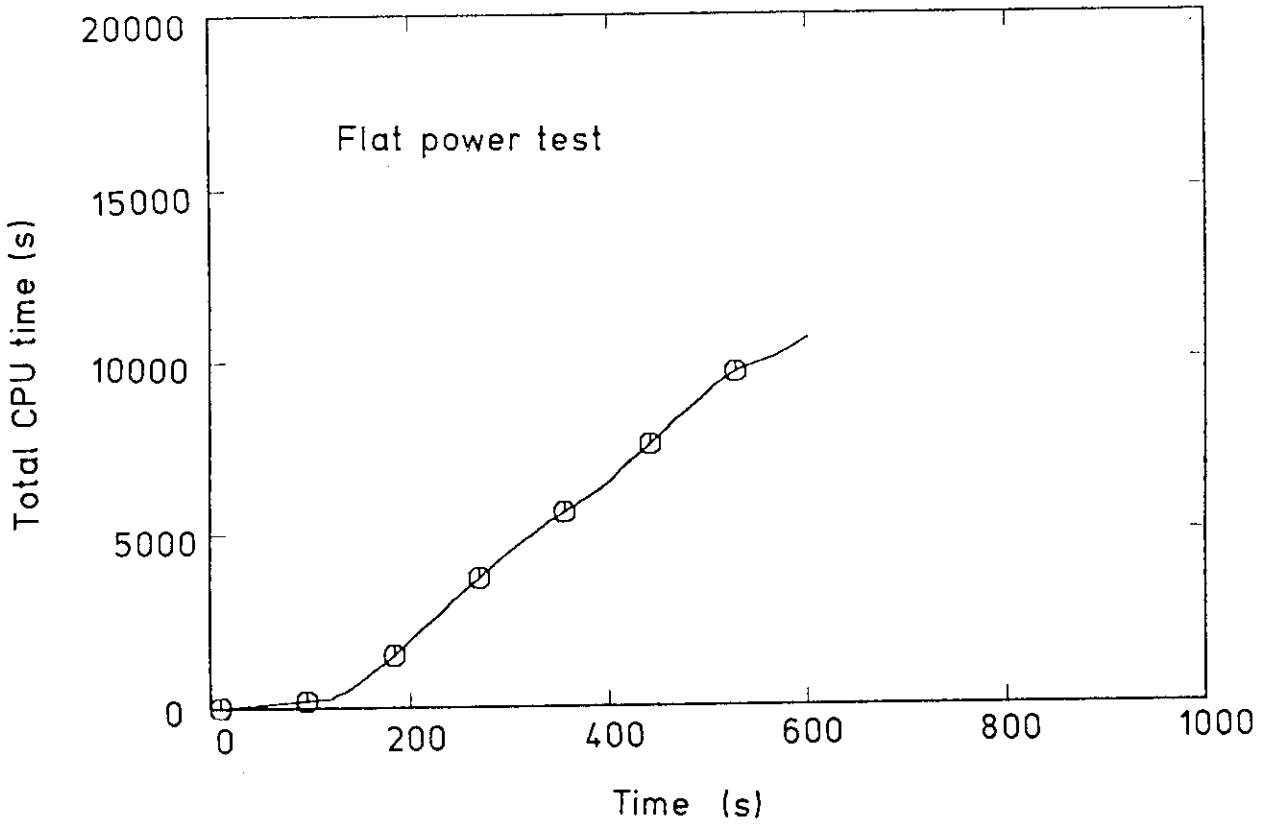

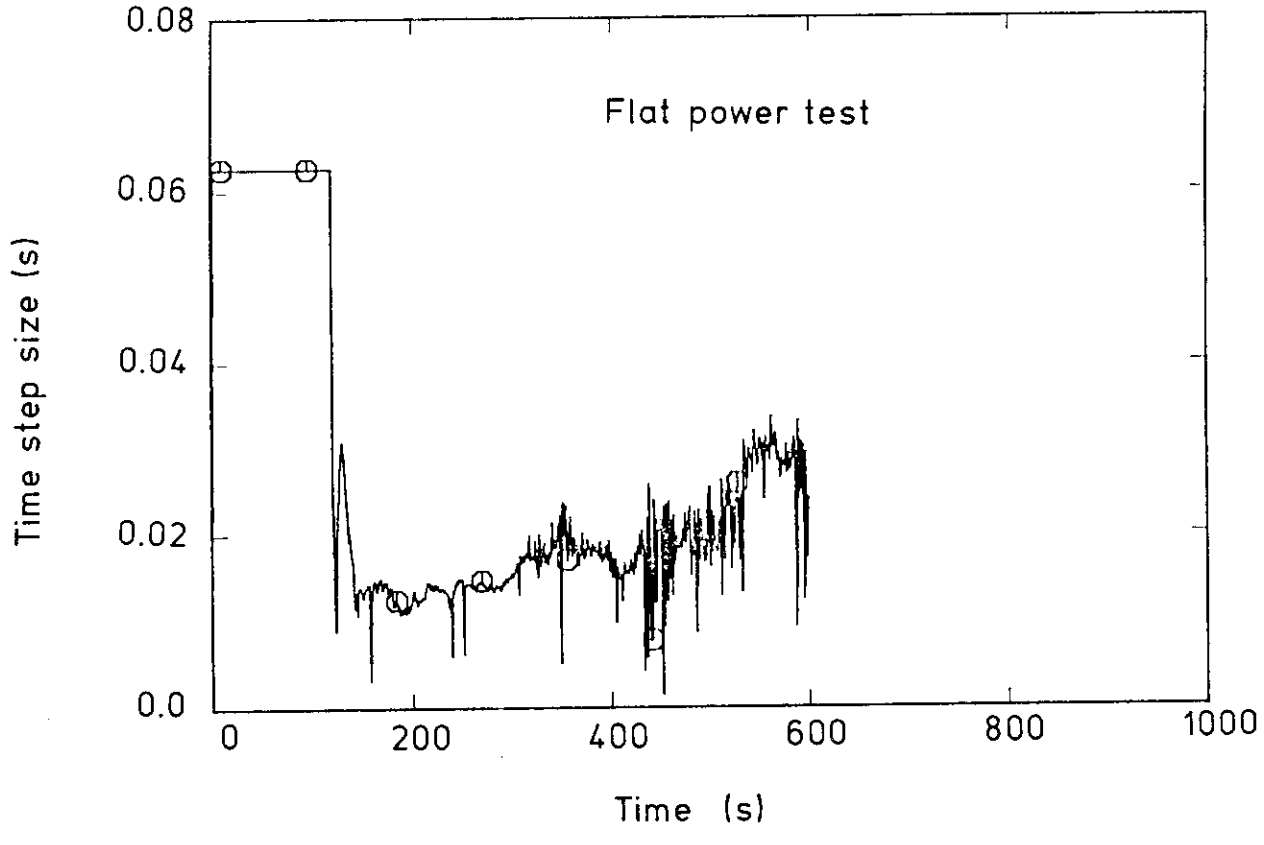

Fig.4.4.1 Total CPU time and time step size for flat power test

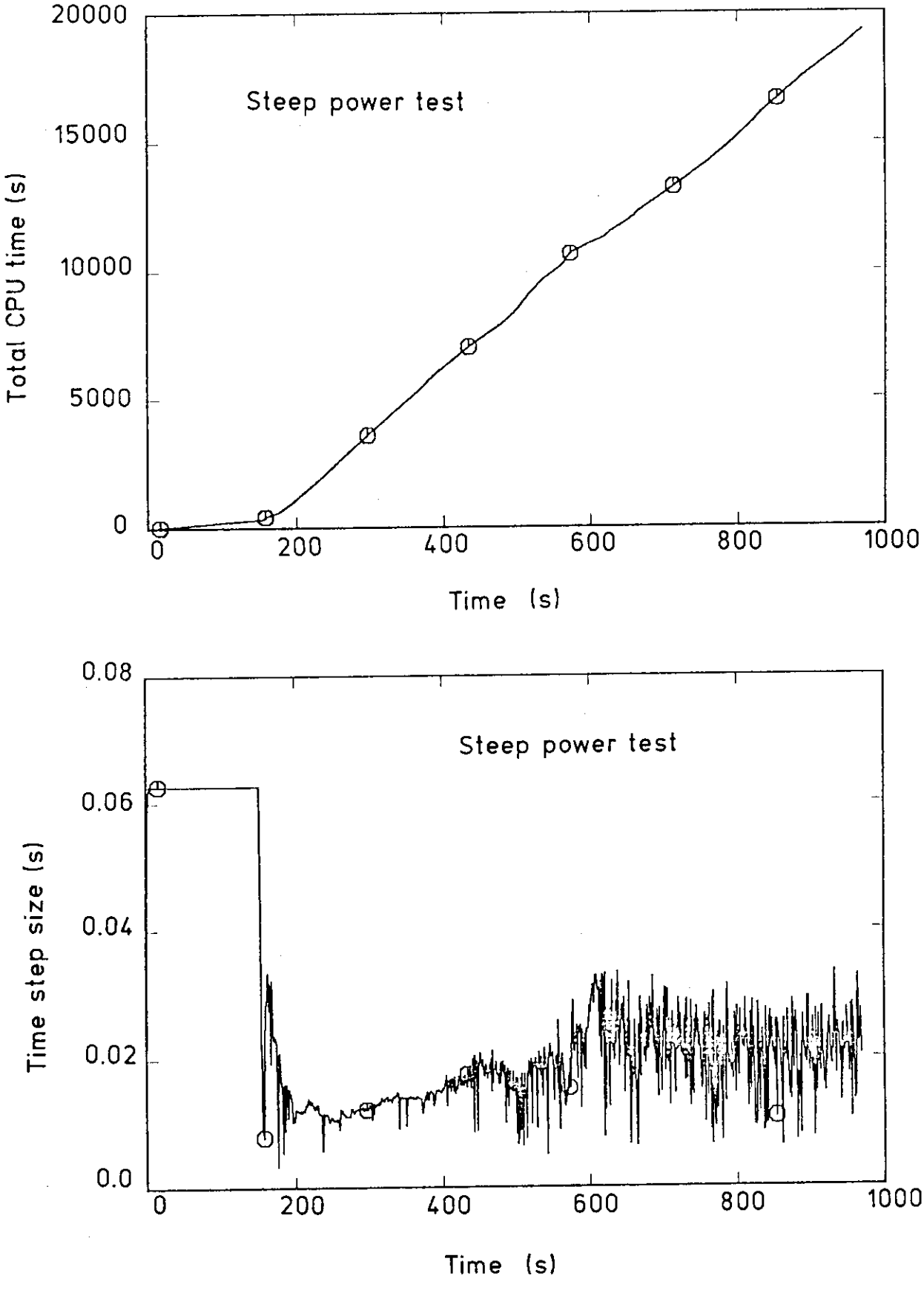

Fig.4.4.2 Total CPU time and time step size for steep power test